

**Understanding molecular strategies of resistance used by the  
malarial parasite, *Plasmodium falciparum***

Jennifer Marquita McDaniels  
Baltimore, Maryland

Bachelor of Science, University of Maryland, College Park, 2012

A Dissertation Presented to the Graduate Faculty  
of the University of Virginia in Candidacy for the Degree of  
Doctor of Philosophy

Department of Biology

University of Virginia  
April 1, 2020

Jennifer Guler (Advisor)  
Christopher Deppmann  
Keith Kozminski  
William Petri  
Yuh-wa Wang

## Abstract

The malaria parasite, *Plasmodium falciparum*, is one of the deadliest human protozoan parasites largely due to its rapid adaptation to overcome antimalarial drug treatment. Work from our group and others have shown that resistance can be accomplished by copy number variations (CNVs) and single nucleotide polymorphisms (SNPs) in the malaria genome. Little is known about how these genetic alterations arise and are propagated to confer enhanced parasite drug resistance. In order to address these gaps in research, this thesis is divided in two parts: resistance and transmission. **Chapter 2** highlights the novel detection of extra-chromosomal(ec) DNA in highly resistant *P. falciparum* parasites. Employing specialized PCR (droplet digital(dd) PCR) and Illumina sequencing we observed high copy numbers over genomic copies, uniquely associated with resistant parasites. The innovative detection strategies outlined in this thesis provided the opportunity to detect an otherwise, invisible molecule. We hope that the data presented in this thesis will lead to new discoveries of ecDNA in other well characterized resistance models. Furthermore, ecDNA provides a new, targetable approach to disrupt transmission of antimalarial resistance. **Chapter 3** investigates for the first time, extracellular vesicles (EVs) harboring endogenously-derived *dhodh* amplicons used by resistant *Plasmodium* parasites. We combined ImageStreamX flow cytometry with cryogenic electron microscopy to characterize vesicle morphology. Also, we used ddPCR to characterize the DNA contents found within EVs. We detected CNVs found in genomic DNA and vesicle-contained DNA. The discovery of genetic material harboring resistance-conferring genes found in

vesicles indicates a novel mechanism of genome evolution adapted by *P. falciparum*. Our results suggest vesicle exchange between a resistant donor and a sensitive recipient parasite may also emerge as a new targetable mechanism to inhibit resistance propagation. **Chapter 4** focuses on the surveillance of molecular markers of chloroquine (CQ) resistance in an endemic country to determine whether or not an antiquated antimalarial, CQ, will be effective once again. Returning to an antiquated antimalarial provides an alternative to our current frontline, artemisinin, aimed to dampened resistance. Resistance profiling in Southwest Uganda during 2010 and 2015 revealed a slow reversal to CQ sensitivity via high resolution melt analysis (HRM). We concluded that the significant regional variation in Uganda as well as other areas of the world emphasizes the need to perform local assessment of resistant profiles. Investigating resistance profiles can be used to inform treatment policies and drug implementation. Overall, we hope that the data generated in this thesis can be used to uncover the Achille's heel of malaria and move the scientific community closer to malaria eradication.

## Dedication

This thesis is first dedicated to Jesus for being my rock and my stronghold.

I would like to express my deep gratitude to Dr. Jennifer Guler, my advisor. I sincerely appreciate your guidance and direction in my research and future aspirations. Your insights are immensely valued. Thank you for your support, patience, and mentorship.

I would like to thank my committee members: Dr. Christopher Deppmann, Dr. Keith Kozminski, Dr. William Petri, and Dr. Yuh-wa Wang. They generously offered their time, expertise, and support. I am extremely grateful. I am specifically thankful to Dr. Kozminski for his support as my first reader.

This thesis was also accomplished with the help of my labmates (both present and former members). I am thankful to Audrey Brown, Maureen Carey-Medlock, Jessica Cooper-Pancake, Luke Dillard, Adam Huckaby, Shiwei Liu, and Michelle Wharton. Thank you for your strong academic discussion, encouragement, and assistance.

I would also like to dedicate my thesis to the entire McDaniels and Langley family. I want to specifically thank my father, Allan McDaniels, my mother, Veronica McDaniels, and my sister, Crystal McDaniels. Your continued support and encouragement allowed me to follow my passions and complete my goals. You all knew that I could push myself to do more than I could have imagined. Thank you for reminding me of His grace and favor. Words cannot express how grateful I am for all of you and your prayers. I also would like to acknowledge my Aunt Sarah, my cousin Shawnette Burke-Asburne, and my cousin Sheri Shearin. Thank you for

being my cheerleaders. Thank you for setting the standard and being excellent role models. I would like to express my deepest gratitude to my grandparents, Leon and Emma Cooper. My grandfather, who, although is no longer with us, continues to inspire and empower me. My grandparents taught me the value of education and encouraged me to be the first doctor in our family. Your values of perseverance, determination, and strength has greatly influenced my work.

I would also like to thank my friends: Joseph Armstead III (late), Hannah Fishman, Amber Griffith, Russell Harrison III, Rachel Jackson, Lamara Johnson, Sierra Lewis, Kiosha Murphy, Gerria Russell, and Djuan Short. Thank you for being a listening ear and always answering the phone when I called. Thank you for being a life style conductor, telling me when I need to break and when I need to go full speed. To Raegan Jackson, may you follow your love for art, science, and discovery. To my new friends: Maria Ali, Ryan Grippio, Trina Kudmozki, Akin Odeleye, Gabriela Paniagua-Stolz, Richard Smindak, Victoria Tucker, Maya Wright, and Xin Yuan. Your guidance and your advice are greatly appreciated. Thank you for your unconditional help and support. Lastly, I would also like to thank Sean Anderson, Kirsnick Ball, Shawn Carter, Kiari Cephus, Kirk Franklin, and Quavious Marshall for presenting me with encouragement through fine music selections.

## Table of Contents

<b>Abstract</b> .....	<b>ii</b>
<b>Dedication</b> .....	<b>iv</b>
<b>Figure list</b> .....	<b>viii</b>
<b>Supplemental Figure List</b> .....	<b>ix</b>
<b>Table List</b> .....	<b>x</b>
<b>Supplemental Table List</b> .....	<b>xi</b>
<b>Appendices List</b> .....	<b>xii</b>
<b>Abbreviations</b> .....	<b>xiii</b>
<b>Chapter 1: Introduction</b> .....	<b>1</b>
1.1 Intracellular development of <i>Plasmodium</i> parasites .....	3
1.2 Antimalarials and resistance .....	6
1.3 Detection of copy number variations (CNVs) .....	10
1.4 Extra-cellular vesicles .....	13
<b>Chapter 2: The generation of extra-chromosomal DNA amplicons in antimalarial resistant <i>Plasmodium falciparum</i></b> .....	<b>20</b>
2.1 Introduction.....	21
2.2 Results .....	23
2.3 Discussion.....	46
2.4 Materials and methods .....	58
<b>Chapter 3: Extra-cellular vesicles containing antimalarial resistance-conferring genes found in <i>Plasmodium falciparum</i> parasites</b> .....	<b>82</b>
3.1 Introduction.....	83
3.2 Results .....	86
3.4 Discussion.....	101
3.3 Materials and methods .....	105
<b>Chapter 4: Persistent <i>pfcr</i> mutations in the genome of the malarial parasite, <i>Plasmodium falciparum</i>, from Southwestern Uganda</b> .....	<b>113</b>
4.1 Introduction.....	114
4.2. Results .....	119
4.3. Discussion .....	122
4.4. Conclusions.....	126

4.5 Materials and methods .....	126
<b>Chapter 5: Discussion and open questions.....</b>	<b>145</b>
Open questions .....	151
<b>References.....</b>	<b>161</b>

## Figure List

<b>Figure 1.</b> Malaria life cycle.....	5
<b>Figure 2.</b> Summary of parasite clones used in this study .....	24
<b>Figure 3.</b> Gel electrophoresis revealed aberrant DNA elements are confined to resistant parasites .....	25
<b>Figure 4.</b> Southern blot detection of <i>dihydroorotate dehydrogenase (dhodh)</i> in ecDNA derived from highly resistant parasites.....	27
<b>Figure 5.</b> Southern blot analysis following restriction digestion revealed ecDNA is resistant to digest.....	34
<b>Figure 6.</b> Highly resistant parasites carry multiple copies of ecDNA enriched in <i>dhodh</i> amplicons.....	37
<b>Figure 7.</b> Digestion with Plasmid Safe ATP-dependent DNase provides insight into ecDNA structure.....	39
<b>Figure 8.</b> Deep sequencing reveals conservation of amplicon boundaries and ecDNA-specific sequence .....	44
<b>Figure 9.</b> Summary of DNA structures predicted by PFGE location and enzymatic analyses.....	47
<b>Figure 10.</b> A model of ecDNA generation and maintenance in <i>Plasmodium falciparum</i> .....	54
<b>Figure 11.</b> Isolation of extra-cellular vesicles (EVs) resulted in a higher density of vesicles .....	87
<b>Figure 12.</b> Morphology of vesicles derived from parasites and uRBCs by Cryo-EM. ....	91
<b>Figure 13.</b> ImageStream revealed that parasite-derived EVs were of a distinct size .....	93
<b>Figure 14.</b> Infected RBCs (iRBCs) secrete vesicles with higher scatter and higher levels of SYBR-positive staining.....	94
<b>Figure 15.</b> Analysis of DNA located inside of wild type (WT) resistant (RT) parasite-derived vesicles.....	97
<b>Figure 16.</b> Visualization of EVs treated in the absence and presence of DNase by ImageStream.....	100
<b>Figure 17.</b> Clinical sample collection sites in Uganda and schematic overview of methods for detection of <i>pfcr</i> t resistant and sensitive genotypes .....	116

<b>Figure 18.</b> PCR and HRM analysis.....	117
---	-----

## Supplemental Figure List

<b>Supplemental Figure 1.</b> Southern blot analysis of additional DSM1 resistant clones all harbored ecDNA with the <i>dhodh</i> gene .....	73
<b>Supplemental Figure 2.</b> Identification of slow-migrating material using an alternative agarose type during PFGE harbors the <i>dhodh</i> gene .....	74
<b>Supplemental Figure 3.</b> Alternative methods were unsuccessful at purifying ecDNA in highly resistant DSM1-resistant parasites .....	75
<b>Supplemental Figure 4.</b> Plasmid Safe (PS) ATP-dependent DNase did not exhibit loci preference.....	77
<b>Supplemental Figure 5.</b> Histogram of sequencing coverage of H1 genomic(g) DNA and gel-incompetent DNA compared to the reference genome.....	79
<b>Supplemental Figure 6.</b> Gating of EVs and merozoites using ImageStream. .	110
<b>Supplemental Figure 7.</b> Parasite derived EVs appeared to contain vesicles bound vesicles .....	111
<b>Supplemental Figure 8.</b> Assessment of DNase activity on DNA associated from uRBCs vesicles .....	112
<b>Supplemental Figure 9.</b> Evaluation of Ct values and confidence % by High Resolution Melt (HRM) assay.....	138
<b>Supplemental Figure 10.</b> Evaluating sequencing profiles of the <i>pfcr</i> t gene in control <i>Plasmodium</i> genomes.....	139
<b>Supplemental Figure 11.</b> Evaluation of LightScanner and HotStarTaq mix performance .....	140
<b>Supplemental Figure 12.</b> Assessment of the impact of narrower normalization regions on genotype calling .....	141
<b>Supplemental Figure 13.</b> Representatives of manual genotype calling .....	142
<b>Supplemental Figure 14.</b> HRM analysis of mixed <i>pfcr</i> t haplotypes using Rotor-Gene Q .....	143
<b>Supplemental Figure 15.</b> Ct values vs confidence % generated by High Resolution Melt (HRM) assay.....	144

## Table List

<b>Table 1.</b> Details of primers used in Southern blot analysis and digital droplet PCR (ddPCR) .....	29
<b>Table 2.</b> Comparison of expected and observed band sizes from Southern blot analysis using the <i>dhodh</i> probe (Figure 5B).....	30
<b>Table 3.</b> Comparison of expected and observed band sizes from restriction digestion analysis.....	32
<b>Table 4.</b> Summary of coverage enrichment at known CNVs .....	43
<b>Table 5.</b> Summary of <i>pfcr1</i> genotypes.....	120

## Supplemental Table List

<b>Supplemental Table 1.</b> Summary of sequencing results .....	68
<b>Supplemental Table 2.</b> Summary of coverage enrichment at chromosome 6 amplicon.....	69
<b>Supplemental Table 3.</b> Summary of highly enriched chromosomal locations from H1 gel-incompetent DNA sample .....	70
<b>Supplemental Table 4.</b> Summary of LUMPY and CNVnator algorithm analysis	72
<b>Supplemental Table 5.</b> High Resolution Melt analysis of clinical samples. ....	133

## Appendices List

<b>Appendix 1.</b> Freeze and squeeze extraction of DNA from agarose gels protocol .....	159
---	-----

## Abbreviations

ACT(s)	artemisinin combination therapy(-ies)
ART	artemisinin
B	BamH1(enzyme)
bp(s)	base pair(s)
CGH	comparative genomic hybridization
Chr	chromosomal DNA
CN	copy number
CNV(s)	copy number variation(s)
CQ	chloroquine
CsCl-EtBr	cesium chloride- ethidium bromide
	centrifugation
Ct	cycle threshold
ddPCR	droplet digital PCR
<i>dhodh</i>	<i>dihydroorotate dehydrogenase</i>
dsDNA	double-stranded DNA
ecDNA	extra-chromosomal DNA
EM	electron microscopy
ESCRT	endosomal sorting complex
EV(s)	extra-cellular vesicles
<i>gch1</i>	<i>GTP cyclohydrolase 1</i>
gDNA	genomic DNA
H1	highly resistant parasite line 1

H2	highly resistant parasite line 2
H3	highly resistant parasite line 3
H4	highly resistant parasite line 4
HRM	high resolution melting
iRBC(s)	infected red blood cell(s)
kb(s)	kilobase pair(s)
L1	low level resistant parasite line 1
M1	mid-level resistant parasite line 1
MC(s)	Maurer's cleft(s)
MaC(s)	manual call(s)
MDA	multiple displacement amplification
<i>mdr1</i>	<i>multiple drug resistance 1</i>
MV(s)	microvesicles
N	NheI (enzyme)
N.D.	not determined
NGS	next generation sequencing
NTC	no template control
O/N	overnight
PCR	polymerase chain reaction
<i>P. falciparum</i>	<i>Plasmodium falciparum</i>
<i>pfcr1</i>	<i>P.falciparum chloroquine resistance transporter</i>
PfCRT	<i>P.falciparum</i> chloroquine resistance transporter
PFGE	pulse field gel electrophoresis

PfPTP2	PfEMP-1 trafficking protein 2
PS	Plasmid Safe ATP-dependent DNase
PV	parasitophorous vacuole
PVM	parasitophorous vacuole membrane
qPCR	quantitative PCR
RBC(s)	red blood cell(s)
RE(s)	restriction enzyme(s)
ROS	reactive oxidative species
SFDA	small fragment-driven DNA amplification
SNP(s)	single nucleotide polymorphism(s)
SP	sulfadoxine-pyrimethamine
ssDNA	single-stranded DNA
SW	Southwest (Uganda)
TVN	tubular-vesicular network
uRBC(s)	uninfected red blood cells
WT1	wild type 1, Dd2
WT2	wild type 2, 3D7

## Chapter 1: Introduction

Malaria, or bad air, is named after the Italian term “mal'aria.” It has plagued the world for over thousands of years. Some of the earliest historical records date back to 2700 BC from China and 2000 BC from Mesopotamia (Cox, 2010). In 1880, Charles Louis Alphonse Laveran discovered the causative agent of malaria (Manson-Bahr, 1938). “He had the good fortune whilst watching a pigmented body in the blood, to witness the eruption of long motile filaments, and thus was able to recognize its living parasitic nature,” recalled by Sir Patrick Manson (Manson-Bahr, 1938).

Since then, the protozoan *Plasmodium* parasites responsible for malaria has consistently evolved to spread in this current day. This phenomenon has been exemplified by the vast diversity of its hosts including apes, reptiles, birds, and humans to name a few ((Faust and Dobson, 2015; Kariuki and Williams, 2020; Martinsen et al., 2008; Prugnolle et al., 2011). Since malaria’s discovery, it has been quite the evolutionarily arms race between the parasite and its human host (Kariuki and Williams, 2020). Human malaria is caused by five different *Plasmodium* protozoan parasites, *Plasmodium falciparum* being the most virulent and deadly (Kariuki and Williams, 2020). Remarkably, *P. falciparum*, has continued to adapt to overcome selective drug, or antimalarial, pressure.

## Summary

This thesis will summarize the key aspects in understanding molecular strategies of resistance used by *P. falciparum*. To this end, I will delineate: 1) the generation of extra-chromosomal(ec) DNA amplicons, defined as a region of DNA that is amplified, in highly resistant DSM1 parasites, 2) a role for extra-cellular vesicles in carrying resistance-conferring genes, and 3) the importance of resistance surveillance in malaria endemic countries. I will describe ecDNA in great detail as it is the first report of endogenously derived genetic elements in response to drug resistance in this organism. Uncovering a mechanism of ecDNA generation and segregation will uncover a new targetable resistance strategy. Previous EV research typically only investigate proteins and RNAs packaged into vesicles, I will address how parasite-derived vesicles carry DNA. This thesis will also shed light on the importance of surveillance of resistance genes in clinical samples. I specifically focus on CQ resistance patterns in Southwestern Uganda. Results produced from this study have the ability to influence drug policies regarding stricter regulations of antimalarial use, distribution, and production. Our findings can also be expanded to other malaria endemic countries to influence antimalarial stringency although Uganda is highlighted.

## Aims

**Aim 1:** To determine ecDNA topology and its sequence

**Aim 2:** To determine whether parasite-derived DNA can be packaged within EVs

**Aim 3:** To assess the resistance profile of *pfcr* mutations in study areas around Mbarara and across Uganda using high resolution melt assays

To reflect the research scope presented in this thesis, the introductory chapter has 4 sections. In the first part, I will provide general background on malaria biology. In the second part, I provide a brief review of antimalarials and effective strategies used by *Plasmodium* to overcome drug challenge with an emphasis on CNVs. Thus, the third part reviews CNV detection methods. In the fourth part, I will describe EVs and its role in malaria pathogenesis.

### **1.1 Intracellular development of *Plasmodium* parasites**

*P. falciparum* has a complex life cycle, developing in both humans and female *Anopheles* mosquitos (Cowman et al., 2016) (see life cycle, **Figure 1**). When an infected mosquito bites a person, parasites make its way to the human liver. There, they undergo schizony, or will be amplified many-fold before bursting into the bloodstream to cyclically infect and destroy red blood cells (RBCs) (Wiser, 2011). A selection of parasites undergoing the asexual erythrocytic cycle transitions to the sexual cycle, forming gametocytes. Mature gametocytes are then taken up by another mosquito during a blood meal. Within the mosquito, male and female gametocytes fuse together forming a zygote. The zygote further develops in oocytes and, eventually, sporozoites. The sporozoites make their way to the mosquito salivary glands. The cycle will continue as the infected mosquito releases sporozoites into another human host (Center for Disease Control and Prevention,

2019). Research in this thesis focuses on the asexual stage that occurs within the RBCs.

The RBC imposes many challenges for the *Plasmodium* parasite, another factor in its complex life cycle. RBCs are terminally differentiated. They are devoid of subcellular organelles and *de novo* lipid and protein biosynthesis machinery (Mohandas and Chasis, 1993). To satisfy the parasite's high nutritional demand and rapid development, it must acquire nutrients from the RBC or the extracellular environment. Although hemoglobin is the parasite's primary source for amino acids, the parasite must also transport isoleucine, L-glutamate, and other solutes (Lauer et al., 1997). Additionally, the parasite must acquire host lipids to support its cellular growth.

Limited biosynthesis of fatty acids occurs in an organelle called the apicoplast, which also contributes isoprenoid precursors and heme (Mitamura and Palacpac, 2003). The parasite has limited nucleotide metabolism and must synthesize pyrimidines *de novo*. For pyrimidine biosynthesis, the parasite can only use glutamine or bicarbonate. One essential step in pyrimidine synthesis involves the transfer of electrons to ubiquinone by dihydroorotate dehydrogenase, DHODH in the mitochondria (Gutteridge et al., 1979).

In turn, the malaria parasite forces many functional and morphological changes upon RBCs. The parasite resides within a protective parasitophorous vacuole (PV) within the RBC, providing yet another transport challenge; cargo needs to be transported across the parasitophorous membrane (PVM), the RBC cytosol, and the RBC membrane.

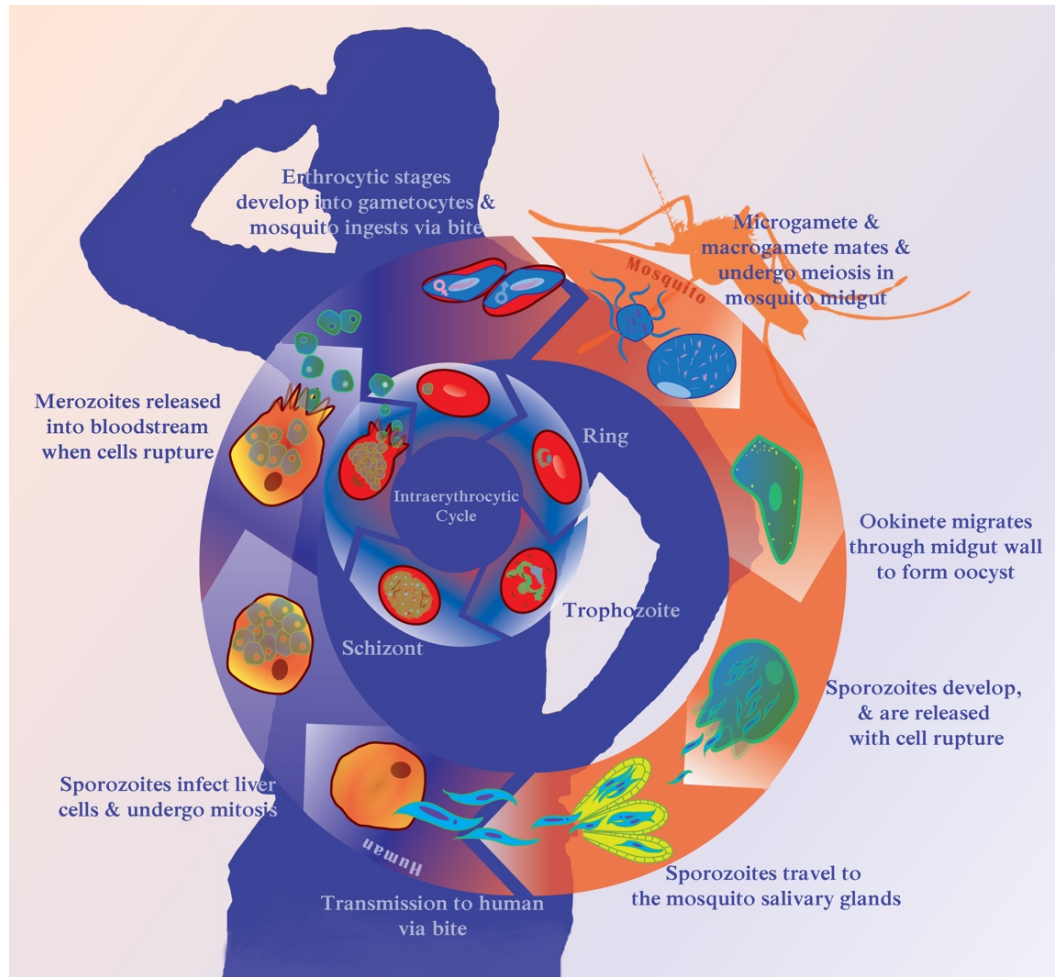


**Figure 1. Malaria life cycle.** To complete its complex life cycle, *P. falciparum* parasites requires both human and mosquito hosts. When in the human, there are 2 important stages, the asexual (inner ring) and sexual stages (outer ring). During the sexual stage, a female *Anopheles* mosquito bites the human host and the parasite continues the sexual stage within the mosquito. Image created by Michelle Warthan, 2017.

In less than two hours following invasion, the malaria parasite strategically remodels the RBC to induce new pathways to acquire nutrients and export proteins from RBC cytosol as well as the extracellular environment. The parasite inserts organelles, increases rigidity and alters RBC permeability to allow the transport of nutrients (Lanzer et al 2006, Rug et al 2014). This includes the formation of *Plasmodium*-specific Maurer's clefts (MCs), which are flat, disc shaped secretory organelles that are about 30nm in diameter (Hanssen et al. 2008). MCs were first thought to resemble Golgi cisternae but do not contain COPII proteins (PfSarp1, PfBet3p, and PfTrs31p) (Adisa et al 2007). The origins of the MCs are unknown but it is thought that MCs can be derived from the PVM or the TVN, which is another proposed mechanism for nutrient uptake (Wickert and Krohne 2007). Furthermore, the dynamics of protein secretion in *Plasmodium* are still poorly understood. The complexity of the *Plasmodium* life cycle leads to an important question: How does trafficking occur over several membranes?

## 1.2 Antimalarials and resistance

Malaria currently pervades Southeast Asia and the sub-Saharan Africa (World Health Organization, 2018). While the development of a malaria vaccine has made recent strides (Adepoju, 2019; Center for Disease Control and Prevention, 2019; RTS,S Clinical Trials Partnership, 2014; van den Berg et al., 2019). We typically rely on antimalarials, drugs that specifically target the malaria parasite, for treatment and control of this disease. Specifically, antimalarials are used in combination—the pairing of 2 or more drugs.

Our current frontline drug is artemisinin (Meshnick, 2002). Artemisinin has an endoperoxide ring and when cleaved, it is activated (Meshnick, 2002; O'Neill et al., 2010). Artemisinin unleashes reactive oxidative species, ROS (Meshnick, 2002; O'Neill et al., 2010); It oxidizes proteins, lipids, and DNA, which eventually leads to the death of the parasite. Southeast Asia has reported the emergence of artemisinin resistance between 2002-2004, specifically located at Myanmar and the Thailand-Cambodia border (Ashley et al., 2014; Müller et al., 2019; Tun et al., 2015). Resistance is characterized by a delay in parasite clearance after ACT treatment and most notably, linked to a *kelch13* mutation in the propeller domain (Ashley et al., 2014; Rosenthal, 2018; Tun et al., 2015). There has been a growing concern regarding the spread of artemisinin resistance to Africa, where there is the highest rate of mortality and malaria cases (Rosenthal, 2018; World Health Organization, 2018). Thus, a large effort is being made to create new antimalarials, revisit former antimalarials (**explored in Chapter 4**), and discover new parasite-specific targets to kill the parasite (explored in **Chapters 2 and 3**).

Prior to artemisinin use, our former frontline drug was chloroquine, CQ. After its development in the 1940s, CQ was particularly effective (Slater, 1993). Coupled with its low cost and ease of manufacturing, it was used in multitudes leading to the first report of resistance in 1959 (Slater, 1993). CQ mode of action involves complex formation with toxic heme moieties that in turn prevent the degradation of hemoglobin to heme (Birnbaum et al., 2020; Burrows, 2015; Sidhu et al., 2002; Tilley et al., 2016). The accumulation of toxic heme intermediates causes swelling and vesiculation of the food vacuole (Langreth et al., 1978). Non-synonymous

SNPs in the *P. falciparum chloroquine resistance transporter*, *pfcr*, gene are linked with CQ resistance (Bray et al., 2005; Krogstad et al., 1992, 1992; Sidhu et al., 2002).

Generally, alteration of the parasite's genome confers resistance and two types of changes have been observed: 1) SNPs or 2) CNVs (Cheeseman et al., 2009; Cowman et al., 2016, 1994; Dharia et al., 2009; Foote et al., 1990; Guler et al., 2013; Kidgell et al., 2006; Koenderink et al., 2010; Kondrashov, 2012; Ribacke et al., 2007; Sidhu et al., 2006; Singh and Rosenthal, 2004). For example, CQ resistance is mediated by SNPs that result in a missense mutations, changing amino acids residues at the 72-76 position (Bray et al., 2005; Sidhu et al., 2002). Functionally, PfCRT is an efflux pump that drains CQ at the food vacuole (Bray et al., 2005; Krogstad et al., 1992). Other SNPs are linked to many other antimalarials like sulfadoxine, pyrimethamine, and atovaquone to name a few (Beghain et al., 2016; Duraisingh and Cowman, 2005; Mita et al., 2009; Roper et al., 2014).

On the other hand, artemisinin resistance is much more complicated due to its broad effects on the parasite (Burrows, 2015; O'Neill et al., 2010). As previously mentioned, a highly conserved gene, *kelch13*, mediates ART resistance (Ashley et al., 2014; Birnbaum et al., 2020; Mbengue et al., 2015; Tun et al., 2015). More recently, it has been shown that *kelch13* mutations impact endocytosis, controlling the amount of hemoglobin available for digestion and the amount of drug that is activated the parasite (Birnbaum et al., 2020). More studies are being done to elucidate artemisinin's mode of action.

CNVs are gains or deletions of genes or groups of genes within the genome. Changes in gene copy number can be either deleterious or provide fitness advantages to an organism that harbors them.

As previously mentioned, *P. falciparum* thrives in a variety of environments throughout its life cycle and exhibits remarkable genetic adaptability in the face of selective pressures. CNVs range in size from a few hundred basepairs to hundreds of kilobase pairs (Cheeseman et al., 2016; Kidgell et al., 2006; Ribacke et al., 2007). The most well-studied example of a *P. falciparum* clinical resistance-conferring genome amplification involves the *multidrug resistance 1 gene*, *mdr1*. This gene is located on chromosome 5 and encodes for a P-glycoprotein efflux pump (Cowman et al., 1994; Foote et al., 1990; Nair et al., 2007; Triglia et al., 1991; Wilson et al., 1989). Additionally, amplification of a region on chromosome 12 that includes *GTP cyclohydrolase 1 gene* (*gch1*), although not directly responsible for resistance, may help compensate for point mutations conferring clinical antifolate resistance (Guler et al., 2013; Kidgell et al., 2006; Nair et al., 2008a). The importance of genome amplification in parasite survival is further emphasized when resistant clones are studied following selection with experimental antimalarials such as inhibitors of cysteine proteases (Singh and Rosenthal, 2004), isoprenoid biosynthesis (Dharia et al., 2009), protein synthesis (Rottmann et al., 2010), and pyrimidine biosynthesis (Guler et al., 2013; Phillips et al., 2015, 2008; Ross et al., 2014). Many questions remain about the genetic basis of CNV formation.

CNVs offer both disadvantages and advantages. CNVs poses vast disadvantages such as alterations in gene dosage, gene expression levels, or neighboring regions, but can also cause gene disruption or fusion (Li and Olivier, 2012). It is also proposed that CNVs offer a stepwise advantage in which the parasite is able to first tune-up its CNVs, subsequently accumulate advantageous SNPs, and finally tune-down CNVs (Guler et al., 2013). Harboring increased copy numbers of certain genes first increases the parasites survival during stochastic SNP accumulation; this means that even if a SNP is deleterious, its impact is diminished due to pseudoheteroploidy.

The *Plasmodium* parasite is highly adaptive and has ability to generate various CNVs as a mechanism of resistance. Until now, there has been no previous investigations linking CNVs to ecDNA in malaria. Thus, the role of ecDNA in resistance remains to be elucidated. More research is needed to map the pathways of resistance in great detail so we can identify an Achille's heel of *Plasmodium*.

### **1.3 Detection of copy number variations (CNVs)**

It is important to choose the appropriate technique and platform for detection. In this section, I discuss common methodologies and their shortcomings, which also covers the methodologies I used throughout the thesis. At the end, I discuss the method that I implemented for my studies.

Quantitative PCR (qPCR) is one method that is commonly used for targeted locus studies (Li and Olivier, 2012). qPCR compares the cycle threshold (Ct) value

of an unknown sample to a reference sample with known copy number (Li and Olivier, 2012; Mehrotra, 2016). One limitation is DNA input is about 5-10ng (Cantsilieris et al., 2013). A newer derivative of qPCR using droplets, called ddPCR, emerged as another CNV detection technique. Using droplet formation, ddPCR allows the end point measurement of ~20,000 individual PCR amplifications from a very small amount of DNA (<0.1ng). The random distribution of DNA into individual droplets facilitates highly accurate quantitation of DNA copy number and enables a smaller fold change measurement compared to qPCR (Hindson et al., 2011; Pinheiro et al., 2012; Whale et al., 2012). Thus, ddPCR is a more sensitive CNV detection method (Weaver et al., 2010; Whale et al., 2012).

Comparative genome hybridization (CGH) and next generation sequencing (NGS) has been an invaluable tool used to determine CNV level over genome-wide targets with high sensitivity. Contrary to qPCR and ddPCR, CGH and NGS require higher DNA inputs (between 0.5-1 $\mu$ g and 1-2 $\mu$ g for CGH arrays and NGS, respectively (Cantsilieris et al., 2013)). CGH arrays compare target DNA to reference DNA by measuring the fluorescent ratio along each chromosomal location (Tim J. C. Anderson et al., 2009; Carret et al., 2005; Li and Olivier, 2012). It has been previously described that one assay is equivalent to thousands of fluorescent *in situ* hybridization experiments (Theisen, 2008). NGS involves alignment of newly synthesized sequence to a reference genome. Most commonly, read depth analysis is used to determine CNV locations (Tim J. C. Anderson et al., 2009). As you scan through an entire genome for imbalances, there is a chance for impactful false positives and negatives (Dennin, 2018).

Combining pulse field gel electrophoresis (PFGE) with Southern blot analysis is another low throughput method to determine copy number. PFGE is used to resolve large chromosomes in the megabase size range (Khan and Kuzminov, 2013; Turmel et al., 1990). Southern blotting is a powerful technique that involves DNA transfer to a nylon membrane followed by the use of specific labelled DNA probes for visualization. Copy number is inferred by the human eye, but post analysis methods used to quantify radiolabeled or fluorescent band intensities normalized to the reference genome are available. DNA input is high at 2–5 $\mu$ g (Cantsilieris et al., 2013).

Overall, CNV detection methods can be used to identify new and novel antimalarial drug targets as it has been done in the past. In this investigation, we propose a novel pipeline modifying from Thuring paired with ddPCR to identify ecDNA (Thuring et al., 1975). This detection pipeline has been manipulated to overcome the limitations of CNV detection. Past studies of ecDNA that involved genome-wide detection like CGH and NGS often overlooked the presence of ecDNA due to: 1) the lack of separation from the chromosomal DNA and 2) the lack of knowledge about its existence (Dennin, 2018). Due to the low sensitivity and high DNA input required for CGH and NGS, I developed an original pipeline of multiple CNV detection methods to study a new form of CNVs; I performed PFGE, Southern blotting, ddPCR, and genome sequencing after isolating ecDNA away from chromosomal DNA to improve the performance of low- and high-throughput methods. This pipeline can be easily adapted to conduct a wide range of ecDNA studies in the presence of a selective driver, not just in *Plasmodium*.

## 1.4 Extra-cellular vesicles

Cell-to-cell communication is mediated by secreted vesicles termed extra-cellular vesicles (EVs). EVs are small membrane-derived vesicles that are 0.1-1 $\mu$ m in diameter that carry cell-type specific RNA, protein, and DNA that can induce signals in targeted cells. Nomenclature is often misused but EV size and origin are two common ways to distinguish types of vesicles. There are three classes of EVs including microvesicles and exosomes (both <0.1 $\mu$ m), and apoptotic bodies (>0.1 $\mu$ m in size) (Delabranche et al., 2012). Another distinction between these classes of vesicles are how they are formed. While apoptotic bodies are vesicles that are released during apoptosis, microvesicles shed and bud directly from the plasma membrane (Johnstone et al, 1987). In contrast, exosomes are formed from late endosomes and are released when multivesicular bodies fuse with the plasma membrane. Exosomes were first discovered while studying maturing reticulocytes (Johnstone et al 1987).

Since 1987, the study of EVs and their role in malaria has been an area of active research. EVs has been associated with *P. falciparum* commitment to the sexual cycle through gametocyte development, which will ultimately assist in the transmission to mosquitos (Mantel et al., 2013a; Regev-Rudzki et al., 2013) **(Figure 1)**.

Regev-Rudzki et al. uncovered the use of DNA packaged into exosomes involved in the parasite commitment to sexual differentiation (Regev-Rudzki et al., 2013). These EVs provided a survival advantage. Resistance-conferring genes were transmitted to neighboring parasites under drug selection. EVs were parasite-

derived and were 80-120nm in size. This study prompts a follow up question: Are endogenously-derived resistant genes packaged into vesicles and transmitted to neighboring parasites? Here, researchers transferred an episomal plasmid. Although this study was the first to implicate EVs in the transfer of drug resistance genes, many questions remain. How are nucleic acids packaged into vesicles? The investigators effectively showed using *in situ* hybridizations that recipient parasites contained newly transferred drug resistance genes; however, they did not show that those necessary genes conferring drug resistance were indeed contained in the EVs. Besides the size, functional characteristics of these EVs including proteins, lipids and structural biology remains to be characterized.

EVs playing an important role malaria pathogenesis is also evident in of Mantel et al. Researchers identified MVs of 100-400nm in size that were released during the asexual cycle prior to egress, a process characterized by mature parasites rupturing their current RBC and invading a new RBC. They showed that the MVs contained parasite material indicating that they are parasite-derived. Remarkably, they found that the parasites can internalize vesicles through immunofluorescent microscopy displaying vesicles located at the nuclear periphery. There are important observations published by Mantel et al. that are in agreement with data previously described by Regez-Rudski et al.: 1) parasites can transmit information into vesicles to neighboring parasites and 2) parasites can internalize vesicles from donator parasites using a trafficking mechanism that is not yet defined.

A number of studies have examined EVs in clinical malaria. The number of EVs are increased with patients that have severe malaria (Combes et al., 2004; Mantel et al., 2013a; Nantakomol et al., 2011; Pankoui Mfonkeu et al., 2010; Sampaio et al., 2017). More recently, it has been shown that vesicle production is amplified during artemisinin resistance; vesicles derived from resistant parasites are inferred to play a role in RBC remodeling and trafficking more protein to the RBC surface membrane (Bhattacharjee et al., 2018).

In general, prior EV work on malaria has been limited to: 1) a small subset of characterized proteins necessary for trafficking i.e. PfPTP2, 2) cargo studies precluding DNA, and 3) the transfer of genes on episomal plasmids, which are not native to the parasite. There is still a great deal of work that needs to be in this area.

In this thesis, I will focus on the first report of endogenously-derived genes packaged into vesicles with a possible role in further propagating resistance. Thus, this study will open up a new avenue for DNA to be further studied in vesicles derived from parasites.

A common challenge when studying vesicles is the lack of standardization in reporting vesicle properties (i.e. size, markers, buoyant density, and so on) and the myriad of isolation methods reported. This may have led to some differences in reports of EV origin and EV occurrence during infection (Sampaio et al., 2017). In the papers I described in detail, exosomes were isolated using density gradient centrifugation by Regev-Rudzki et al. and MVs were isolated using a combination of sucrose differential centrifugation and filtration by Mantel et al. The isolation

methods in the general EV field also vary widely, which results in numerous vesicle related studies with little overlapping characteristics. For example, centrifugation at 2000xg can isolate apoptotic vesicles, 10,000-20,000xg can isolate microvesicles and 100,000-200,000xg can be used to isolate exosomes (Szatanek et al., 2015). Ultracentrifugation, which is the most commonly used method, can isolate all 3 different type of vesicles; however, physical damage to the vesicles can occur (Konoshenko et al., 2018). Density gradient ultracentrifugation (facilitated through the use of sucrose or iodixanol) is inefficient at isolation large vesicles (Szatanek et al., 2015).

The current literature reports that *Plasmodium* secretes both exosomes and microvesicles. However, *Plasmodium* is devoid of major exosome proteins involved in its biogenesis from multivesicular bodies (ESCRT I and II, (Mantel and Marti, 2014)), which introduces doubt about the presence of canonical exosomes despite the appropriate size range of the vesicles. The general lack of EV markers and proper sizing guidelines leads to difficulties with EV characterization.

A well-recognized issue for the study of EVs in malaria is that uninfected RBCs (uRBCs) release EVs. This 'background' source of EVs necessitates a better approach to distinguish uRBCS from parasite-infected RBCs (iRBCs) (Kuo et al., 2017). To complicate this issue further, parasite-derived vesicles also contain host-specific markers such as stomatin, a lipid raft protein (Babatunde et al., 2018) or human nucleic acids (Babatunde et al., 2018; Mantel and Marti, 2014). There are also a few parasite-specific markers available. One way to overcome these issues, lies in expanding studies with *Plasmodium*-derived vesicles, which

is explored in **Chapter 4**. Here, I present new EV research that specifically distinguishes vesicles from iRBCs and uRBCs.

It is a long journey for vesicles, as they are transported across various organelles of the parasite including the Golgi, endoplasmic reticulum, tubular-vesicular network (TVN) to the plasma membrane, the parasitophorous vacuole (PV) and the PV membrane (PVM), finally to the Maurer's cleft (MC) of the RBC before export through the RBC membrane (Martin et al., 2009; Soni et al., 2016) (referenced in **Chapter 1**). Most of what we know is centered around the secretion of PfEMP1, an essential virulence protein found on the surface of RBCs involved in cytoadherence (Baruch et al., 1995; Boddey et al., 2009; Kraemer and Smith, 2006; Smith et al., 1995).

There are two proposed models for protein export and thus, these models can be extended to vesicles export in *Plasmodium* (Boddey et al., 2009). The first model makes use of processing a transmembrane PEXEL-like sequence found on vesicles to be sorted to the Golgi and the parasitophorous vacuole using a general secretory pathway involving COPII machinery. Then, vesicles are transported to MCs and then to the RBC membrane. The second model suggests the use of a different PEXEL-like sequence and its complementary receptor that directly sorts vesicles to the PVM. In general, an export pathway to the host RBC remains speculative (Boddey et al., 2009; Crabb et al., 2010; Haase and de Koning-Ward, 2010; Mundwiler-Pachlatko and Beck, 2013). Another important consideration is the possibility of exported vesicles devoid of a PEXEL sequence, as many characterized proteins that takes residency in the MCs are PEXEL-negative

(Mundwiler-Pachlatko and Beck, 2013). This then begs the question: are there other key proteins, lipids, etc. required for the efficient sorting of vesicles that are undiscovered?

In either case, after vesicles leave the PVM, vesicle may stop at MC transiently. Vesicles to be exported are found to have PFPTP2, a MC protein deemed to be essential (Babatunde et al., 2020; Maier et al., 2008; Regev-Rudzki et al., 2013). Another family of proteins, SNAREs, are predicted to play a role in trafficking; however, once again, little is known about their role in the unique trafficking pathways found in *P. falciparum* (Parish and Rayner, 2009). It is suggested that an endocytosis-like pathway is one way for the vesicles to be internalized but on its own, a mature RBC is devoid of any internal membranes to assist in endocytosis (Mantel and Marti, 2014).

So why study vesicles? Despite many unknowns, *P. falciparum* vesicular research is an exciting area due to its potential for identifying new therapeutic approaches. Vesicles can be loaded with antimalarials or vaccines for long lasting effects reviewed in (Sampaio et al., 2017). Transmission-blocking approaches, which prevent cell-to-cell communication between parasites, also presents itself as a new resistance strategy. Furthermore, there has been no published studies that addresses whether or not endogenously-derived DNA is packaged into vesicles.

We aimed to expand on the previous results of Regev-Rudzki et al. while determining if endogenously-derived, resistance-conferring genes are packaged into vesicles. I hope this study will lead to new insights of parasite-specific proteins

to further elucidate the trafficking pathways used in malaria. I also hope these studies can assist in the development of a likely mechanism in support of horizontal gene transfer, which can be a valuable method applied *in vivo*. These studies warrant a better understanding of why increased levels of EVs are linked to severity of disease. One possible explanation is that parasites are increasing their communication using genetic material, which confers enhanced survival for the parasite. To conclude, EV studies similar to this one will help to disrupt a resistance strategy used by the *P. falciparum*.

## **Chapter 2: The generation of extra-chromosomal DNA amplicons in antimalarial resistant *Plasmodium falciparum***

This section is a version of a manuscript currently written for submission to the Molecular Microbiology Journal. The figures and tables have been renumbered to maintain sequence with other figures and tables in this dissertation.

Jennifer M. McDaniels<sup>1</sup>, Adam C. Huckaby<sup>1</sup>, Sabrina A. Carter<sup>1</sup>, Sabrina Lingeman<sup>1</sup>, Audrey Francis<sup>1</sup>, Molly Congdon<sup>2</sup>, Webster Santos<sup>2</sup>, Pradipsinh K. Rathod<sup>3</sup>, and Jennifer L. Guler<sup>1, 4</sup>

<sup>1</sup>Department of Biology, University of Virginia, Charlottesville, Virginia 22903 USA,

<sup>2</sup>Department of Chemistry, Virginia Tech, Blacksburg, Virginia 24061 USA,

<sup>4</sup>Departments of Chemistry and Global Health, University of Washington, Seattle, Washington 98195-1700 USA, <sup>4</sup>Division of Infectious Diseases and International Health, Department of Medicine, University of Virginia, Charlottesville, Virginia 22903 USA

Author contributions:

Conceived and designed the experiments: JMM SAC PKR JLG

Performed the experiments: JMM ACH SAC SLL MC AF JLG

Analyzed the data: JMM ACH SAC MC JLG

Contributed reagents, materials, and/or analysis tools: WS PKR JLG

Wrote the paper: JMM JLG

## 2.1 Introduction

A major factor that contributes to genome plasticity in a variety of organisms is extra-chromosomal (ec)DNA. EcDNA contains extra gene copies that exist outside of the genome and are often observed at high copy numbers in organisms under strong selection. As evidence for their contribution to genome plasticity, genes that confer fitness benefits are enriched in ecDNA (Beverley et al., 1984). Although pioneer works in *Leishmania* protozoan parasite (Beverley et al., 1984), ecDNA has now been reported in various eukaryotes including yeast (Møller et al., 2015) human cancers (Albertson, 2006; Hastings et al., 2009; McGill et al., 1993; Verhaak et al., 2019; Wu et al., 2019), mammalian cells (Dillon et al., 2015), and another protozoan species *Trypanosoma* (Wagner and So, 1992). The diversity of ecDNA is exemplified in the reported sizes that range from a few hundred base pairs to mega base pair molecules (Dennin, 2018; Paulsen et al., 2018a). Although their size and composition vary depending on the organism, one consistent theme is the importance of ecDNA in rapid adaptation.

*Plasmodium falciparum*, the deadliest malaria parasite, killed ~435,000 people in 2018 (World Health Organization, 2018). This organism is known for its adaptability, both in response to the human immune system (Scherf et al., 2008) and drug treatment (Qidwai, 2020). However, the presence of endogenously-derived ecDNA after drug selection has never been reported in any *Plasmodium* species.

During our studies of a family of parasites that were selected with the novel antimalarial, DSM1 (Guler et al., 2013), a few key observations led us to

hypothesize that ecDNA may be present in highly resistant *P. falciparum*. First, we observed genomic copy number variations of the target gene, *dhodh*, (termed *dhodh* amplicon) located on chromosome 6 and these resistance-conferring amplicons were rapidly gained with elevated antimalarial pressure. Second, the amplified unit was precisely conserved during subsequent selections, providing evidence that they were not generated *de novo* at every step. Lastly, the resistance level, although correlated, was not directly proportional to the detected amplicon copy number; two DSM1 resistant clones exhibited ~10 amplicon copies as detected by qPCR, but one of them (termed H1 for high level resistance) showed ~10-fold higher EC<sub>50</sub> than the other (termed M1 for mid-level resistance, **Figure 2**). Overall, these observations indicated the presence of an independent DNA element that contributes to resistance yet can be rapidly increased or decreased in order to balance benefit with fitness effects.

Upon further study of this experimental system, we definitively identified ecDNA in highly DSM1 resistant *P. falciparum* parasites. We used an electrophoresis-based purification scheme combined with a variety of highly sensitive DNA analysis methods to expose resistance-conferring genes outside of the chromosomal genome. We then employed enzymatic digestions to explore the structure of multiple forms of ecDNA; Interestingly, two forms were detected, although we speculate that only one (a large complex circular form) is biologically relevant. The carriage of resistance genes on ecDNA has wide-reaching implications, as it provides a new target to limit the development of resistance.

Understanding how these ancillary forms of DNA are generated and their function holds high importance for our understanding of adaptation in general.

## 2.2 Results

In our initial study of drug resistance mechanisms in *Plasmodium*, we selected for resistant parasites using multiple levels of DSM1 selection (Guler et al., 2013) (see schematic in **Figure 2** showing the relationship between L, M, and H clones). In order to investigate the physical nature of genomic amplicons, we assessed the chromosomal pattern of DSM1 resistant clones using pulse field gel electrophoresis (PFGE) (**Figure 3A**). Although chromosomes 6-10 are similar in size (predicted to be 1.4-1.7Mb based on the 3D7 genome (PlasmoDB, (Aurrecochea et al., 2009)) a shift in position of chromosome 6 in the resistant clones was evident (**Figure 3A** and **4A**). Chromosome 6 from the DSM1-resistant clone, termed “L1” for low level resistance, appeared slightly larger due to the predicted insertion of amplicons into the native genome location (**Figure 3A**). However, in another DSM1-resistant clone, termed “H1” for high level resistance, the pattern of chromosomes in this area of the gel was completely altered (**Figure 3A**). Prompted by this result, we ran the gels under a number of additional PFGE conditions. Those that allowed visualization of the broadest range of DNA sizes revealed an additional element of DNA present in the H1 clone (**Figure 3B**). This “gel-competent” ecDNA element runs independently from intact chromosomes as a heterogeneous smear regardless of PFGE run parameters (see various run conditions in *Materials and Methods*).

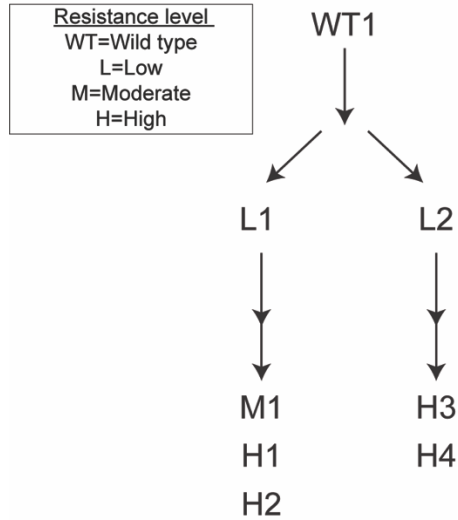


**Figure 2. Summary of parasite clones used in this study.** Wild type (WT1) *P. falciparum* was selected with 0.3 $\mu$ M of DSM1 in two steps; the first step selected for low level (L) resistant parasites and the second step selected for moderate (M) or high level (H) resistant parasites.  $EC_{50}$  values and amplicon copy numbers are as follows: L1 (1 $\mu$ M, 4), L2 (1 $\mu$ M, 4), M1 (7 $\mu$ M, 8), H1 (62 $\mu$ M, 10), H2 (85 $\mu$ M, 12), H3 (36 $\mu$ M, not determined), H4 (49 $\mu$ M, 12). Values were previously reported in and clone names adapted from (Guler et al., 2013). Not shown: Wild type 2 (WT2) represents Hb3 (0.1 $\mu$ M, no resistance).

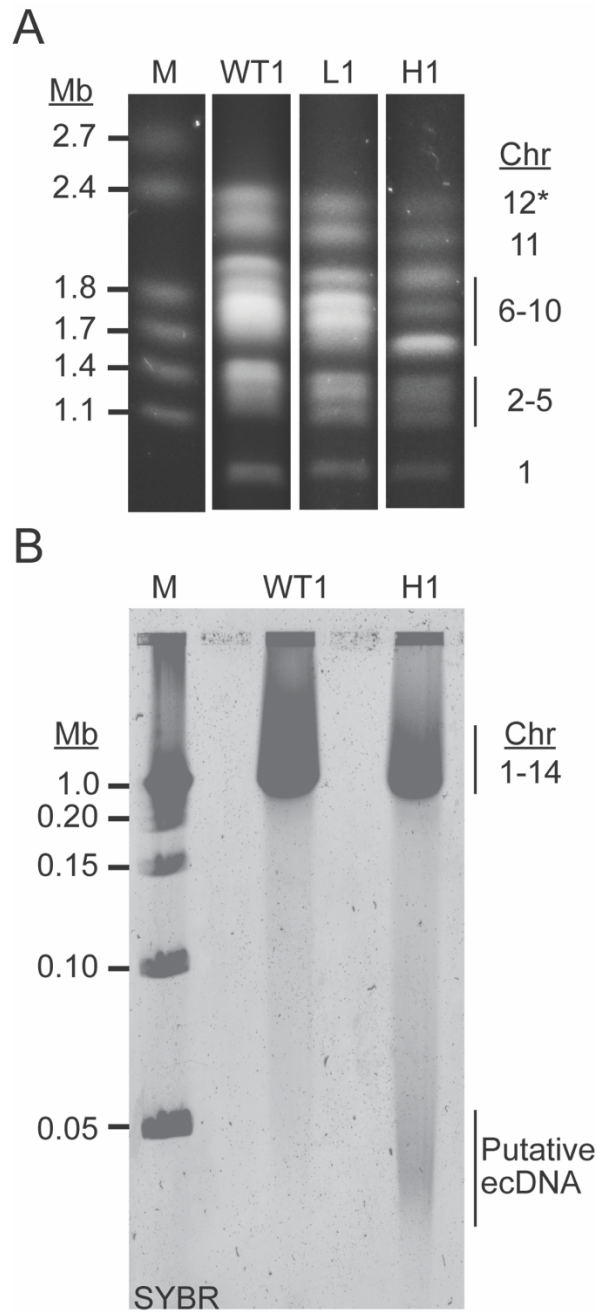


**Figure 3. Gel electrophoresis revealed aberrant DNA elements are confined to resistant parasites. A.** Altered pattern of chromosomes from resistant clones

(L1 and H1) compared to wild type 1 (WT1) migrated from agarose plugs. PFGE running conditions: 50hr, 3V/cm, 250-900sec switch rate, stained with 1 $\mu$ g/mL ethidium bromide and imaged on a UV transilluminator. M, marker (1-3.1Mb, BioRad 170-3667). \*Chromosome 13 and 14 ran above chromosome 12 and appeared as expected in all clones. **B.** Detection of extra-chromosomal(ec) DNA in the H1 clone from agarose plugs. PFGE running conditions: 17hr, 6V/cm, 1-10sec switch rate, stained with 1XSYBR Safe DNA stain and imaged using the Typhoon 9410 Variable Mode Imager (see Materials and Methods for settings). M, marker (0.05-1Mb, BioRad 170-3635); chr, chromosome; L1, low level resistant clone; H1, high level resistant clone; WT1, Dd2.

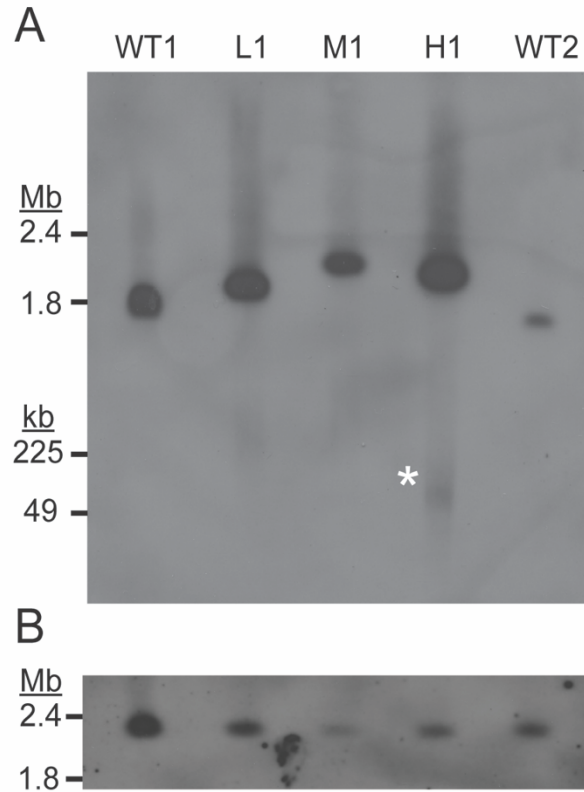


**Figure 4. Southern blot detection of *dihydroorotate dehydrogenase (dhodh)* in ecDNA derived from highly resistant parasites.** Agarose plugs with low (L1), moderate (M1), and highly resistant parasites (H1) are displayed after a PFGE run. **A.** Southern blot is probed with the *dhodh* amplicon probe (Table 1). The expected size of WT1 chromosome is 1.5Mb and WT2 chromosome 6 is 1.4Mb (PlasmoDB (Aurrecoechea et al., 2009)). Exposure time: 8hr. **B.** Southern blot probed with single copy reference gene 1 (Table 1). An additional housekeeping gene was also performed (single copy reference gene 2, Table 1, data not shown). The expected size of WT2 chromosome 11 is ~2Mb (PlasmoDB, PlasmoDB (Aurrecoechea et al., 2009)). DNA size was determined with 1-3.1Mb and 0.05-1Mb markers (Bio-Rad 170-3667 and 170-3635). Exposure time: 7hr. PFGE running conditions: 50hr, 3V/cm, 250-900sec switch rate. WT1, Dd2; WT2, 3D7; White dashed box, ecDNA.

To further investigate the origin and size of the putative ecDNA, we performed Southern blot analysis on PFGE gels using probes for gene sequences within the amplified region from chromosome 6 (*dhodh* amplicon, **Table 1**) as well as those outside the amplicon (external, single copy reference gene 1 and 2, **Table 1**). Using this approach, we determined that the gel-competent ecDNA was only detected when probing for a gene within the amplicon from high level resistant H clones (**Figure 4A** and **Supplemental Figure 1**). We did not detect the gel-competent ecDNA when probing for 2 genes located on chromosomes 7 and 11 (**Figure 4B** and **Supplemental Figure 1**). Because of this result, we ruled out general genome degradation as the source of the observed smear. We conclude that the gel-competent ecDNA is derived from amplified regions of the genome.

During these studies, we made additional informative observations. Firstly, using the *dhodh* amplicon probe, we determined the relative sizes of chromosome 6 in wild type and resistant parasites (see summary in **Table 2**). Chromosome 6 from low and moderate L and M clones, which are expected to have ~4 and ~8 copies of the amplicon, respectively (**Figure 2** and **Table 3**), migrated at the expected size on the PFGE gel (**Figure 4A**). However, chromosome 6 from the H1 clone, which is predicted to harbor ~10 copies of the amplicon (**Figure 2** and **Table 2**), runs well below the predicted size. In fact, the observed H1 chromosome 6 band ran below that from the M clone with fewer predicted amplicon copies (**Table 2, Figure 4A**). This inconsistency indicated that both ecDNA and chromosomal amplicons were contributing to the high level of resistance in H clones.

**Table 1. Details of primers used in Southern blot analysis and digital droplet PCR (ddPCR)**

Method	Probe Name	PlasmoDB Gene ID	Gene Name	Chr	CN	Sequence
Southern blot	<i>dhodh</i> amplicon	PF3D7_0603300	<i>Dihydro-orotate dehydro-genase</i>	6	Multicopy	F-TTGGTACCATAACCCCAAGG R- CCCTCCTGATGCAATAATGG
	Single copy ref. gene 1	PF3D7_1132900	<i>H protein</i>	11	Single copy	F-AAGTGCTTCTTCCCAGTTGTG R- CCCTTGCCCTTTATTTTCAA
	Single copy ref. gene 2	PF3D7_07177700	<i>seryl tRNA synthetase</i>	7	Single copy	F- TGCCGAACCTTGATGACTTTG R- TGC GTTGT TTAAGCTCCTG
ddPCR	<i>dhodh</i> amplicon	PF3D7_0603300	<i>Dihydro-orotate dehydro-genase</i>	6	Multicopy	F-TCCATTCGGTGTTGCTGCAGGATTT GAT <sup>†</sup> R-TCTGTAAC TTTGT CACAACCCATATTA <sup>†</sup> 56FAM/CATTATTGCATCAGGAGGGA/MGBNFQ
	Single copy ref. gene 2	PF3D7_07177700	<i>seryl tRNA synthetase</i>	7	Single copy	F- GGAACAATTCTGTATTGCTTTACC <sup>†</sup> R- AAGCTGCGTTGTTTAAAGCTC <sup>†</sup> VIC/ACATGAAGAAATGATACAAACA/3MGBE <sub>c</sub>
	Single copy ref. gene 3	PF3D7_0831700	<i>heat shock protein 70</i>	8	Single copy	F- GAATCGGTTTGTGCTCCAAT <sup>‡</sup> R- CAACTGTTGGTCCACTTCCA <sup>‡</sup> 5HEX/AGCAGGAATGCCAGGAA/3MGBE <sub>c</sub>
	<i>mt-cyb</i>	mal_mito_3	<i>cytochrome b</i>	Mito.	Multicopy	F- AGCAAGTCGATATACACCAGATG R- CAAGAGAAGCACCTGTTGCG 56-FAM/AAGAGAATTATGGAGTGGATG GTGTTT/3MGBE <sub>c</sub>

<sup>†</sup>Original primer reference (Guler et al., 2013).

<sup>‡</sup>Original primer reference (Ngwa et al., 2013).

Chr, chromosome

**Table 2. Comparison of expected and observed band sizes from Southern blot analysis using the *dhodh* probe (Figure 5B)**

Resistance level	Clone	Average # of amplicons	Predicted increase in size <sup>†</sup> (Mb)	Expected size (Mb)	Observed size (Mb)
Wild type	WT1	1	-	1.5 <sup>‡</sup>	~1.8
	WT2	1	-	1.4 <sup>‡</sup>	<1.8
Low	L1	4	0.292	~2.1	1.8-2.4
Moderate	M1	8	0.584	~2.4	1.8-2.4
High	H1	10	0.730	~2.5	1.8-2.4 <sup>§</sup>
	H4	12	0.876	~2.6	1.8-2.4

<sup>†</sup>qPCR # of amplicons x amplicon size (Guler et al., 2013).

<sup>‡</sup>The size of WT1 (Dd2) chromosome 6 was estimated after alignment of sequencing reads ((Guler et al., 2013) to the WT2 (Hb3) chromosome 6 (PlasmoDB) (unpublished data)).

<sup>§</sup>H1 chromosome 6 appears smaller than that from M1, despite an increased number of amplicons. Next Generation Sequencing revealed a ~10kb deletion on chromosome 6 in a related clone (H2, Guler et al., 2013), but this does not account for the size difference.

Second, we routinely observed DNA remaining in the well of the PFGE gel (**Supplemental Figure 2A**). Since previous studies found that circular DNA of  $\geq 30$ kb in size is readily trapped in the loading well and the region immediately below called the compression zone (Cole and Tellez, 2002; Gurrieri et al., 1999; Khan and Kuzminov, 2017, 2013; Turmel et al., 1990), we investigated the presence of larger sized ecDNA elements. Indeed, if we used a different grade of agarose (that allowed larger DNA fragments to enter the gel, see *Materials and Methods*), we detected amplicon specific supra-chromosomal DNA in all of the H clones by Southern blotting (**Supplemental Figure 2B and C**). This observation suggested that there is a second form of ecDNA that is termed “gel-incompetent” because it is well-bound under standard PFGE conditions.

Next, we used restriction digestion analysis followed by PFGE and Southern blot analysis to further investigate the structure of genomic amplicons and the two ecDNA forms (see **Figure 5A** for digestion schematic). We chose restriction sites both within (NheI) and outside (BamHI) of the amplified region with probes that are complementary to sequence both inside (termed *dhodh* amplicon, **Table 1**) and outside of the amplicon (termed external, **Table 1**). Overall, the detected fragments were of the expected size and pattern from both *dhodh* and external amplicon probes (**Table 3** and **Figure 5B**). The most significant observation during these studies was that the gel-competent ecDNA remained intact after digest for all H clones (**Figure 5C**); thus, it was resistant to restriction digestion.

**Table 3. Comparison of expected and observed band sizes from restriction digestion analysis**

Probe	Category	Clone (# of amplicons)	Expected band size (kb)		Observed band size (approximate) (kb)	
			B	B+N	B	B+N
Amplicon- specific (dhodh, Table 1)	No CNV	WT1	79.2	55.4	80	50
	L1 clone derived	L1 (4)	298 <sup>†</sup>	73.4/55.4	200	1. <80 2. 50 <sup>‡</sup>
		H1 (10)	736 <sup>†</sup>	73.4/55.4	>200	1. <80 2. 50 <sup>‡</sup>
		H2 (12)	882 <sup>†</sup>	73.4/55.4	>200	1. <80 2. 50 <sup>‡</sup>
		L2 clone derived	L2 (4) H4 (12)	79.2 79.2	55.4 55.4	80 80
	No CNV	WT1	79.2	55.4	80	50
Clone-specific (External probe, Table 1)	L1 clone derived	L1 (4)	298 <sup>†</sup>	55.4	ND	ND
		H1 (10) H2 (12)	736 <sup>†</sup> 882 <sup>†</sup>	55.4 55.4	>200 >200	50 50
	L2 clone derived	L2 (4) H4 (12)	79.2 79.2	55.4 55.4	80 80	50 50

<sup>†</sup>This value is dependent on the number of amplicons present in the genome.

Those listed assume 4 (L2) and 10 or 12 (H1 and H2 clones) copies of the L1 amplicon, respectively.

<sup>‡</sup>This band is only present once in genome despite amplicon, so band intensity is lower than band 1

CNV, copy number variation; B, BamHI restriction enzyme; N, NheI restriction enzyme; ND, not determined.

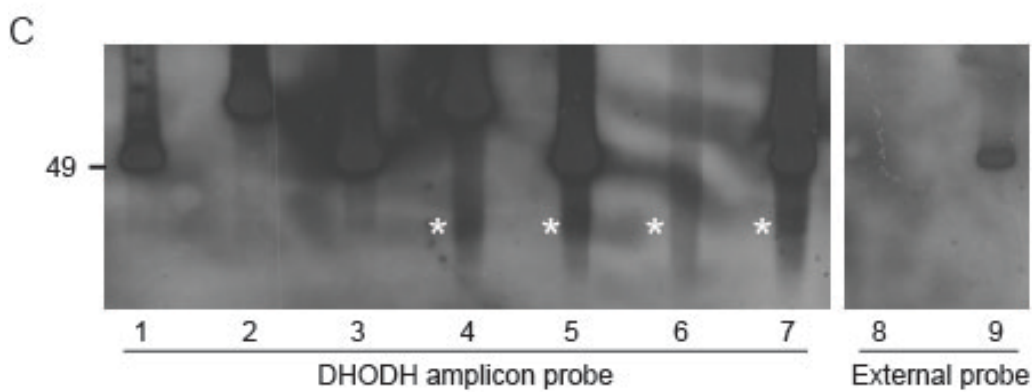
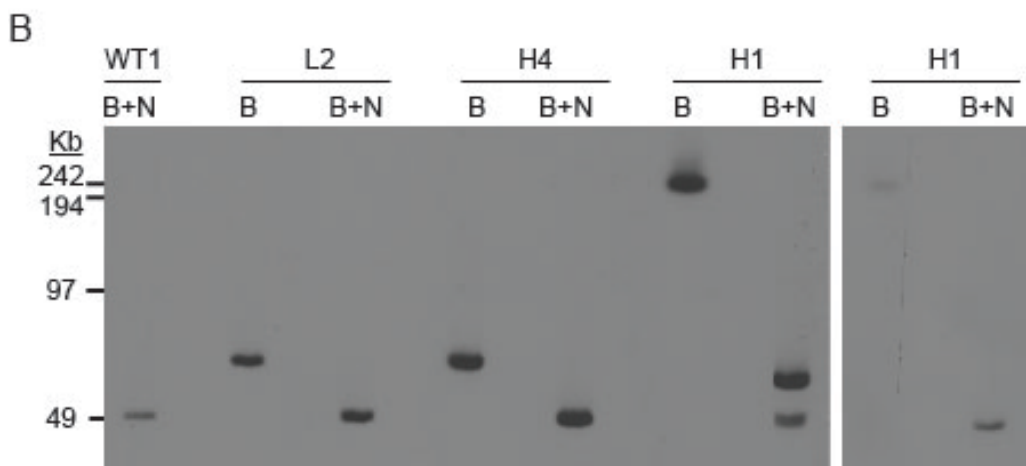
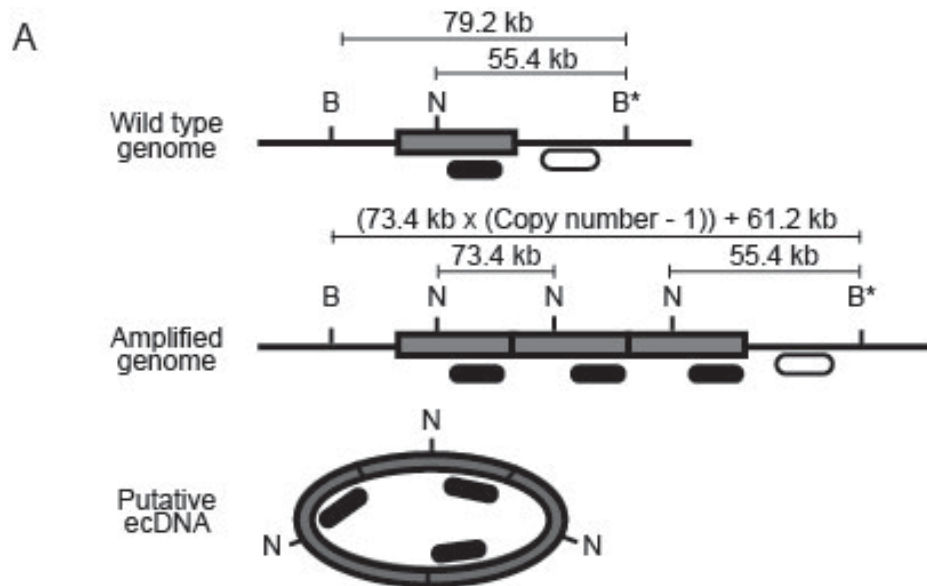


**Figure 5. Southern blot analysis following restriction digestion revealed ecDNA is resistant to digest. A.** Schematic of digestion pattern in wild type and amplified genomes for L1-derived clones only (H1) and ecDNA (expected and observed band sizes are also displayed in Table 3). All restriction sites were predicted from the WT2 reference genome but confirmed in sequencing reads from WT1 and L clones. For the L2-derived clones (L2 and H4), all probes and cut sites are contained within the amplicon from L2-derived clones. **B and C.** Two exposures of a Southern blot hybridized with the *dhodh* amplicon probe (Table 1, lanes 1-7) and the external probe (Table 1, lanes 8-9). WT1 (B alone) has been omitted for simplicity, but appears the same as L2 (B, lane 2). Digest of clones L1 and H2 (B and B+N) appear the same as H1 (lanes 6 and 7). **B.** Exposure times: Lanes 1-7, 30min; Lanes 8-9, 3hr. **C.** Exposure time: Lanes 1-7, 15hr; Lanes 8-9, 17hr. PFGE running conditions: 50hr, 3V/cm, 250-900sec switch rate; DNA source: parasite agarose plugs; B, BamHI; N, NheI; B+N, double restriction digest; grey square, *dhodh* amplicon; black ellipse, *dhodh* probe; white ellipse, external probe located outside *dhodh* amplicon (H1 only); B\*, due to varying lengths of the *dhodh* amplicon (Guler et al., 2013), the B\* site is located within L2 and H1 clones; White asterisk, ecDNA that is resistant to restriction digest; WT1, Dd2.

Further proof of the resistance of ecDNA to restriction digestion came from experiments with another set of H clones that were derived from a distinct L clone (L2, **Figure 2**). The amplicon in these clones is longer than those from L1-derived clones and therefore, includes a unique BamHI site within the amplicon (see digestion schematic in **Figure 5A**). After BamHI digestion, ecDNA from L1- and L2-derived H clones showed the same 'smear' persistence (**Figure 5C**, lanes 5 and 7); this result indicates that this effect is restriction site-independent and confirmed that cutting did not occur in either sample. As expected, the persistent gel-competent ecDNA was not detected when DNA from H clones was hybridized with the external probe (**Figure 5A and C**, lanes 8 and 9). Furthermore, since we did not detect an increase in the intensity of bands beyond what is expected from digestion of chromosomal copies alone (i.e. 4-fold for the L clone and 10 to 12-fold for H clones, **Figure 5B and Table 2**), we conclude that the well bound, gel-incompetent ecDNA is also not impacted by these enzymes.

Since other methods were not effective in isolating DNA away from chromosomal DNA (**Supplemental Figure 3**), we took advantage of the electrophoretic separation of these elements from the chromosomes and purified the DNA elements directly from the PFGE agarose gels. We then used droplet digital(dd) PCR to quantitatively measure enrichment of the resistance-associated gene in three gel regions of interest: the loading well (location of gel-incompetent ecDNA), the chromosomal region (location of previously described tandem amplicons), and the smear (location of gel-competent ecDNA). This method was particularly useful for our studies for several reasons: 1) the yield of ecDNA from

the PFGE gel was below levels required to run conventional quantitative PCR, 2) ddPCR assays can be multiplexed to accurately assess multiple loci within a single reaction, and 3) droplet partitioning diluted contaminating material from purifications (*i.e.* agarose). Using this approach, we calculated a ratio between resistance-conferring (*dhodh*, termed D) and single copy genes (*seryl tRNA synthetase* termed S). For this study, we hypothesized that samples with enriched numbers of ecDNA will generate a D:S ratio that is greater than the chromosomal copies of the amplicon. While chromosome material from an H clone yields a mean D:S ratio of ~8 (*i.e.* 8 copies of *dhodh* to one copy of *seryl tRNA synthetase*), we measured an enrichment for both the gel-incompetent and -competent ecDNA elements (average D:S ratio of 20 and 106, respectively, **Figure 6**). In comparison, wild type samples generated a consistent copy number of ~1, with no amplicons detected in either the extracted gel and loading well region (**Figure 6**). The highly sensitive ddPCR analysis unequivocally shows that the ecDNA elements are enriched in the resistance-conferring gene.

We utilized the Plasmid Safe (PS) ATP-dependent DNase to gain additional structural insight into the different ecDNA elements isolated from the gel. This enzyme preferentially digests linear DNA, while leaving circular DNA mostly intact. To examine its specificity on *Plasmodium* DNA, we PS-treated genomic DNA purified from cell lysates, linear chromosomal DNA isolated from gels, and complex structural forms of the mitochondrial genome that are also entrapped in the gel loading well and evaluated the remaining material with ddPCR (**Figure 7A**).

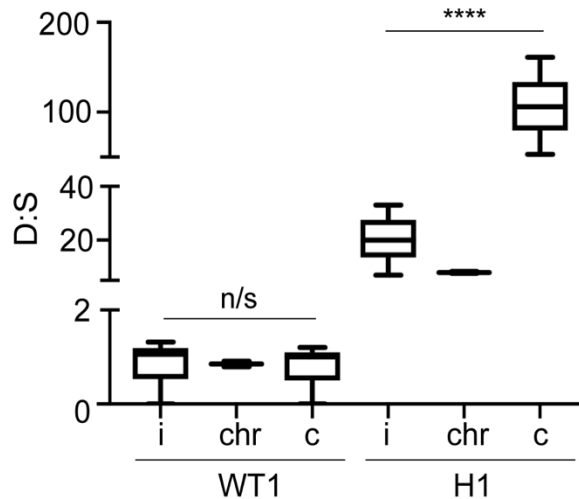


**Figure 6. Highly resistant parasites carry multiple copies of ecDNA enriched in *dhodh* amplicons.** A box and whisker plot summarizing the observed ratio of *dhodh* gene copies (denoted as D, a multicopy gene in the amplicon) to *seryl tRNA synthetase gene* copies (S, a single copy reference gene) as measured by droplet digital (dd)PCR. Samples were extracted from 3 regions of the PFGE gel prior to ddPCR: 1) the loading well, which following electrophoresis, retains gel-incompetent DNA (i), 2) the chromosomal (chr) region where chromosomes 1-14 are expected to run using specific parameters, and 3) the lowest region that harbors gel-competent DNA (c) that runs between 50-200kb. Average ratio (line in the center of the box) measured in the H1 well, chr, and smear regions are 20, 7.95, and 106, respectively. Average ratio measured in the WT1 well, chr, and smear regions are 1.06, 0.85, and 1.0, respectively. Expected chromosomal copy number is shown in Figure 1. WT1, Dd2; H1, high level resistant clone; i, gel-incompetent DNA; chr, chromosome; c, gel-competent DNA; \*\*\*\*,  $p < 0.0001$  significance; n/s, not significant; Error bars represent Poisson confidence intervals (upper hinge, 75<sup>th</sup> percentile; lower hinge, 25<sup>th</sup> percentile);  $n=3$ .

Here, in addition to *dhodh*, we probed for a known multicopy gene, *cytochrome b*, located on the mitochondrial genome; once again, we compared these multicopy genes to single copy genes (*hsp70* or *seryl tRNA synthetase*) to determine a C:S or C:H ratio, respectively. We included one other single copy gene as a control, *heat shock protein 70*. This experiment showed that the PS enzyme: 1) indiscriminately degrades genes that sit on the linear chromosomes (i.e. genes on chromosomes 6, 7, and 11 were degraded equally well, averaging 91% degradation at three separate loci, **Supplemental Figure 4A-D**) and 2) leaves complex/circular forms of DNA mostly intact (average of 36% degradation at the *cytochrome b* mitochondrial locus, **Figure 7B**). When we assessed the impact of the PS enzyme on isolated ecDNA, we observed almost complete digestion of the gel-competent form (smear, average of ~93% degradation at the *dhodh* locus, **Figure 7C**). When performing the PS digestion on gel-derived DNA in wild type parasites, the enzyme performed equally well at two different loci; there was no significant difference between *dhodh* and a single copy reference gene after PS digestion (mean of 79% and 84% degradation, respectively, **Figure 7D**). Importantly, the PS enzyme displayed limited digestion of gel-incompetent ecDNA (average of ~42% degradation at the *dhodh* locus, **Figure 7E**). This latter result is not due to a general lack of PS digestion since assessment of a single copy gene in the same sample showed high levels of degradation (76%, **Figure 7D**). From this experiment, we concluded that gel-competent ecDNA is largely linear due to high levels of PS degradation and gel-incompetent ecDNA is mostly complex/circular due to PS protection.

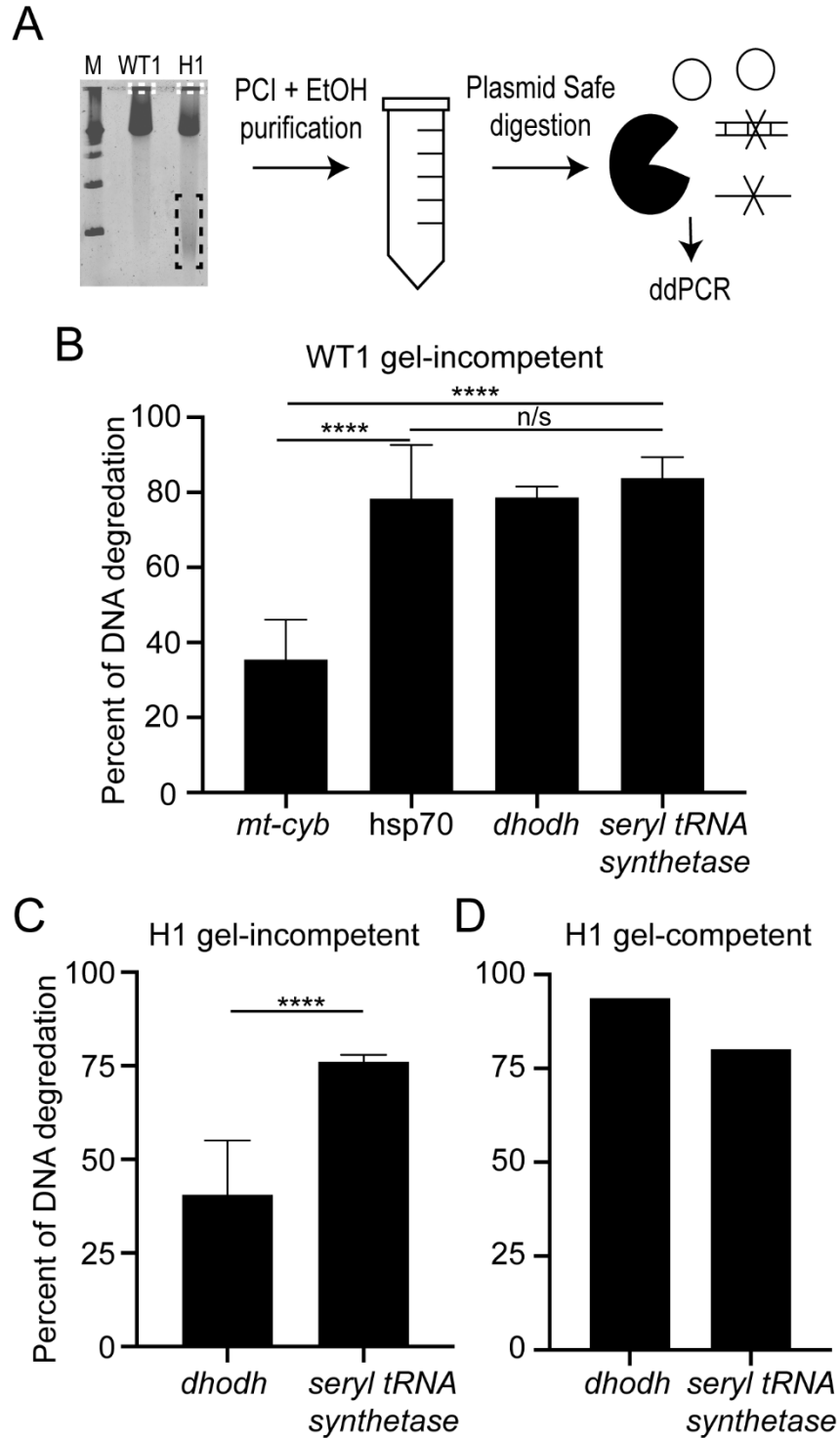


**Figure 7. Digestion with Plasmid Safe ATP-dependent DNase provides insight into ecDNA structure. A.** Schematic of DNA digestion approach. PCI, phenol-chloroform-isoamyl alcohol; EtOH, ethanol. WT1, Dd2; H1, high level

resistant clone; ddPCR, droplet digital PCR. **B-D**. Percent of DNA degradation is calculated by dividing the number of DNA positive droplets after digestion as measured by ddPCR by the number of DNA positive droplets before digestion then multiplying by 100. Each sample is probed for a multicopy gene (*mt-cyb* or *dhodh*) and a single copy gene (*hsp70* or *seryl tRNA synthetase*) to determine enzyme susceptibility of each type of locus. **B**. DNA derived from the loading well of WT1. n=3 **C** and **D**. DNA derived from the loading well of H1 (n=3) or lower region of the H1 gel (n=1), respectively. Both locations are thought to contain ecDNA. Note: the analysis presented in panel D was only completed once due to difficulties in purifying enough material. WT1, Dd2; H1, high level resistant clone; *mt-cyb*; *cytochrome b*; *dhodh*, *dihydroorotate dehydrogenase*; *hsp70*, *heat shock protein*; error bars denote standard error; \*\*\*\*,  $p < 0.0001$ ; n/s, not significant,  $p > 0.05$ .

To explore the sequence of the gel-incompetent ecDNA elements, we amplified DNA isolated from the PFGE well and performed short read sequencing on the resulting material (see basic sequencing statistics in **Supplemental Table 1**). Base calling accuracy (i.e. Q scores) and the mean library insert size of the amplified material was equivalent to that from a non-amplified genomic DNA sample from the same clone. While levels of contaminating bacterial reads were similar between the two samples (18% and 21% of total reads for H1 genomic DNA and H1 gel-incompetent ecDNA, respectively), the well-derived material had a drastically lower level of human read contamination (87% vs 0.02% of total unmapped reads for H1 genomic DNA and H1 gel-incompetent ecDNA, respectively, **Supplemental Table 1**). These results are likely due to 1) an equal contribution of bacterial products from reagents to each sample type and 2) electrophoretic depletion of degraded human DNA from the well DNA. After the removal of non-*Plasmodium* reads, >75% of the reads from both samples aligned to the *P. falciparum* genome and these reads represented a similar range of total A/T content (78.7 and 80.9%, **Supplemental Table 1**).

Reads from the amplified well-entrapped material covered the majority of the *P. falciparum* genome (**Supplemental Figure 5**, >90% of the genome was covered by >1 read). This result is not surprising given that 1) chromosomal sequence is detected in the loading well during the ddPCR assays (i.e. single copy genes on chromosome 7 and 11, **Figure 6**) and 2) whole genome amplification using multiple displacement amplification (MDA) is effective at amplifying very low amounts of DNA (Hosono et al., 2003; Wang et al., 2009). However, much less of

the genome is covered by higher levels of reads in the gel-incompetent ecDNA (**Supplemental Figure 5**, ~50% less of the genome is covered by 10-reads), which is either due to the biased nature of MDA amplification or the limited representation of the genome in the well. We detected an enrichment of the mitochondrial genome in the gel-incompetent material (>75-fold enrichment over the nuclear genome compared to ~30-fold enrichment in the genomic DNA sample, **Table 4**). Read-based enrichment of the mitochondrial genome in the loading well agrees with our ddPCR analysis (**Figure 7B**) and previous reported studies (Preiser et al., 1996).

When comparing the read coverage across the *dhodh* amplicon relative to that from the entire chromosome 6, we observed very high enrichment of the amplicon in the gel-incompetent material (a mean of ~170-fold, **Table 4**) and conservation of the amplicon boundaries with those from genomic DNA (**Figure 8**). Additionally, we discovered an A/T-rich (88.2%), 714bp sequence found specifically within the *dhodh* amplicon of the gel-incompetent ecDNA; this region is drastically over-enriched (**Figure 8** and **Supplemental Table 3**). We termed this the “super-peak” due to a maximum coverage of >36,000-fold and a mean coverage of >25,000-fold (**Figure 8** and **Supplemental Table 3**). The coverage of the full ~70kb *dhodh* amplicon including the super-peak is 604x (**Table 4**) and excluding the super-peak is 55x (**Table 4, see footnote**). Initially, we suspected that the extremely high coverage at this region is due to an artifact of the DNA amplification method; if we exclude this particular region, we estimated a similar number of *dhodh* amplicons as for ddPCR (~15 copies, **Table 4** and **Figure 6**).

**Table 4. Summary of coverage enrichment at known CNVs**

Samples	Chromosome 6 coverage			Mitochondrial genome coverage		Chromosome 5 coverage		
	Chr 6	<i>dhodh</i> amplicon	CN	<i>mt-cyb</i>	CN <sup>†</sup>	Chr 5	<i>mdr1</i> amplicon	CN
H1 genomic DNA	6.5x	79x	<b>12</b>	286.6x	32	8.6x	29x	<b>3</b>
H1 gel-incompetent DNA <sup>‡</sup>	3.6x	604x <sup>‡</sup>	<b>170<sup>§</sup></b>	683.5x	76	5x	14x	<b>3</b>

Samples were aligned to the WT1 (Dd2) reference genome using Geneious analysis (Geneious Prime 2019). CN, copy number (calculated by dividing mean coverage of the amplicon by the coverage of the remainder of the chromosome); *dhodh*, dihydroorotate dehydrogenase; published copies 8-10 (Guler et al., 2013); *mt-cyb*, mitochondrial *cytochrome b*; published copies 20-150 (Lane et al., 2018); *mdr1*, *multidrug resistance protein 1*, published copies 2-3 (Triglia et al., 1991). Chromosome (chr) 5 and 6 coverage is calculated as the mean across the chromosome, excluding amplified regions.

<sup>†</sup>Copy number of mitochondrial genome relative to nuclear genome.

<sup>‡</sup>This sample was isolated from the loading well of a PFGE gel and amplified using a DNA amplification kit to generate enough material for sequencing.

<sup>§</sup>This amplicon includes the super-peak region detailed in Supplemental Table 2. Without this region, the estimated CN is 15 copies.

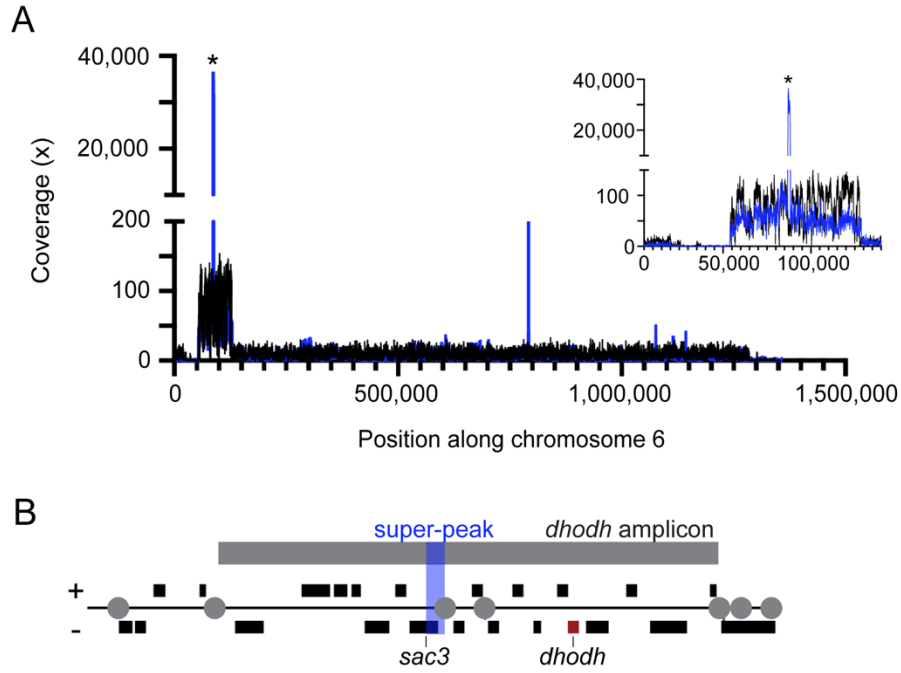


**Figure 8. Deep sequencing reveals conservation of amplicon boundaries and ecDNA-specific sequence.** **A.** Visualization of H1 genomic DNA (black line) compared to H1 gel-incompetent DNA (blue line) coverage using Integrative Genomics Viewer Software (IGV 2.4.10). Enrichment of a <1kb region partially spanning the *sac3* gene (PlasmODB ID: PF3D7\_0602600) is overrepresented at 36,636-fold (asterisk, termed super-peak). Samples were aligned to the WT1 (Dd2) reference genome. The inset (right) emphasizes the super-peak found within the *dhodh* amplicon and the shared amplicon boundaries. **B.** Schematic displaying relative gene locations (black boxes) and the super-peak location (blue shaded region) within the full *dhodh* amplicon (grey box, top) adapted from (Guler et al., 2013). H1, high level resistant clone; red box, *dhodh* gene, grey circles, location of long A/T tracks involved in CNV formation; black boxes, genes with +/- orientation.

Indeed, other small regions of the genome are over-amplified in the well-derived sample (**Figure 8A** and **Supplemental Table 3**), although not to the same extent (mean of ~240-fold). Analysis of discordant reads at this location revealed that copies of the amplified region that make up the super-peak are arranged in a tandem head-to-tail orientation (**Supplemental Table 4, Supplemental Figure 6A** and **C**). This result is similar to the known orientation of chromosomal copies of the *dhodh* amplicon ((Guler et al., 2013) (**Supplemental Figure 6D**)). However, we do not detect this pattern in other over-amplified regions (data not shown), likely because MDA tends to create chimeric reads or randomly connected sequences that occur due to template switching during high polymerase processivity (Lasken and Stockwell, 2007). Due to the extreme level of over-amplification and read orientation across this region, the super-peak is likely to represent a sequence that was present prior to WGA steps and therefore, may hold biological significance. A targeted analysis of this region in non-amplified sample is precluded by the high A/T content of this region (88.2%), which makes the design of specific PCR primers impractical.

Finally, in order to understand whether the ecDNA phenomena is restricted to the *dhodh* amplicon in H clones, we evaluated the level of other known copy number variations in the well-derived material. We observed similar enrichment levels between genomic DNA and gel-incompetent material for *mdr1* amplicons located on chromosome 5 (expected: 2-3-fold, (Triglia et al., 1991), observed: 3-fold for both sample types, **Table 4**). The *gch1* amplicon on chromosome 12, however, was drastically underrepresented in the gel-incompetent material and

overrepresented in the genomic DNA (expected: ~2-fold, (Tim J. C. Anderson et al., 2009; Guler et al., 2013), observed 6-and 0-fold, respectively, **Table 4**).

## 2.3 Discussion

We have identified ecDNA in DSM1 resistant *P. falciparum* parasites; this is the first observation of endogenously-derived ecDNA in any *Plasmodium* species generated after drug selection. By combining the physical separation of DNA elements directly from the parasite with sensitive DNA analysis methods (i.e. Southern blots and ddPCR), we revealed two different migration patterns: one ecDNA element readily entered the gel and another remained trapped in the loading well. Although detected separately, we predict that there is a single ecDNA element that becomes fragmented during electrophoresis to generate the two forms. This element, and its degradation products, are only detectable in highly DSM1 resistant parasites (**Supplemental Figure 1**) and they are confined to genes within the *dhodh* amplicon (**Figures 4, 5, 6, and 7**). This latter finding suggests that ecDNA is derived from the original chromosomal 6 location of the amplicon and thus, likely contributes to resistance. This contribution is bolstered by the additive effect between ecDNA and genomic copies in the highest level of resistance (**Figure 2, clones H1-H4**). Since we observed it in all of the H clones tested, including those from independent selections (**Figures 4, 5B, and Supplemental Figure 1 and 2**), ecDNA may also be *required* for high level resistance. Below, we summarize information on various characteristics of *P.*

*falciparum* ecDNA. Additionally, we discuss potential mechanisms for the generation of ecDNA in malaria as well as the implications of their role in malaria.

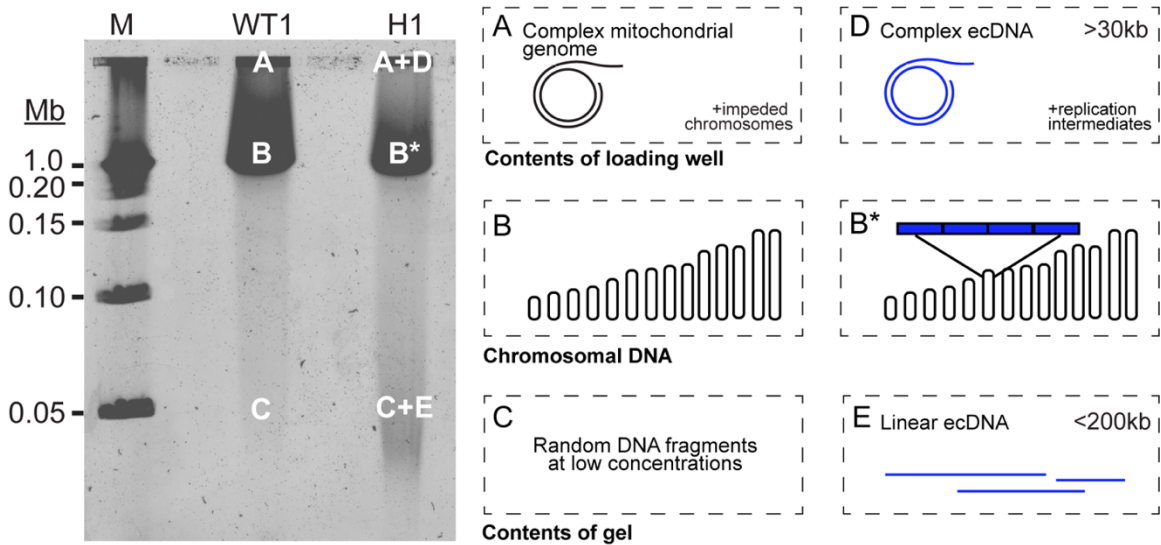


**Figure 9. Summary of DNA structures predicted by PFGE location and enzymatic analyses.** **A.** After PFGE electrophoresis, the loading well contains complex circular forms of the mitochondrial genome (Figure 6) and a small proportion of entrapped nuclear chromosomes and their replication intermediates. **B.** The prominent chromosomal band contains linear chromosomes 1-14. Under these PFGE conditions, individual chromosomes are not resolved (Figure 2B). **B\*.** For highly resistant clones, the size of chromosome 6 varies due to the presence of multiple *dhodh* amplicons (blue boxes) (Figure 2). **C.** The location of small nuclear DNA fragments by stochastic breakage from chromosomes by electrophoresis. **D.** In highly resistant parasites, the loading well contains complex circular forms of ecDNA along with accompanying replication intermediates (Figure 6), which may contain stretches of fragile linear DNA. **E.** Location of linear

ecDNA elements that break from complex circular forms. WT1, Dd2; H1, high level resistant clone.

*Gel-competent ecDNA.* We first observed the gel-competent ecDNA in H clones as a heterogenous smear of <200kb (**Figures 3B, 4A, 9C and E**). Since the boundaries of the smear vary depending on the PFGE conditions (compare **Figure 4A** to **Supplemental Figure 1**), it was difficult to assign an exact size range to this element. ddPCR analysis after purification from the PFGE 'smear' showed a high enrichment of the *dhodh* amplicon relative to a single copy gene on a different chromosome (106 copies to 1, **Figure 6**). We presume that smaller fragments of chromosomes break off during electrophoresis at a low rate, but exacerbated breakage from the large ecDNA element lead to the detection of higher levels of *dhodh* in this gel region (see *Relationship Between Two ecDNA Forms* below). By digesting this fragmented ecDNA form with enzymes, we gained information about its structure (**Figures 5 and 7**); gel-competent ecDNA was resistant to restriction digestion, which indicated either a: 1) supercoiled conformation, 2) single-stranded sequence, 3) a modification (*i.e.* methylated), or 4) tight association with a protein (*i.e.* histones or single-stranded binding proteins). The latter two possibilities were less likely because the BamHI restriction enzyme is not blocked by DNA methylation and we performed extensive detergent lysis and proteinase K digestions prior to PFGE analysis (see *Materials and Methods*). Furthermore, the high susceptibility to PS, which selectively digests linear DNA over circular elements, precluded a supercoiled circular structure. Therefore, we

conclude that gel-competent ecDNA is a linear, single-stranded DNA element (**Figure 9E**). Although we propose that this ecDNA form is not biologically relevant (i.e. it is an artifact of our separation method), cellular single-stranded ecDNA may impact gene expression (Dillon et al., 2015; Paulsen et al., 2019; Sun et al., 2019). Further investigations are required to determine its role in malaria.

*Gel-incompetent ecDNA.* We identified another form of ecDNA in H clones that is distinct from the gel-competent ecDNA described above. Instead of entering the gel, this ecDNA form remains in the PFGE loading well (**Figure 9D**). This phenomenon, termed 'entrapment', was previously described during PFGE analysis of large ( $\geq 30$ kb), circular or highly branched recombination intermediates from other species (Beverley, 1988; Gurrieri et al., 1999; Khan and Kuzminov, 2017, 2013; Turmel et al., 1990) (**Figure 9A**). In *P. falciparum*, some forms of the mitochondrial genome are also entrapped in the PFGE well (Preiser et al., 1996). Due to this characteristic, as well as its enrichment over the nuclear genome (Lane et al., 2018; Preiser et al., 1996; Vaidya and Arasu, 1987), we were able to use entrapped mitochondrial DNA as an internal control during our studies. When digesting well material with PS, we observed partial protection from enzyme degradation for both the mitochondrial genome (inferred by *cytochrome b* detection, **Figure 7B**) and gel-incompetent ecDNA (inferred by *dhodh* detection, **Figure 7D**). The conserved structure between the gel-incompetent ecDNA and the mitochondrial genome in this organism indicates that there may be conserved replication strategies to effectively generate high numbers of circular DNA elements.

*Relationship Between the Two ecDNA Forms.* Our studies show that both types of ecDNA are derived from the resistance amplicon and, therefore, they either share a common origin or one is generated from the other. Since linear DNA elements are not maintained in replicating parasites and transfection of *P. falciparum* is only possible with supercoiled, circular episomes (O'Donnell et al., 2001a; Donald H. Williamson et al., 2002; Wu et al., 1995), we propose that the linear ecDNA element is generated after breaking from the more complex gel-incompetent element (**Figure 9D and E**). In preparation for PFGE analysis, parasites are embedded within agarose without any DNA purification steps and therefore, DNA breakage occurs during electrophoresis steps. Given the parallels with the structure of the mitochondrial genome mentioned above, it is possible that the gel-incompetent ecDNA contains stretches of fragile single-stranded DNA. Random breakage across these regions to generate a heterogeneous mixture of sizes also explains the diffuse nature of the gel-competent elements (**Figures 3B, 4A, and 9E**).

*ecDNA Sequence.* A number of techniques, including deep sequencing, show that the gel-incompetent ecDNA element shares major homology with the amplicon on chromosome 6 (**Figures 4-8**). Additionally, the chromosomal amplicon and the enriched ecDNA amplicon show no detectable differences in their boundaries or orientation, indicating that the full 75kb *dhodh* amplicon is conserved on the ecDNA molecule (**Figure 8, Supplemental Table 4, and Supplemental Figure 6**). This result indicates that the amplified locus may be protected in a specified location in the nucleus or through epigenetic marks that

limit further recombination. On the other hand, these shared features add to the difficulty in purifying ecDNA away from the genome and the recognition of unique features.

Deep sequencing of this region did reveal one feature that was unique to ecDNA: a small highly A/T-rich region of the amplicon was greatly overrepresented in well-derived material (asterisk, **Figure 8B, 8C**, and **Table 7**, termed the super-peak).

This region encompassed a portion of the upstream UTR and 5' end of the gene for the SAC3 domain-containing protein (PlasmoDB gene ID: PF3D7\_0602600), which possess phosphoinositide phosphatase activities (Wengelnik et al., 2018). While it is possible that the super-peak is an artifact of the sample preparation (as introduced in the *Results*), we are confident of its biological importance due to the excessive overrepresentation of this region combined with the predicted head-to-tail orientation of the copies (**Supplemental Table 4 and Supplemental Figure 6**).

The high A/T-richness (~90%) and tandem arrangement of the super-peak sequence is reminiscent of *Plasmodium* replication origins and centromeres, which are both short A/T-rich repeats that are arranged in tandem (Agarwal et al., 2017; Gardner et al., 2002; Iwanaga et al., 2010; Matthews et al., 2018; Singh et al., 2003). Although, replication origins used by *Plasmodium* have not been extensively explored, 400-500bp intergenic sequences of >75% A/T-content can serve as replication initiation sites (Agarwal et al., 2017; Matthews et al., 2018). The average centromere in *Plasmodium* is 4-4.5kb in length containing a 2-2.5kb

A/T-rich repeat (Verma and Surolia, 2018). Perhaps the super-peak sequence serves as a binding scaffold to increase the translation rate of a nearby protein target (Davies et al., 2017), such as SAC3 itself or nearby DHODH.

Alternatively, this sequence may have a role in the maintenance of the ecDNA element. Past studies linked the stability of transfected episomes in malaria parasites with A/T-rich centromere-like elements, which increases the efficiency of mitotic segregation (Iwanaga et al., 2012, 2010; Verma and Surolia, 2018). It is conceivable that the super-peak sequence (<1kb and ~90% A/T-content) can function in a similar manner during segregation of ecDNA.

*ecDNA Generation.* Previous studies have defined two common mechanisms for ecDNA generation: replication-dependent or replication-independent. There is robust evidence linking ecDNA generation with replication errors such as polymerase stalling or replication fork stalling (Bzymek and Lovett, 2001; Coquelle et al., 1998; Dennin, 2018; Paulsen et al., 2018b; Schimke et al., 1986; Toledo et al., 1993; Varshavsky, 1981; Vogt et al., 2004; Wolfson et al., 1991). More recently, polymerase slippage at short repeats followed by a microdeletion at the chromosome have been implicated in ecDNA generation (Dillon et al., 2015); however, this mechanism appears to produce small single-stranded DNA of <400bp and is therefore not likely contributing to our large single-stranded ecDNA (**Figure 3B**). On the other hand, replication-independent mechanisms show the production of ecDNA through excision and ligation of chromosomal DNA irrespective of replication activities (Cohen, 2001; Cohen and Segal, 2009; Cohen and Lavi, 2009; Gresham et al., 2010; Hull et al., 2019;

Paulsen et al., 2018b). One outcome of replication independent generation is the loss of genetic material as ecDNA is formed through excision from the chromosome; one study found that it's the repetitive sequences are lost at the chromosomal location (Cohen and Lavi, 2009). To investigate this further, more work will be targeted to finding deletions.

While we cannot say for sure which of the above mechanisms is contributing to the generation of *Plasmodium* ecDNA, we propose a model that integrates our previous studies on chromosomal amplicons (Guler et al., 2013; Huckaby et al., 2019) with the current experimental validation of ecDNA structure (**Figure 10**). After the formation of amplicons (**Figure 10, Part 1**), large stretches of homology between the amplicons mediate recombination. This process can lead to the expansion of amplicons (as described in (Guler et al., 2013), **Figure 10, Part 1**), as well as the formation of ecDNA (as described here, **Figure 10, Part 2**). For the latter, excision of variable sized portions of the chromosome that contain few or multiple amplicons followed by ligation of the molecule produces a circular form. As mentioned above, the excision step is supported by evidence of deletion in this genomic region. Additionally, the circularization step is supported by the resistance of the gel-incompetent ecDNA form to nuclease degradation (**Figure 7E**).

While the paths to more amplicons or ecDNA may not be mutually exclusive, this stochastic model indicates that ecDNA may be generated more often than it can be detected. Although we have not been able to visually detect signs of ecDNA in parasites other than the highly resistant H1-4 clones (**Supplemental Figure 1**) or computationally detect the presence of amplicons at

lower levels in the genome (i.e. *mdr1*, **Table 3**), improved detection methods, including new efforts to computationally identify circular DNA from sequencing

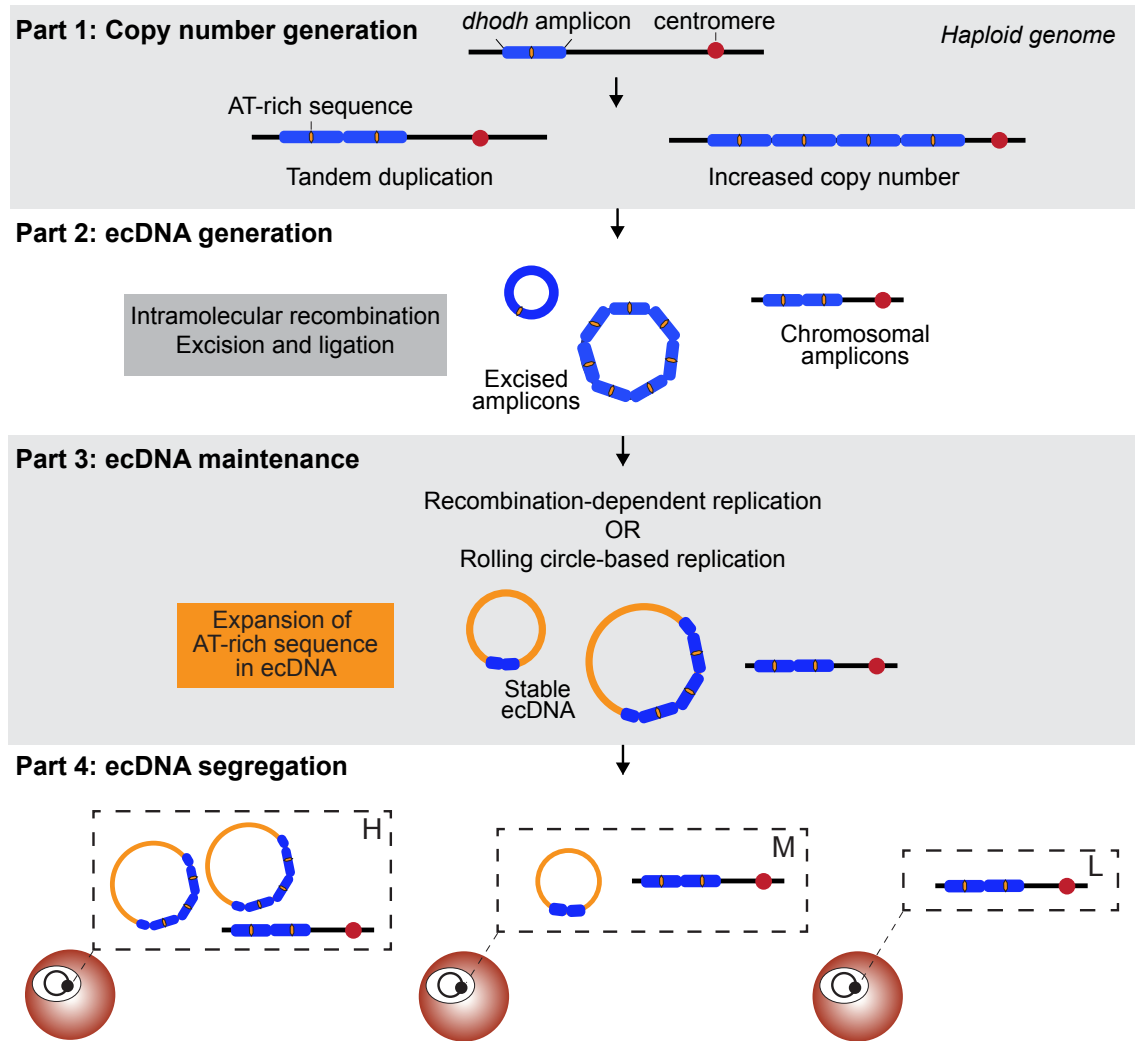


**Figure 10. A model of ecDNA generation and maintenance in *Plasmodium falciparum*.** **Part 1** summarizes the paths to generate few to many tandem *dhodh* amplicons on chromosome 6 (blue boxes) under drug selection. *Dhodh* amplicons do not contain known centromere sequences (red circle) but they do harbor a short, highly AT-rich sequence in the center of the amplicon that is expanded in ecDNA molecules (yellow region). **Part 2** illustrates the generation of ecDNA by

intramolecular recombination followed by excision and ligation. Based on previous studies and PFGE/ Southern, we predict that excised ecDNA can contain few or many amplicons (although higher numbers may facilitate segregation) and that some amplicon copies remain on chromosome 6 after excision. **Part 3** highlights proposed mechanisms of replication that may contribute to maintenance of ecDNA. We speculate that the expansion of the short, highly AT-rich sequence (yellow region, >35,000-fold enriched over other sequences, termed “super-peak”) may occur during replication. Additionally, this sequence constitutes large portions of the ecDNA molecule and may contribute to ecDNA stability through enhanced segregation or impact gene expression from the molecule. **Part 4.** The presence of ecDNA dictates the level of resistance achieved by the parasites (H, high level resistance; M, mid-level resistance; L, low level resistance). Unequal segregation of ecDNA into daughter parasites, even in a clonal parasite line, likely contributes to the growth phenotype observed in highly resistant parasites (Guler et al., 2013).

data, hold promise for future studies of malaria ecDNA (Deshpande et al., 2019; Prada-Luengo et al., 2019; Wu et al., 2019). Improved detection methods, including new efforts to computationally identify circular DNA from sequencing data are promising for future studies of malaria ecDNA (Deshpande et al., 2019; Prada-Luengo et al., 2019; Wu et al., 2019).

*ecDNA Maintenance.* In considering the maintenance of ecDNA, we once again draw on parallels with the mitochondrial genome. A recombination-dependent mechanism is responsible for the replication of the mitochondrial genome and maintenance of transfected episomes in *P. falciparum* (O'Donnell et al., 2001a; Preiser et al., 1996). A conserved mechanism may participate in the replication of ecDNA; on the other hand, D-loop and/or rolling circle replication, as used for the *P. falciparum* apicoplast genome (Milton and Nelson, 2016; D. H. Williamson et al., 2002), may be acting on ecDNA. Either process would explain two prominent characteristics of *P. falciparum* ecDNA: 1) the entrapment in PFGE gels due to the formation of massive complexes of single- and double-stranded DNA (Viret et al., 1991) and 2) the heterogeneity of the smear due to the creation of varying lengths of linear tails during active replication (O'Donnell et al., 2001a). Furthermore, the complex non-linear nature of replication intermediates would confer partial susceptibility to PS and the creation of single-stranded DNA would confer resistance to restriction enzymes. For these reasons, we propose that these pathways are also involved in replication of ecDNA (see **Figure 10, Part 3**).

Once replicated, ecDNA must be segregated during cell division so that daughter cells can maintain their selective advantage. Although ecDNA shares close identity to a region of chromosome 6 (position 61,619-158,072 (Guler et al., 2013)), this region does not contain a centromere (predicted position at 477,751-482,751 (Hoeijmakers et al., 2012)). Other possibilities for segregation include: 1) direct tethering as has been reported in other organisms (Guler et al., 2013; Kanda et al., 2007; Kanda and Wahl, 2000; Sau et al., 2019), 2) hitchhiking due to its large size as has been observed for *P. falciparum* episomes (O'Donnell et al., 2001b), and 3) use of repetitive regions as pseudo-centromeres, as we suggest above for the super-peak (see *ecDNA Sequence* above). In all of these cases, unequal segregation is likely (**Figure 10, Part 4**). This characteristic could contribute to the growth phenotype observed for H clones (Guler et al., 2013); only the proportion of parasites that receive enough ecDNA survive in the highest levels of the antimalarial.

*Implications of ecDNA in malaria.* In light of the identification of ecDNA in highly DSM1 resistant parasites, it is important to consider whether ecDNA generation could contribute to resistance in other antimalarial contexts. Due to its effect on DNA synthesis, DSM1 inhibits likely causes replicative stress, which could trigger pathways that drive copy number variations and/or ecDNA generation (as in (Arlt et al., 2009, 2009; Bindra et al., 2004)). However, copy number variations are not specific to this drug resistance model; amplicons are observed in parasites resistant to a range of antimalarials with a number of cellular targets (Tim J.C. Anderson et al., 2009; Cheeseman et al., 2009; Cowman et al., 1994;

Foote et al., 1990; Kidgell et al., 2006; Nair et al., 2008a, 2008b; Triglia et al., 1991; Wilson et al., 1989). Therefore, we speculate that ecDNA would be present in these cases as well but perhaps harder to detect. EcDNA abundance, strength of selection, as well as the methods employed (single cell verses population-based), will certainly affect the detection of this DNA element in other contexts.

## 2.4 Materials and methods

### 2.4.1 DSM1 and parasite clones.

DSM1 is a triazolopyrimidine that specifically and potently inhibits the *P. falciparum* dihydroorotate dehydrogenase enzyme of pyrimidine biosynthesis (Phillips et al., 2008) DSM1 resistant parasites were previously selected according to the scheme depicted in (**Figure 2**) (Guler et al., 2013). For this manuscript, we simplified the naming scheme to represent low, medium, and high levels of resistance (**Figure 2**).

### 2.4.2 Parasite culture.

*P. falciparum* parasites were grown *in vitro* at 37°C in solutions of 2-3% hematocrit (serotype A positive human erythrocytes) in RPMI 1640 (Invitrogen, Waltham, Massachusetts, USA) medium containing 28mM NaHCO<sub>3</sub> and 25mM HEPES, and supplemented with 20% human type A positive heat-inactivated plasma in sterile, sealed flasks, flushed with 5% O<sub>2</sub>, 5% CO<sub>2</sub>, and 90% N<sub>2</sub> (Haynes et al., 1976; Rathod et al., 1992; Trager and Jensen, 1976). Cultures were maintained with media changes 3 times each week and sub-cultured as necessary to maintain parasitemia below 5%.

#### 2.4.3 Pulse field gel electrophoresis (PFGE).

Parasites embedded in agarose plugs for PFGE electrophoresis were made from synchronized trophozoite-schizont *P. falciparum* parasites according to previous protocols (Hernandez-Rivas and Scherf, 1997). Briefly, erythrocytes were lysed with 0.15% saponin (Acros Organic™, Thermo Fisher Scientific, Waltham, MA, USA), parasites were washed in sterile phosphate buffered saline, and  $5 \times 10^8$  parasites/mL were resuspended in 1.6% certified low melting point agarose (Bio-Rad Laboratories Inc., Hercules, MA, USA) at 37°C ( $2.5 \times 10^8$  parasites/mL final). 100µl aliquots were cooled in plug molds before transferring to cell lysis buffer (10mM Tris-HCl pH 8, 0.5M EDTA, 1% sodium lauryl sarcosinate) for storage. To eliminate parasite proteins prior to PFGE analysis, parasite plugs were incubated with 2mg/ml proteinase K (Thermo Fisher Scientific) in cell lysis buffer at 37°C for two 24hrs incubations (with a buffer replacement between each). Plugs were loaded into the well of 1% pulse field-certified gel in 0.5X Tris/Boric acid/EDTA buffer (Bio-Rad Laboratories, Inc.) and run at 14°C on the PFGE-DR system with PFGE DNA standards (Bio-Rad Laboratories, Inc.) at various conditions (see figure legends for marker information and running conditions for each gel). Completed gels were stained with either ethidium bromide (1µg/ml, Bio-Rad Laboratories, Inc.), SYBR Safe DNA Gel Stain (1:10,000, Life Technologies, Carlsbad, CA, USA) or SYBR Gold Nucleic Acid Gel Stain (1:10,000, Invitrogen, Carlsbad, CA, USA). Gels were visualized using either UV transillumination, Typhoon 9410 Variable Mode Imager (SYBR settings: fluorescence, Laser: blue

(488nm), Emission filter: 520BP40), or Gel Doc XR+ Gel Documentation (Bio-Rad Laboratories, Inc.).

#### *2.4.4 DNA transfer, probe labeling and Southern blot analysis.*

Following PFGE, ethidium bromide-stained DNA embedded within the gels was nicked by UV treatment (60mJ/ 600 x 100µJ on a short wave/ 254nm UV transilluminator). Gels were soaked in 0.4N NaOH/ 1.5M NaCl for 15min prior to 24-48hrs alkaline transfer to nylon (Zeta-Probe membrane, BioRad). Membranes were rinsed in 2x saline sodium citrate and dried before probing. Candidate probe sequences were amplified from the WT1 *P. falciparum* genome using primers listed in (**Table 1**). The PCR protocol was 94°C for 3min, followed by 30 rounds of 94°C for 30sec, 55°C for 1.5min, and 68°C for 1.5min and an extension step of 68°C for 5min. PCR products were cloned into TOPO-TA (Life Technologies) and confirmed by Illumina sequencing. Confirmed probes were labeled with digoxigenin (DIG): dNTP (1:6-1:9) using the PCR DIG Probe Synthesis Kit (Roche Applied Science, Indianapolis, IN, USA) at the cycling conditions listed above.

For Southern blotting, membranes were pre-hybridized in DIG Easy Hyb™ (Roche Applied Science) for 30min at 42°C. Probes were denatured for 5min at 95°C and immediately chilled in ice water prior to being added to pre-warmed hybridization buffer at a concentration of 500-800ng/mL. Following an 18-24hrs incubation at 42°C, probed membranes were washed twice for 5min in 2X SSC/ 0.1% SDS at room temperature and then twice more for 15min in 0.5X SSC/ 0.1% SDS at 50°C. DIG-labeled probe was detected on the membrane using the DIG Luminescent Detection Kit (Roche Applied Science) according to the

manufacturer's instructions. Membranes were exposed to film and developed to visualize probe pattern. Prior to re-probing, membranes were stripped twice for 15min in 0.2M NaOH/ 0.1% SDS at 37°C and washed for 5min in 2xSSC.

#### *2.4.5 Restriction digestion prior to Southern blot analysis.*

Restriction sites were predicted from the WT2 reference genome, but confirmed in sequencing reads from WT1, L1, and L2 clones generated during a previous study (**Figure 2**) (Guler et al., 2013). Restriction digest of parasite plugs was performed as previously described (Hernandez-Rivas and Scherf, 1997). Briefly, plugs were washed three times in TE buffer (10mM Tris-HCl pH8, 1mM EDTA), treated with 1mM phenylmethanesulfonylfluoride (Sigma-Aldrich, St. Louis, MO, USA ) for 2hrs at room temperature to inactivate proteinase K (Thermo Fisher Scientific), and washed three additional times in TE for 30min. Plugs were then equilibrated in restriction endonuclease buffer (with bovine serum albumin) prior to incubation with 200U/mL of enzyme (BamHI and/or NheI, New England Biolabs) at 37°C for 18hrs. Digestion was stopped by adding 50mM EDTA prior to running on PFGE, transferring, and probing as above.

#### *2.4.6 Standard DNA isolation.*

Genomic DNA (gDNA) and other sources of DNA (see below) were purified for prior to ddPCR as done previously (Guler et al., 2013). Briefly, parasites were lysed with 0.1% L-loril sarkosil (Teknova) in the presence of 200µg/mL proteinase K (Thermo Fisher Scientific) overnight at 37°C. Nucleic acids were then extracted with phenol/chloroform/isoamyl alcohol (25:24:1), pH 7.8-8.1 (Invitrogen, Waltham, MA, USA) using Phase Lock Gel, Light tubes (5 Prime Theaetetus Inc, San

Francisco, CA, USA). Following RNA digestion with 100µg/ml RNase A (Thermo Fisher Scientific) for 1hr at 37°C, gDNA was extracted twice more as above, once with chloroform, and, then ethanol precipitated using standard methods. DNA quantitation was performed using the Qubit double-stranded DNA High Sensitivity kit per the manufacturer's instructions (Thermo Fisher Scientific).

#### *2.4.7 DNA isolation from agarose gels.*

Regions of the gel with target DNA were excised from the PFGE agarose gels using a sterile razor and purified using a modified "freeze and squeeze" method (Thuring et al., 1975). The agarose block was placed in a sterile microcentrifuge tube with 500µl of nuclease-free water. Samples were heated for 65°C for 20min and transferred to a -80°C freezer. Following an overnight incubation, the samples were thawed at room temperature and centrifuged for 30min at 20°C at 17,000xg (instead of physically squeezing the gel between thumb and index finger, as performed in the original protocol). The supernatant was transferred to a new tube and DNA was purified using phenol/chloroform/isoamyl alcohol (Invitrogen) followed by ethanol using standard methods (see *Standard DNA Isolation* above). Purified DNA was quantified before use in downstream analyses by Qubit DNA quantitation (Qubit Fluorometer, Thermo Fisher Scientific, see **section** on Genomic DNA Purification).

#### *2.4.8 Droplet digital PCR and analysis.*

Droplet digital (dd)PCR was used to investigate the success of ecDNA purification. The PCR step was performed using QX200™ EvaGreen® ddPCR™ Supermix (Bio-Rad Laboratories, Inc.) or ddPCR probe Supermix (Bio-Rad Laboratories,

Inc.) with 5pg- 1ng of DNA. The EvaGreen® assays used 75-150nM multiplexed primers (a single copy reference gene was run in the same reaction as the multi-copy gene by varying the primer concentrations (McDermott et al., 2013; Miotke et al., 2014)) (**Table 1**). The PCR protocol for EvaGreen® assays was 95°C for 10min, followed by 39 rounds of 94°C for 30sec and 60°C for 1min, 4°C for 5min and 90°C for 5min. The TaqMan probe assay used 600nM for VIC probes and 900nM for FAM probes (final) multiplexed primers combined with a 50µM (final) probe (McDermott et al., 2013; Miotke et al., 2014) (**Table 1**). The reactions also contained one of the following detection probes: *Cytochrome b* probe 56-FAM/AAGAGAATTATGGAGTGGATGGTGT/3MGBEc, *Dihydroorotate dehydrogenase* (*dhodh*) probe 5'-56-FAM/CATTATTGCATCAGGAGGGA/3MGBEc-3', *heat shock protein 70 (hsp70)*, and *seryl tRNA synthetase* probe-5'-5HEX/ACATGAAGAAATGATACAAACA/3MGBEc-3'. The PCR protocol for probe-based was 95°C for 10min, followed by 40 rounds if 95°C for 30sec and 60°C for 1min. *Seryl tRNA synthetase* and *heat shock protein 70* and served as a single copy reference gene 2 and 3, respectively; *Cytochrome b* and *dihydroorotate dehydrogenase* served as multicopy genes (**Table 1**). Droplet generation (prior to PCR cycling) and fluorescence readings (post-PCR cycling) were performed per the manufacturer's instructions. The majority of samples measured fluorescence from a minimum of 8000 droplets, although droplet counts below this were allowed for crude lysate material or digestion analysis. The ratio of positive droplets containing an amplified gene (*dhodh*, *D* or *cytochrome b*, *C*)

versus a single-copy gene (*seryl tRNA synthetase, S or hsp70, H*) was calculated by Quantasoft (BioRad Laboratories, Inc., D:S, C:S, or C:H ratio) and averaged between replicates. Poisson confidence intervals were provided by the software and the extreme values were reported (*i.e.* min and max across all experiments).

#### *2.4.9 Digestion of linear DNA with Plasmid Safe ATP-dependent DNase.*

To increase the efficiency of linear DNA degradation, samples were first treated with a double restriction digest using NheI (10,000 units/mL, New England Biolabs Inc.) and NdeI (10,000units/ mL, New England Biolabs Inc.) at 37°C for 30min to expose more free ends and to shorten linear DNA fragments. To remove residual protein and restriction buffer, samples were purified post-digestion using phenol/chloroform/isoamyl alcohol (Invitrogen) followed by ethanol using standard methods (see *Standard DNA Isolation* above). Purified samples were then treated with 1 unit of Plasmid safe ATP-dependent DNase (Epicentre Technologies Corp., Madison, WI, USA) per 10µl reaction for 30min at 37°C, followed by an inactivation step at 70°C for 30min according to the manufacturer's instruction. Samples were evaluated by ddPCR for Plasmid Safe activity.

#### *2.4.10 DNA amplification, Illumina sequencing, and analysis.*

To reach an optimal concentration for sequencing (>10ng), we purified DNA from the PFGE loading well and we amplified the DNA first using the Repli-g Mini Kit (Qiagen). Repli-g was chosen as a strategy to achieve multiple displacement amplification (MDA), which is a common strategy for extra-chromosomal DNA studies (Jørgensen et al., 2015). The following components were added per 50µl reaction: 5µl of template DNA (<10ng), 5µl of denaturation buffer, 10µl of

neuralization buffer, and a 30µl reaction mix (of 1µl of Repli-g Phi 29 polymerase and 29µl of Repli-g Mini reaction buffer) per manufacturer's instructions. Samples were then incubated at 30°C for 16-18hrs and, then, heat inactivated at 65°C for 3min. Genomic DNA from wild type and highly resistant parasites was purified as described above (see *Standard DNA Isolation* above). Prior to sequencing, *dhodh* amplicon in the range of 7 to 10 was confirmed using ddPCR. Also, no DNA amplification (ie MDA methodology) and no enzymatic digestions was performed on genomic DNA used in these studies. In preparation for Illumina sequencing, all DNA samples were sonicated in 50 µl screw cap tubes (microtube-50, Covaris Inc.) using the Covaris M220 Focused Ultrasonicator (Covaris, Inc, Woburn, Massachusetts, USA). Specific settings achieved an average fragment size of 300bp (Duty cycle: 10%, Intensity: 4.5, Cycles per burst: 200, Time: 120sec), as assessed using the Agilent High Sensitivity DNA 1000 Kit on an Agilent 2100 Bioanalyzer (Agilent Biotechnologies, Santa Clara, CA, USA). Fragmented samples were prepared for sequencing using the NEBNEXT® Ultra™ II DNA Library Prep Kit (NEB, Inc.) for the Illumina MiSeq platform with paired end reads (2x150bp). After library construction, DNA size and concentration were assessed again using an Agilent 2100 Bioanalyzer (Agilent Biotechnologies).

First, we used a pairwise alignment to a WT1 (Dd2) reference genome (PlasmoDB release 20190829) using the Geneious® and Integrative Genomics Viewer (IGV 2.4.10) Software. % mapped reads to reference genome, Q score, average read length, and depth of coverage was used to evaluate reads and the alignment. We removed contaminants using Geneious® paired with BLAST searches. In parallel,

BBtools (38.33) and FastQC (Version 0.11.8, <http://www.bioinformatics.babraham.ac.uk/projects/fastqc/>) was also used to evaluate reads in the same manner. We used BBtools to trim adapter sequences and low-quality reads. Remaining unmapped reads that did not align to the *Plasmodium falciparum* Dd2 genome, was then blasted (NCBI database) to determine % contamination with sequences that aligned to other organisms using Geneious®. After evaluation, human and bacterial read contamination were removed by aligning the reads to the human hg19 and top 3 bacterial genomes from BLAST using BMAP (version 38.33, <https://sourceforge.net/projects/bbmap/>). Unmapped reads from this step were used for alignment and CNV analysis. BBmap alignment options included a minimum of 95% identity, max indels of 3, a minimum of two seed hits, and quick match and fast modes enabled. An example command is as follows: `bbmap.sh minid=0.95 maxindel=3 bwr=0.16 bw=12 quickmatch fast minhits=2 path=/path/to/masked/genome -Xmx32g in=input.fastq.gz outu=reads_of_interest.unmapped.fastq.gz outm=contaminating_reads.fastq.gz` (Huckaby et al., 2019).

Two algorithms, CNVnator, which call CNVs using read-depth, and LUMPY, which calls CNVs using discordant reads, was used to further evaluate copy number variations after BWA-MEM was used to align reads with default settings to the Dd2 genome (PlasmoDB release 32). QualiMap 2 was also used to evaluate the quality of reads and the number of reads that aligned to the *Plasmodium* genome (see **Supplemental Table 1**). The LUMPY algorithm offered location of CNV, length of

CNV, and pieces of support its calling, paired ends, and split reads (see **Supplemental Table 4**). The CNVnator algorithm offered location of CNV and an estimation of copy number using 1000bp bins to calculate read depth (see **Supplemental Table 4**). Methods for these algorithms were followed and previously reported in (Huckaby et al., 2019). Lastly, to determine the orientation of the amplicon (tandem or reverse tandem duplication) discordant reads were visually inspected at the breakpoints using IGV 2.4.10 (**Supplemental Figure 6**).

### Supplemental Table 1. Summary of sequencing results

Samples	Q score (mean)	Insert size (mean bp)	% A/T	Total reads	% Mapped to <i>P. falciparum</i> genome <sup>†</sup>	% Unmapped reads that align to bacterial genomes	% Unmapped reads that align to the human genome	% of genome covered by >1 read
H1 genomic DNA	36.4	144.5	78.7	1,559,730	95.9	18	87	91
H1 gel-incompetent DNA <sup>‡</sup>	36.3	142.2	80.9	1,198,484	96.4	21	0.02	90

Sequencing reads were mapped to the WT1 (Dd2) reference genome (PlasmoDB release 20190829) using two independent algorithms; the Geneious alignment algorithm (Geneious Prime 2019) and BMAP alignment algorithm (version 38.33) produced similar results for contaminating bacterial and human genomes (Geneious results are presented here). <sup>†</sup>Reads were mapped to the *P. falciparum* genome following removal of contaminating reads. <sup>‡</sup>This sample was isolated from the PFGE well and amplified using multiple displacement amplification in order to generate enough material for sequencing. % genome covered by >1 read was determined using Qualimap 2.2.1.

**Supplemental Table 2. Summary of coverage enrichment at chromosome 6 amplicon**

Samples	Chromosome 6 Coverage			Chr. 6 % A/T <sup>‡</sup>
	Minus <i>dhodh</i> amplicon	Super-peak only <sup>†</sup>	Estimated CN	
H1 genomic DNA	6.5x	42x	6.5 <sup>§</sup>	79.1
H1 gel- incompetent DNA <sup>†</sup>	3.6x	25,641x	7,223	85.8

Geneious analysis (Geneious Prime 2019) of super-peak inclusion and exclusion is presented. The super-peak is defined by location 86,429-87,143bp (-) (aligned to the WT1(Dd2) genome) on chromosome 6, which is also found within the *dhodh* amplicon. This specific 714bp region covers an intergenic region and as well as part of a genic region corresponding to the *sac3 domain-containing, putative protein*, (PF3D7\_0602600). <sup>†</sup>This sample was isolated from the loading well of a PFGE gel and amplified using a DNA amplification kit to generate enough material for sequencing. <sup>‡</sup>For comparison, the H1 super-peak A/T content is 88.2%. CN, copy number; *dhodh*, *dihydroorotate dehydrogenase*. <sup>§</sup>This region is underrepresented compared to the CN of 12 for the *dhodh* amplicon.

**Supplemental Table 3. Summary of highly enriched chromosomal locations from H1 gel-incompetent DNA sample**

Chromosome	Location	Size (bp)	Max Coverage	Mean Coverage
1	32,130-37,106	4,985	151	150.4
	99,965-100,377	413	150	150
	241,037-242,089	1,054	151	150.7
	418,189-418,437	249	151	150.8
6	<b>86,429-87,143</b>	<b>714</b>	<b>36,636</b>	<b>25,641</b>
	788,760-789,239	482	232	174.2
9	2,794-6,432	3,653	151	146.7
	166,841-171,721	4,906	151	142.8
	244,334-244,610	297	118	61.6
	556,692-557,096	415	72	48.2
	2,794-6,432	3,653	151	146.7
	166,841-171,721	4,906	151	142.8
10	192,663-194,034	1,374	151	151
	345,325-345,715	508	1499	1048.9
11	1,489,486-1,489,770	286	127	81.3
12	589,733-590,245	557	131	74.7
	1,047,359-1,047,727	432	2013	1238
	1284219-1,284,726	526	115	76.9
13	1,643,674-1,644,457	802	157	122.5
	2,293,426-2,293,693	268	243	143.5
14	426,901-427,229	334	665	377.8

---

Mean (minus super-peak)	1,505	336.5	238.975
-------------------------	-------	-------	---------

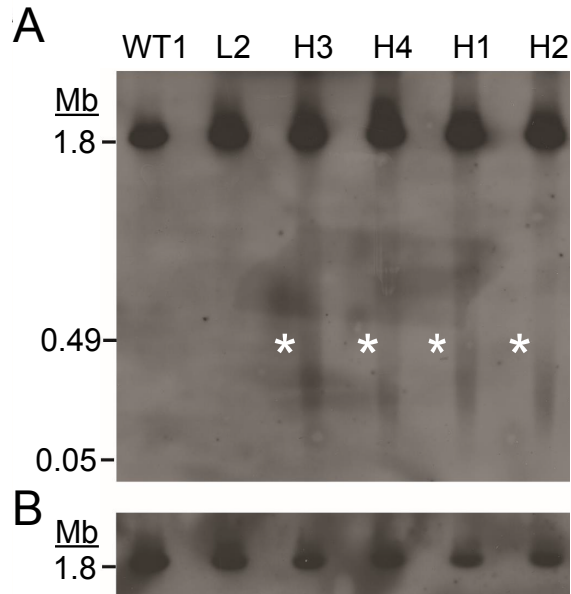
---

The *dhodh* amplified region termed super-peak is bolded. Highly enriched locations are defined as coverage regions above the respective chromosome coverage (mean of 5.5X coverage across the whole genome).

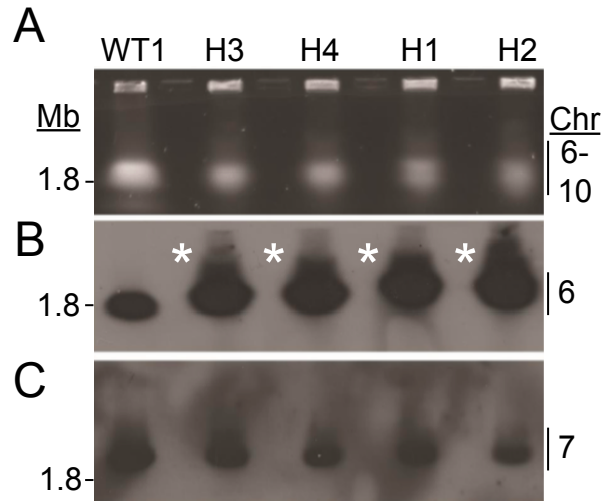
**Supplemental Table 4. Summary of LUMPY and CNVnator algorithm analysis**

Clone	Chr	ID	Orientation of amplicon	LUMPY pieces of support/ paired end/ split read	LUMPY start site (bp)	LUMPY end site (bp)	CN number (CNVnator)
H1 gDNA	6	DHODH amplicon	Tandem	34;23;11	53,835	127,352	8.5
H1 gDNA	6	SAC3 domain containing protein, putative	Tandem	4;1;3	86,429	87,143	N.D.
H1 gel-incompetent	6	DHODH amplicon	Tandem	32; 25; 7	53,835	127,352	N.D.
H1 gel-incompetent	6	SAC3 domain containing protein, putative	Tandem	22,341; 7,947; 14,394	86,429	87,143	N.D.

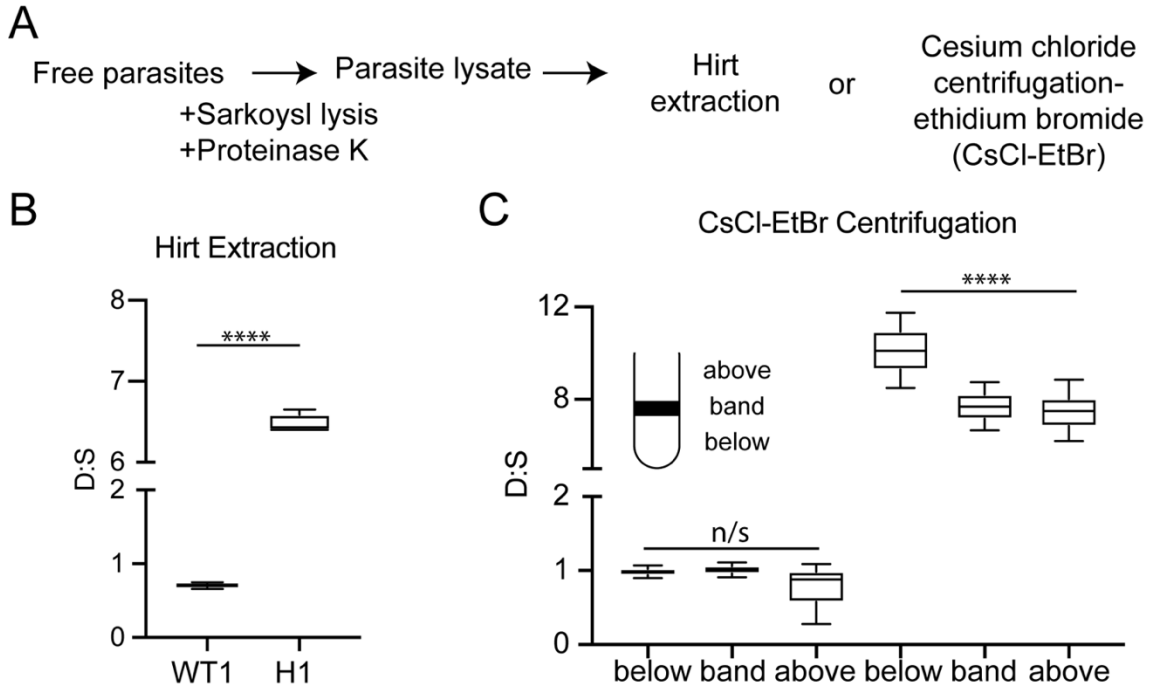
LUMPY and CNVnator are algorithms used to call copy number variations and breakpoint locations (Layer et al., 2014 and Abyoz et al., 2011). CNVnator was unable to call read depth analysis but visual inspection of bam file showed an increase in coverage indicating the presence of copy number variations. N.D., not determined.



**Supplemental Figure 1. Southern blot analysis of additional DSM1 resistant clones all harbor ecDNA with the *dhodh* gene.** **A.** Southern blot hybridized with *dhodh* amplicon probe (Table 1). Exposure time: 11.5hr. White asterisks, putative ecDNA. **B.** Southern blot hybridized with single copy reference gene 2 (Table 1). Exposure time: 16.5hr. The expected size of WT1 chromosome is 1.5Mb (PlasmoDB (Aurrecochea et al., 2009)). DNA size was determined with 0.05-1Mb and 5-120kb markers (BioRad 170- 3635 and 170-3624). DNA source: parasite agarose plugs made from wild type (WT1), low level resistant clone (L2), and high level resistant clones (H1-H4). CHEF running conditions: 17hr, 6V/cm, 1-10sec switch rate. *dhodh*, dihydroorotate dehydrogenase; WT1, Dd2.

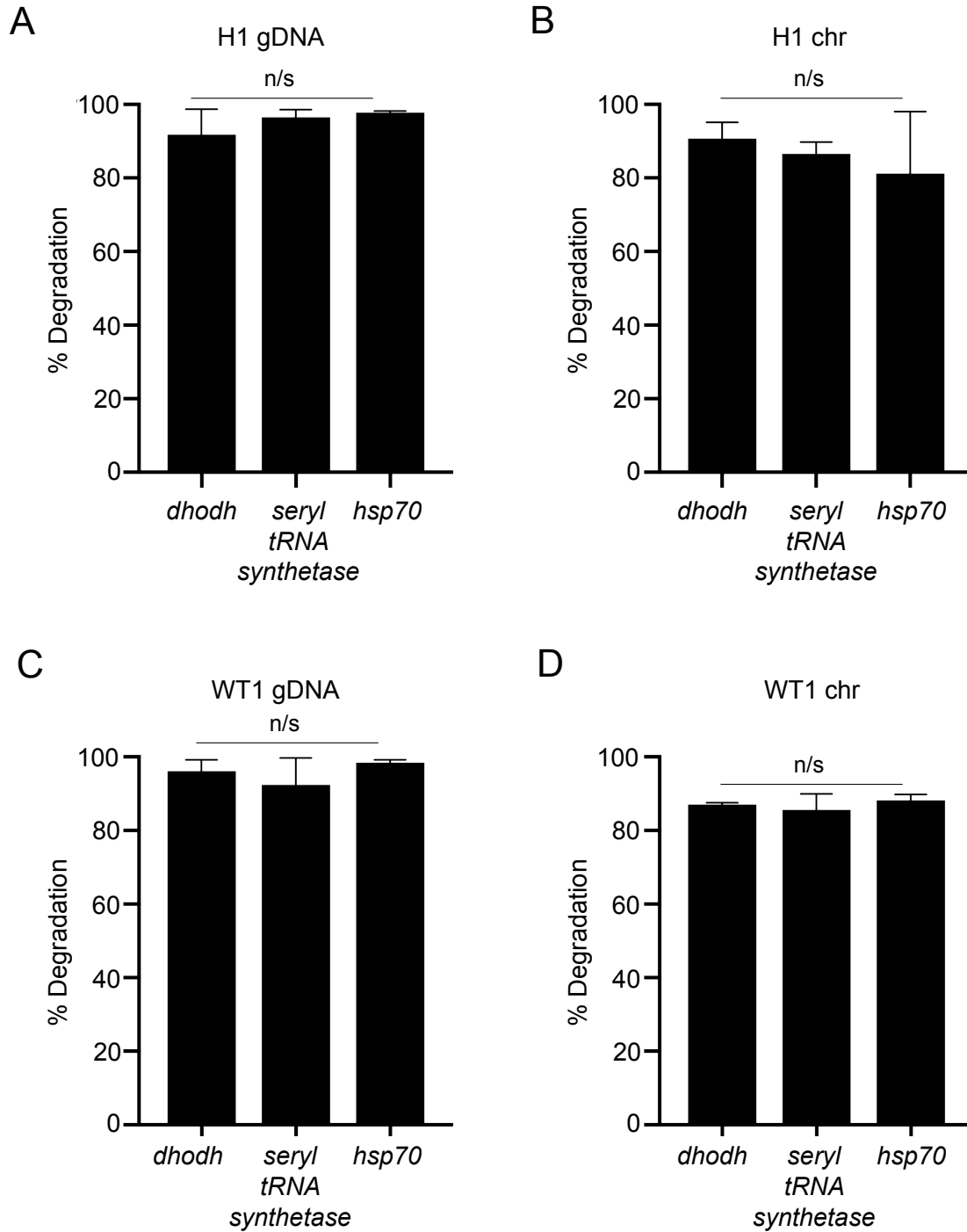


**Supplemental Figure 2. Identification of slow-migrating material using an alternative agarose type during PFGE harbors the *dhodh* gene.** Only the top portion of the gel including the well and larger chromosomes are displayed. **A.** A PFGE gel stained with 1 $\mu$ g/mL ethidium bromide. Chromosomes 6-10 has co-migrated at chosen electrophoresis parameters. **B.** Southern blot hybridized with *dhodh* amplicon probe (Table 1). Exposure time: 6hr. White asterisks, putative slow-migrating extra-chromosomal amplicons restricted to resistant parasites (H3, H4, H1, and H2). **C.** Southern blot hybridized with single copy reference gene 2 (Table 1) absent of high molecular weight DNA element. Exposure time: 16hr. DNA source: parasite agarose plugs made from wild type (WT1) and high level resistant clones (H1-H4 clones). Type of agarose used: 1% pulse field certified agarose (instead of megabase-certified agarose compare to Figure 3. PFGE running conditions: 24hr, 6V/cm, 60-90sec switch rate. WT1, Dd2.



**Supplemental Figure 3. Alternative methods for the purification of ecDNA in highly resistant DSM1-resistant parasites.** *Note: These methods were considered unsuccessful at enriching DNA because we did not detect enrichment levels beyond what is expected from chromosomal amplicons.* **A.** Experimental scheme for the isolation of ecDNA. Parasites were isolated from red blood cells and then treated with a detergent and Proteinase K to release DNA in a 24hr incubation. Parasite lysate was subjected to Hirt Extraction, when DNA is purified using sodium dodecyl sulfate (SDS) and high concentration of salts, or CsCl centrifugation, when DNA is purified using isopycnic separation. **B** and **C.** Box and whisker plots depicting D:S ratio (dhodh: seryl tRNA synthetase) measured using ddPCR. Both isolation methods produced reproducible results that matched chromosomal estimates (Guler et al. 2013). n=6. **C.** Cesium chloride-ethidium bromide centrifugation of WT1 and H1 parasites produced a single visible band. The below band, band, and above band fractions (inset) were isolated, purified,

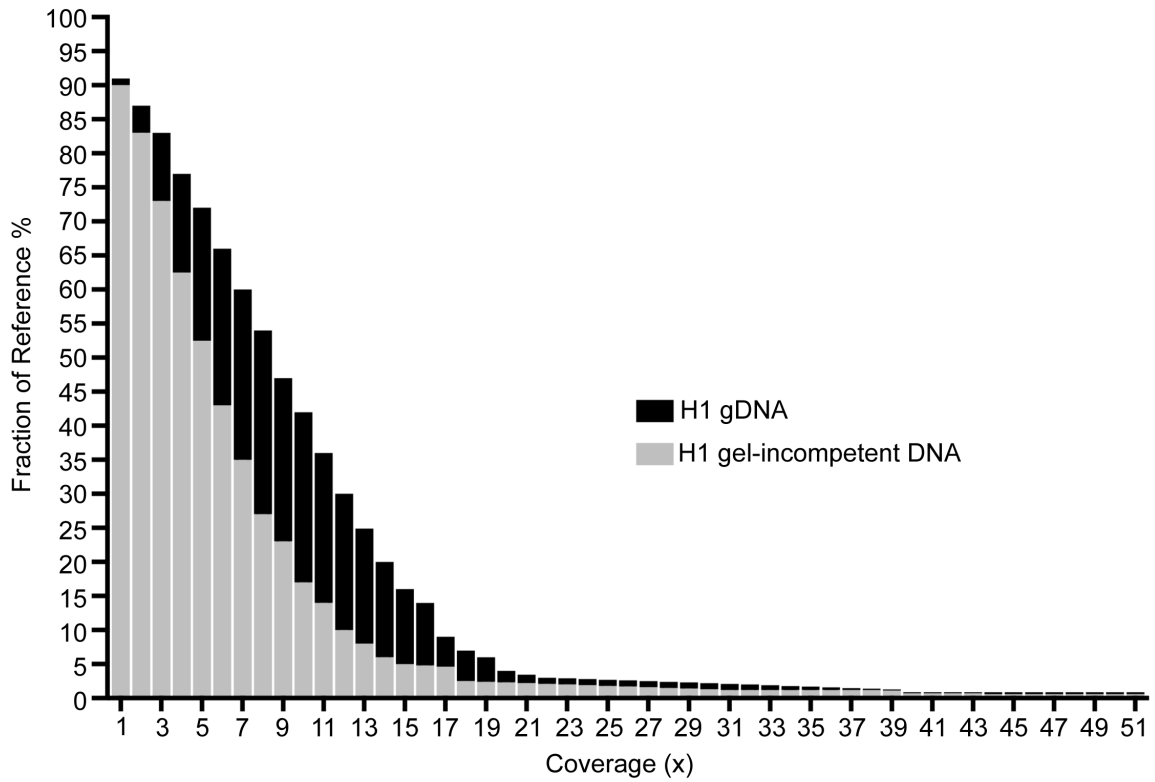
and measured. WT1, wild type 1, Dd2; H1, high level resistant clone; ddPCR, droplet digital PCR. Error bars represent Poisson confidence intervals (upper hinge, 75th percentile; lower hinge, 25th percentile). \*\*\*\*,  $p < 0.0001$ ; n/s, not significant.



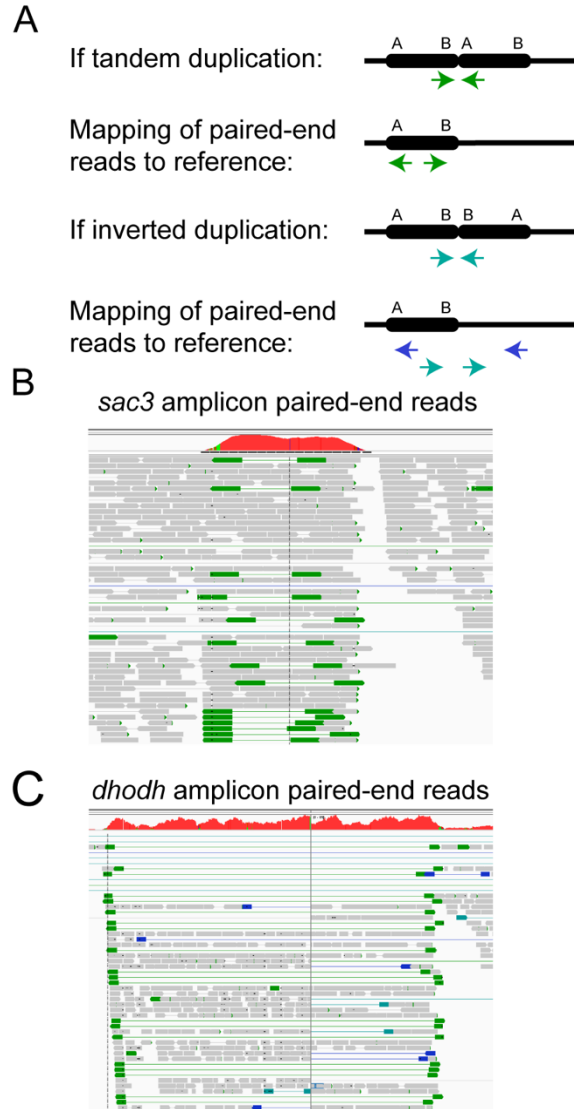
**Supplemental Figure 4. Plasmid Safe (PS) ATP-dependent DNase did not exhibit loci preference.** No significant differences after PS digestion were observed at 3 different loci across the parasite genome. DNA samples were either extracted directly from red blood cells as genomic DNA (gDNA, **A** and **C**) or extracted from the chromosomal region of PFGE agarose gels (**B** and **D**). The

percent of DNA degradation is calculated by dividing positive droplet counts after digestion as measured by ddPCR by the number of positive droplets before digestion then multiplying by 100. Each sample is probed for a multicopy gene (*dhodh*) and a single copy gene (*hsp70* or *seryl tRNA synthetase*) to determine enzyme susceptibility. gDNA, genomic DNA; chr, chromosome; *dhodh*, *dihydroorotate dehydrogenase*, chromosome 6; *seryl tRNA synthetase*, chromosome 7, and *hsp70*, chromosome 11; WT1, wild type 1, Dd2; H1, high level resistant clone; n=3.

### Genome Fraction Coverage



**Supplemental Figure 5. Histogram of sequencing coverage of H1 genomic(g) DNA and gel-incompetent DNA compared to the reference genome. Plot was created using Qualimap 2.2.1.**



**Supplemental Figure 6. Orientation of discordant reads at *sac3* super-peak position and *dhodh* amplicon is indicative of tandem duplication. **A.** Schematic of a tandem duplication, which illustrates paired-end reads pointing outwards and an inverted duplication, which illustrates paired reads pointing in the same direction. **B.** IGV image of paired reads at the super-peak. The super-peak includes the *sac3* domain-containing, putative protein found on chromosome 6 at position 86,429 - 87,143bp. H1 gel-incompetent DNA is sequenced and the paired ends are aligned to the WT(Dd2) reference genome. **C.** IGV image of paired reads of the *dhodh* breakpoints matches previously reported tandem duplication (Guler**

et al., 2013). Due to size of the amplicon, boundaries of reads are shown in a split screen. Reads were analyzed using Integrative Genomics Viewer Software (IGV 2.4.10) and does not depict the total reads at those locations. Colored arrows, discordant reads; green arrows depict tandem duplications and blue and teal arrows depict an inverted duplication.

## **Chapter 3: Extra-cellular vesicles containing antimalarial resistance-conferring genes found in *Plasmodium falciparum* parasites**

Jennifer M. McDaniels<sup>1</sup>, Jessica Pancake<sup>1</sup>, Sabrina Carter<sup>1</sup>, Jennifer Kniss<sup>1</sup>,  
Audrey Francis<sup>1</sup>, and Jennifer L. Guler<sup>1,2</sup>

<sup>1</sup>Department of Biology, University of Virginia, Charlottesville, Virginia 22903 USA,

<sup>2</sup>Division of Infectious Diseases and International Health, Department of Medicine,  
University of Virginia, Charlottesville, Virginia 22903 USA

Author Contributions:

Conceived and designed the experiments: JMM JP JLG

Performed the experiments: JMM JP SC JK AF JLG

Analyzed the data: JMM JP SC JK AF JLG

Contributed reagents, materials, and/or analysis tools: JLG

Wrote the paper: JMM JLG

### 3.1 Introduction

Extra-cellular vesicles (EVs) are membranous structures secreted from intracellular organelles or the plasma membrane. There are 3 classes of EVs: 1) exosomes, which are formed from late endosomes and are released when multivesicular bodies fuse with the plasma membrane, 2) microvesicles, which shed and bud directly from the plasma membrane, and 3) apoptotic bodies, which are vesicles released during apoptosis (Johnstone et al 1987). They serve as a mode of communication between cells, and are considered transport “containers” for different signaling molecules such as proteins, nucleic acids, lipids, metabolites and other small molecules.

A number of human pathogens have co-opted EVs for disease propagation and life cycle progression (Mantel and Marti, 2014; Montaner et al., 2014; Ofir-Birin et al., 2018; Regev-Rudzki et al., 2013; Sampaio et al., 2017; Schorey et al., 2015). Interestingly, drug resistance can be transferred using EVs in response to different cellular stressors, providing a fitness advantage. Alteration of gene expression, reduction of drug effectiveness at target sites, and sequestration of cytotoxic drugs to limit bioavailability has been directly (or indirectly) mediated by EV-carried signaling molecules (Maacha et al., 2019; Regev-Rudzki et al., 2013; Siquella et al., 2017; Soekmadji and Nelson, 2015).

One pathogen that produces EVs is *P. falciparum*, the protozoan parasite responsible for malaria. In 2018, there was an estimated 228 million cases and 405,000 deaths (World Health Organization, 2018). EVs and their role in malaria has caused considerable interest within the community due to the observation of elevated EV levels in patients with severe malaria (Combes et al., 2004; Mantel et

al., 2013a; Nantakomol et al., 2011; Pankoui Mfonkeu et al., 2010; Sampaio et al., 2017). Recent studies have also shown that *P. falciparum* can transfer episomal plasmids in EVs, transferring drug resistance to sensitive parasites (Regev-Rudzki et al., 2013). This is particularly interesting because the successful transfer of an episomal plasmid suggests a new molecular mechanism of resistance. We hypothesize that endogenous resistance-conferring genes are a likely EV-bound component associated with drug resistance and increased parasite fitness. There has been a concerted effort to limit and control resistance in *Plasmodium*. One emerging strategy is to prevent cellular communication between parasites via vesicles, ultimately blocking the transfer of drug resistance.

There have been two seminal works (Mantel et al., 2013a; Regev-Rudzki et al., 2013) that described the mechanism of how EVs influence the parasite transition from the red blood cell (RBC) asexual stage to the sexual stage, which can be transmitted to mosquitoes. It is proposed that EVs aid in density sensing amongst parasites (Mantel et al., 2013a; Regev-Rudzki et al., 2013); however, the exact mechanism of how this process is activated or regulated is not known. The difference in these two studies lies in its cargo: study one describes protein cargo that is enriched in parasite proteins with minimal red blood cell (RBC)-specific proteins, suggesting that the RBC plays a small role in EV biogenesis and gametocyte production (Mantel et al., 2013b; Mantel and Marti, 2014). Study two describes that transfer of a Maurer's cleft (MC) protein and DNA cargo to parasites under drug pressure, suggesting that environmental stressors are involved in EVs production and, ultimately causes increased levels of gametocytes.

Previous work sheds light on how *Plasmodium* parasites are able to communicate with each other and continue to cause disease. Work from Regev-

Rudzki et. al. also highlighted an important discovery; parasites were able to transmit resistance genes carried on episomal plasmids. This is important due to the possibility that information can be readily passed between parasites to avoid the harmful effects of drug pressure. One thing that is unclear is how much information one parasite is able to communicate with another via EV transport. To date, little is known about the storage limitation of DNA when found in vesicles and secretory pathway that allows genetic material flow to from parasite to parasite.

Here, we collected EVs derived from *in vitro* cultures of RBCs infected with sensitive and drug resistant *P. falciparum* parasites (iRBCs) with uninfected RBCs (uRBCs) serving as a control. We combined ImageStreamX flow cytometry (ImageStream) and cryogenic electron microscopy (Cryo-EM) technologies to uniquely distinguish EVs derived from iRBCs and uRBCs. We found, on average, the iRBC-derived vesicles are larger and have higher granular complexity than the uRBC-derived vesicles. This might suggest more (and larger) cargo is being exchanged between parasites. We also assessed the vesicular content derived from drug resistant iRBCs by droplet digital(dd) PCR. To our surprise, vesicles from drug resistant parasites concealed DNA with copy number variations (CNVs) in addition to harboring CNVs at its home chromosomal location. In this report, we present the novel finding that *Plasmodium* parasites are able to transfer endogenous resistance-conferring genes without the use of an episomal plasmid. Taken together, these results are significant due to implications that EVs may be involved in the propagation of resistance. This work furthered our knowledge from prior work in the field.

### 3.2 Results

In an effort to investigate the diverse nature of EVs, we assessed 2 different approaches to examine vesicle morphology derived from uRBCs and iRBCs. We aimed to capture the highest, and most diverse population of EVs. We collected EVs from transwell plates (used similarly in (Regev-Rudzki et al., 2013)) and directly from large culture flasks. Transwell plates contained multiple wells with a porous insert separating parasites from vesicles. The insert has a 0.4 $\mu$ m filter. Large culture flasks do not have a barrier to limit dispersion of larger cellular components; thus, this method leads to contamination with cellular debris and small invasive parasite stages (termed merozoites). Gating strategies used are described in the Results section and see **Supplemental Figure 6**. Following, vesicles were purified using the Invitrogen Total Exosome Isolation Reagent kit. To more directly identify DNA associated with vesicles, we also assessed the proportion of vesicles staining positive with SYBR DNA binding fluorescent dye prior to ImageStream analysis.

ImageStream was used to analyze and compare the physical properties of the vesicles isolated from culture flasks and transwell plates. ImageStream has the capabilities to quantify vesicles that are <1 $\mu$ m and detect fluorescent markers (Lannigan and Erdbruegger, 2017). Given the same starting volume and parasitemia, we found that culture flasks provided the highest number of EVs per volume. On average, the density measured were ~5,000,000 and ~10,000,000 objects/mL for transwells and flasks, respectively (**Figure 11B and C**).

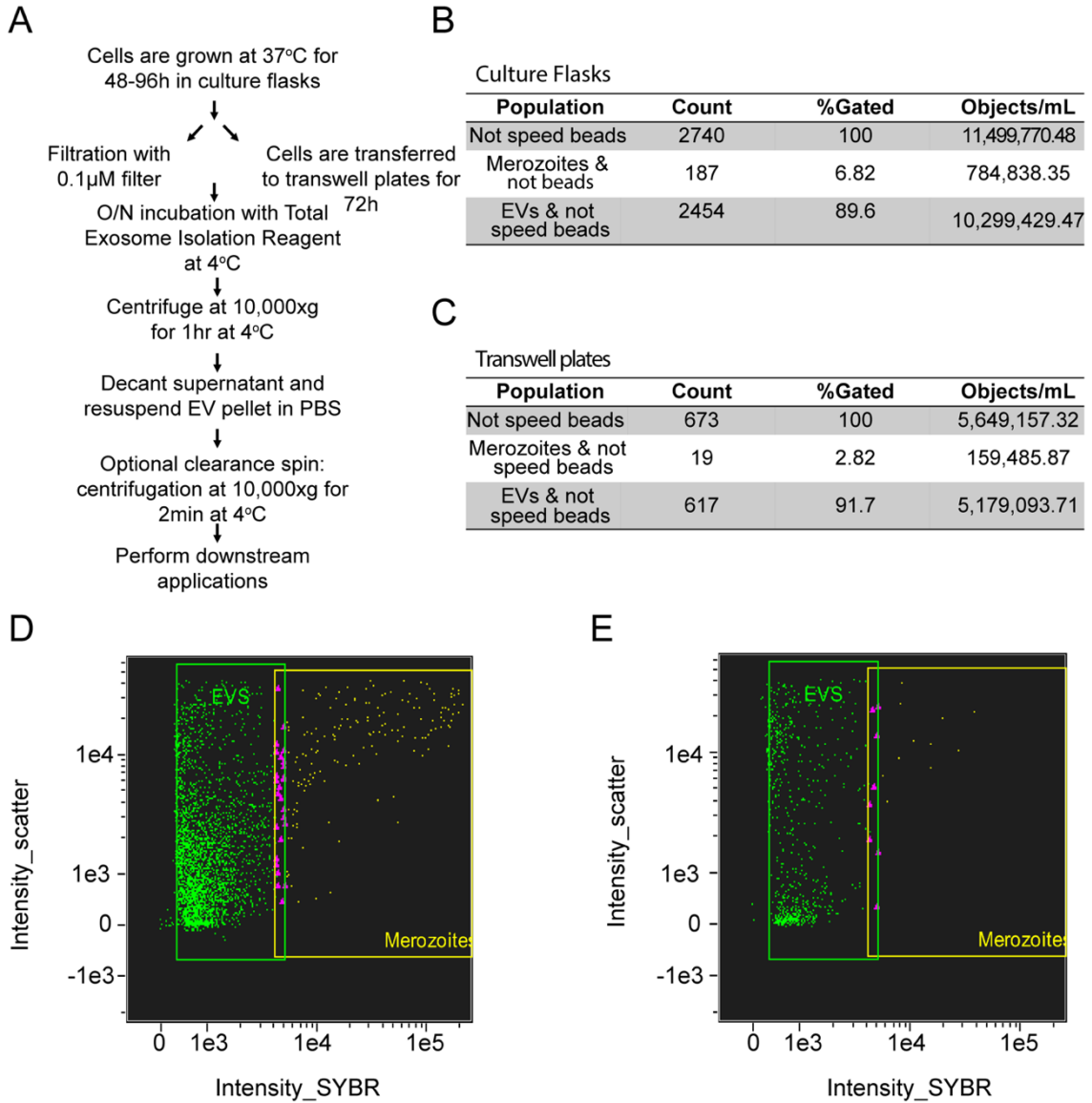


**Figure 11. Isolation of extra-cellular vesicles (EVs) resulted in a higher density of vesicles.** **A.** Overview of isolation scheme using Total Exosome Isolation Reagent Kit. **B-E.** Representative summaries and plots of vesicles isolated from culture flasks and transwell plates. Density is represented as objects/mL. EVs positively stained for SYBR DNA fluorescent dye (green) are derived from **(D)** culture flasks or **(E)** transwell plates. Merozoites are shown in (yellow) at lower density. . Forward intensity scatter represents heterogeneity of observed EV population. Higher heterogeneity is shown in panel **(D)**. Speed beads

scatter signals are used to calibrate the flow of the samples for camera synchronization (Erdbrügger et al., 2014). n=2.

We concluded that vesicles harvested from ~2 transwell plates are equivalent to the density of vesicles harvested from 1 flask; this result was observed regardless of the smaller filtration pore size used following propagation in flasks.

From visual interrogation, it is also clear that we have isolated more EVs of higher heterogeneity starting from culture flasks than transwell plates (compare **Figures 11D to 11C**). EVs derived from culture flasks showed low SYBR fluorescence intensity with mid to high scatter. On the other hand, EVs derived from transwell plates showed low SYBR fluorescence intensity with majority low scatter (**Figures 11D to 11C**). As mentioned, we also detect more merozoites that co-purified with our vesicles using culture flasks. Merozoites are distinctly displayed as high SYBR fluorescence intensity and high scatter using ImageStream (compare **Figures 11D to 11C**). Through gating, we eliminated the characterization of merozoites from our studies by precluding particles falling in the merozoite gate and particles that overlapped with our merozoite and EV gate (pink, **Figures 11D and 11E**). Gates are used to distinguish specific populations based on 2 dimensions of scatter or fluorescence (Dominical et al., 2017). For downstream applications, we only investigated vesicles isolated from culture flasks.

Next, we investigated morphological differences between uRBCs and iRBCs using cryo-EM and ImageStream. In our uRBCs and iRBCs samples, we also detected vesicles heterogenous in nature. On average, isolated vesicles were predominantly 200-300nm; although small EVs of 50-100nm were detected (**Figure 12**). Most EVs were smooth and round in appearance with a discernible lipid bilayer present (**Figure 12**). We also detected a smaller fraction of vesicles

containing an intracellular compartment with another discernible lipid bilayer (**Supplemental Figure 7**). Although vesicles harboring other vesicles were reported in Sisquella et al., we are uncertain if they are biologically relevant or an artifact of the isolation methodology. In a large proportion of the vesicles, we observed an electron dense area within the EVs (**Figure 12**). Based on previous studies, this dark area is predicted to be lipoproteins such as very low density lipoproteins (VLDL), low density lipoproteins (LDL) or high density lipoproteins (HDL) (Lázaro-Ibáñez, 2019; Poliakov et al., 2009; Yuana et al., 2013).

Flow cytometry revealed a similar heterogenous population of vesicles; however, we detected a distinct population iRBC-derived EVs that were distinguishable by its large side scatter (**Figure 13**). Side scatter is fluorescent measurement taken when the laser beam perpendicularly intersects the vesicles; while forward scatter and size may be roughly correlated, side scatter roughly correlates with cellular granularity (Basiji et al., 2007). We noticed a distinct shoulder specific to EVs derived from parasite (**Figure 13**, white arrow). Our data indicates that iRBC-derived vesicles have a higher internal complexity, possibly due to internal structures and other particulates. Thus, vesicles that fall in the range of side scatter of  $1e4$ - $1e5$  may be used differentiate iRBC-derived vesicles from uRBC derived vesicles.

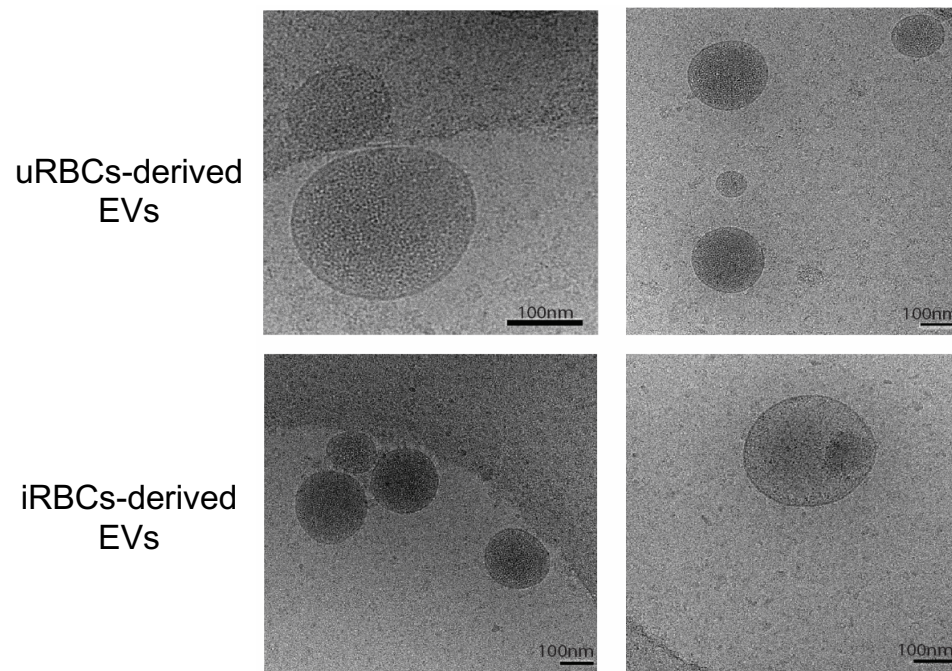


**Figure 12. Morphology of vesicles derived from parasites and uRBCs by Cryo-EM.** Each individual panel exemplifies the typical vesicle morphology for the group specified to the left. Dark areas, areas of low-high electron density; scale bar, 100nm.

Next, we investigated the DNA content of vesicles released from uRBCs and iRBCs (**Figure 14**). We hypothesized that vesicles derived from iRBCs contain more DNA than uRBCs because mature RBCs lack nuclei. We measured the fraction of vesicles that positively stained for SYBR using ImageStream. This experiment illustrated that iRBCs derived vesicles had a higher concentration of DNA associated with its vesicles (**Figure 14B**). We expect that the low fraction of vesicles that are SYBR-positive is due to the fact that vesicles were cultured in human serum, a large contributor of contaminating human DNA (**Figure 14A**). Again, merozoites were precluded from our studies after gating, and thus, were not contributing the SYBR-positive vesicles we observed.

In order to differentiate the topology of DNA from SYBR-positive vesicles, we investigated whether DNA is contained within vesicles or associated with its outer membrane. For these experiments, we assessed vesicles derived from a DSM1 drug-resistant parasite. The resistant parasite line H1 (C710-1a) harbored copy number variations for the *dihydroorotate dehydrogenase* gene (*dhodh*) (Guler et al., 2013). *Note: This parasite line was renamed for thesis consistency; for further details see Guler et al, 2013.* To perform this experiment, we incubated vesicles in the presence of a DNase for 140min (Ronquist et al., 2012). After the enzyme was inactivated and removed using phenol-chloroform extraction, we lysed the vesicles, releasing its inner contents. We predicted two different results. If the DNA is located within the vesicle, the DNA should be protected against DNase degradation; therefore, detectable by ImageStream and ddPCR.

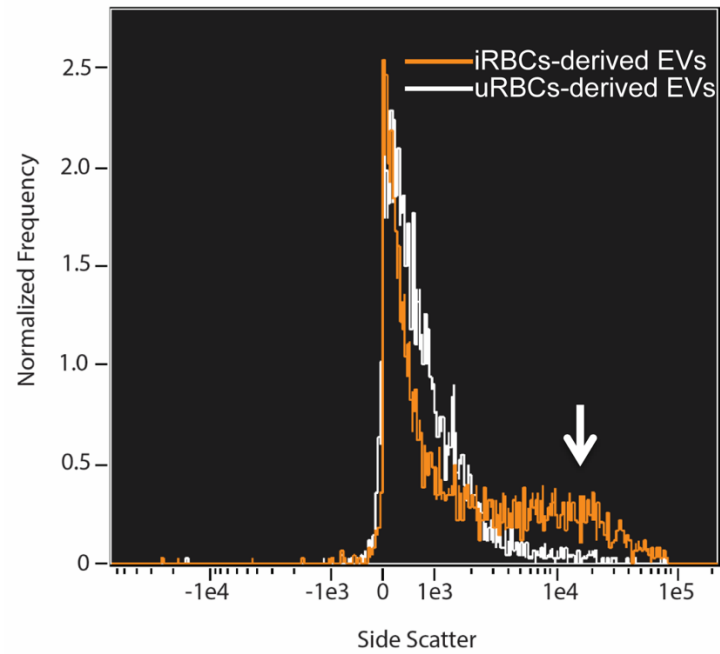


**Figure 13. ImageStream revealed that parasite-derived EVs were of a distinct size.** Overlaid histogram showing the population of parasite-derived vesicles (orange) and uRBC-derived vesicles (white). Arrow (shoulder), a unique EV population derived from parasitized red blood cells. n=3.

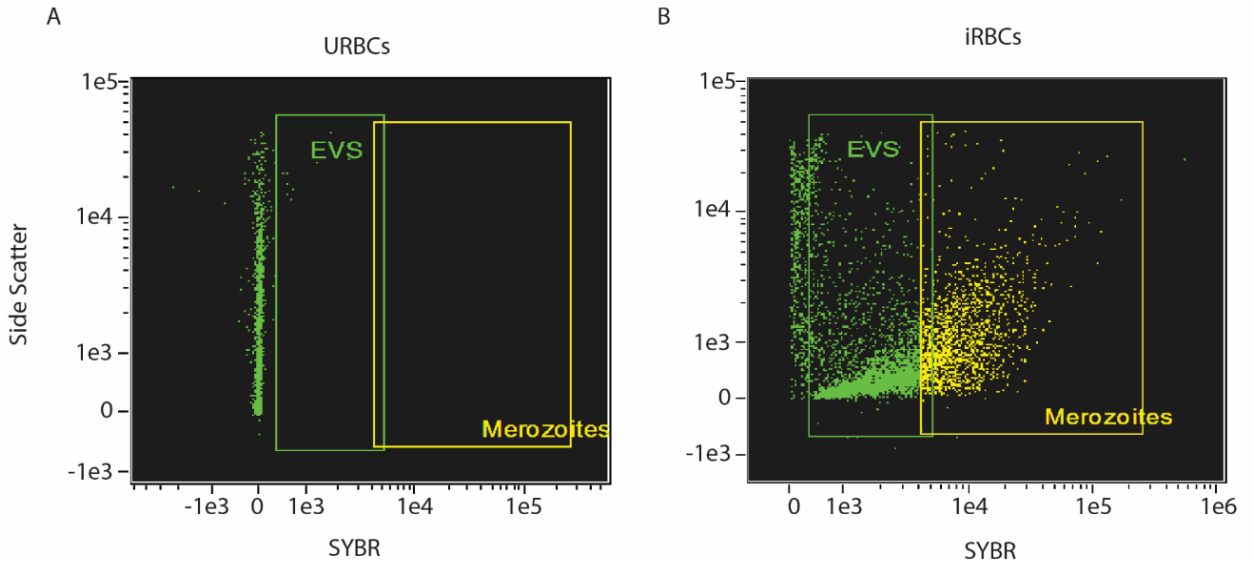


**Figure 14. Infected RBCs (iRBCs) secrete vesicles with higher scatter and higher levels of SYBR-positive staining.** ImageStreamX flow cytometry is used to characterize vesicles derived from (A) uninfected RBCs (uRBCs) and (B) iRBCs. Larger vesicles scatter more light and appear further along the y-axis. The x-axis detects the SYBR-fluorescent dye that binds to DNA. As the concentration of DNA increases, the further it will appear along the x-axis. Two gates were created to differentiate EVs from merozoites. Merozoites are gated by size and DNA content. n=2.

If the DNA is associated with the outside of the vesicle, the DNA should be susceptible to DNase degradation; therefore, not detectable by ImageStream and ddPCR. In a preliminary experiment, we first assessed the quality of the DNA that remained following DNase treatment of vesicles by qPCR. We also sought to investigate the origin of DNA found within vesicles. We assessed two different *Plasmodium* genes at two different loci (*18s ribosomal DNA*, chromosome 1 and *dhodh*, chromosome 6) and two different human genes at two different loci (*gapdh*, chromosome 12 and *beta tubulin*, chromosome 6) (**Figure 15A**). We detected both pairs of genes. To highlight, *Plasmodium* genes found inside of the parasite-derived vesicles provides further support that genomic DNA is packaged into vesicles (Sisquella, 2017). The *Plasmodium* genes were distinguished by their relatively low Ct values while the human genes were distinguished at higher Ct values (**Figure 15A**). This result implies that *Plasmodium* DNA is of higher quality and concentration over human DNA. The human host DNA that we detected in this study is contributed by human serum (Babatunde et al., 2020; Sisquella, 2017). We believe that it is highly degradable and its properties are reflected by the result of >1000-fold lower concentrations following DNase treatment.

We predict that *Plasmodium* DNA is protected from DNase treatment because majority is located inside of vesicles and human DNA is susceptible to DNase treatment because majority is located on the outside of vesicles, perhaps bound to the outer membrane of RBCs. Without the untreated qPCR control conclusions are loosely stated; however, we have reason to believe the DNase enzyme is highly active and does indeed degrade human DNA (**Supplemental Figure 8**). In a separate control, it is clear from visual interrogation that the DNase enzyme decreases the number of SYBR-positive vesicles (**Supplemental Figure**

8). Vesicles derived from uRBCs are displayed; vesicles falling into the merozoite gate are vesicles with high SYBR intensity and not merozoites (**Supplemental Figure 8A**). In the absence of parasites (merozoites), we are certain that the source of DNA is: from human contamination and readily degraded in the presence of DNase, which further supports our claim.

Next, we aimed to expand on the results of a previous study conducted by (Regev-Rudzki et al., 2013) in which an episomal plasmid was transmitted between parasites under drug selection. We hypothesized that resistant parasites can package endogenously-derived resistance conferring genes in vesicles to communicate with neighboring parasites also under selection. We utilized ddPCR to measure CNVs (**Figure 15B**). ddPCR is a specialized form of PCR that is used to measure a gene of interest (*dhodh*, D) relative to a single copy reference gene (*seryl tRNA dehydrogenase*, S), generating a ratio that indicates enrichment (D:S). As a control, we utilized extracted genomic DNA from resistant (RT, C710-1a) and DNA from WT1 (Dd2). The published *dhodh* gene copy number is 7-10 and 1 for RT and WT1, respectively (Guler et al., 2013).

When we measured the vesicle DNA from resistant parasites, we observed a copy number of 6.0 (**Figure 15B**). This result indicates that parasites are capable of harboring endogenous resistance-conferring genes into vesicles. Second, we observed *dhodh* CNVs presumably found within the vesicle as CNVs are also present in the resistant parasite genome. Interestingly, after performing a DNase treatment, copy number declines to almost half at 3.6 copies. This is also ~2-3 fold lower than genomic DNA copies (7-10) (Guler et al., 2013).

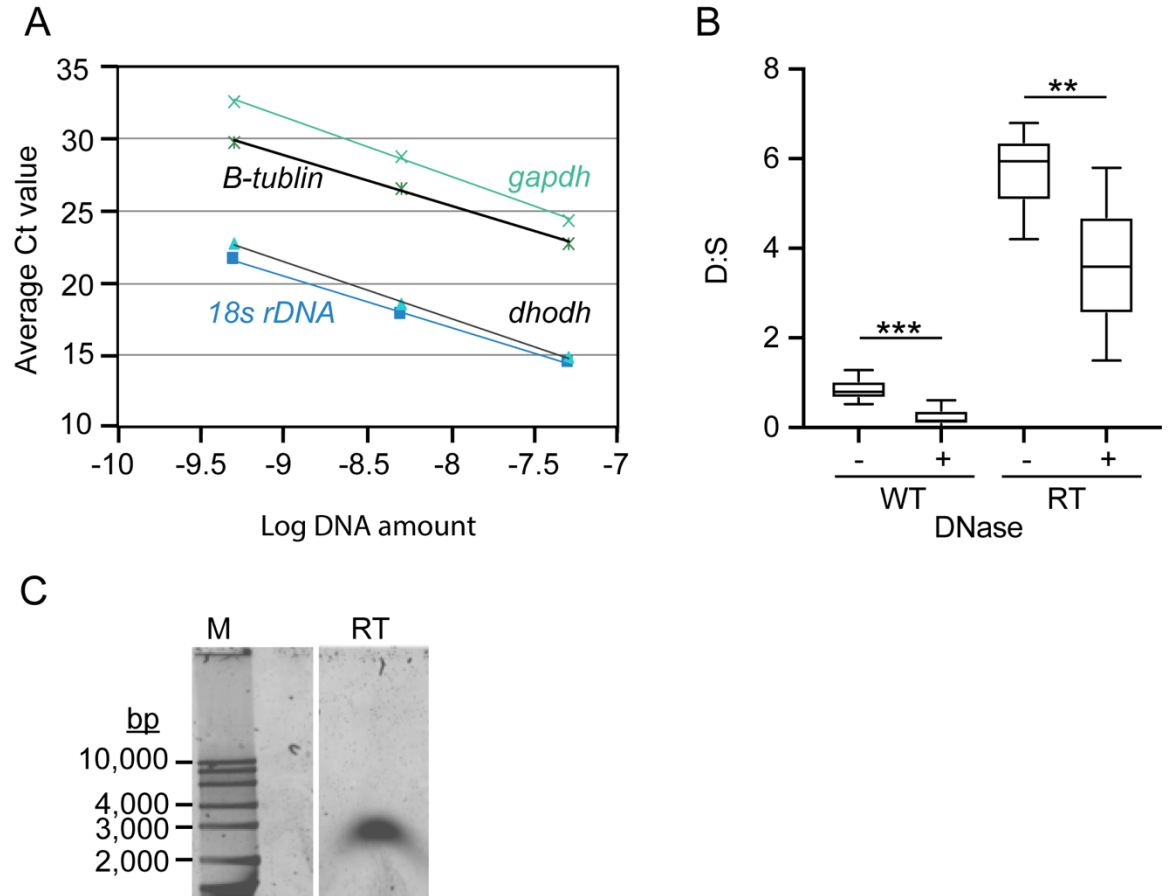


**Figure 15. Analysis of DNA located inside of wild type (WT) resistant (RT) parasite-derived vesicles** **A.** qPCR analysis was used to estimate parasite and human DNA located within vesicles using the standard curve method. Prior, DNA associated with the outer membrane of vesicles and free DNA was removed using a DNase enzyme. After digestion, WT DNA was probed for parasite specific genes: *dihydroorotate dehydrogenase* (*dhodh*, lower black line) and *18s ribosomal DNA* (*18s rDNA*, blue line) and human specific genes: *tubulin beta-1 chain* (*B-tubulin*, higher black line) and *glyceraldehyde 3-phosphate dehydrogenase* (*gapdh*, green line). Ct, cycle threshold. **B.** Box and whiskers plot summarizing copy number variation analysis of DNA found within vesicles using droplet digital (dd) PCR. DNA was treated with DNase as in **(A)**. Then, vesicle-bound DNA was extracted and

treated in the presence (+) or absence (-) of DNase. The observed ratio is calculated using the number of *dihydroorotate dehydrogenase*, *dhodh*, gene copies (denoted as D, a multicopy gene in the *dhodh* amplicon) to the number of seryl *tRNA synthetase gene* copies (S, a single copy reference gene). DNA derived from WT vesicles displayed a mean of 0.80 when absent of digestion and 0.15 when digestion was performed. DNA derived from RT vesicles displayed a mean of 6.0 when absent of digestion and 3.60 when digestion was performed. Analysis of ddPCR was performed using the QuantaSoft Bio-Rad Software. \*\*\*,  $p=0.0003$ ; \*\*,  $p=0.0047$ ; Error bars represent Poisson confidence intervals (upper hinge, 75<sup>th</sup> percentile; lower hinge, 25<sup>th</sup> percentile);  $n=5$ . **C.** Preliminary study of an observed ~4kb DNA fragment detected in RT parasite-derived vesicles. DNA was assessed using pulse field gel electrophoresis and stained with 1xSYBR Safe.

The decrease in copy number suggests that *Plasmodium* parasite DNA is located partially protected in vesicles. While majority of parasite DNA is found inside the vesicle, perhaps, some fragments of DNA is bound to the membrane or span the membrane. On the other hand, wild type parasite DNA is significantly degraded (mean of 0.80 to 0.15, **Figure 15B**), implying that wild type DNA is not preferentially packaged into EVs. These experiments have also illustrated that with the detection of *seryl tRNA synthetase*, genomic DNA is found within vesicles.

Further analysis of the EV-DNA derived from resistant *Plasmodium* parasites led to a preliminary result assessing the size of DNA contained vesicles revealed that DNA of ~4kb in length (**Figure 15C**). The size of the DNA may indicate that there is a size limitation for cargo enforced by the vesicle. More detailed analyses are required to determine the average size of DNA located within vesicles derived from iRBCs compared to uRBCs with a higher sample size.

Lastly, we aimed to visualize the EVs by ImageStream before and after DNase digestion (**Figure 16**). We report a 79.7% reduction in the number of SYBR-positive vesicles derived from uRBCs (compare **Figure 16A** to **16B** and **Figure 16D**). Unfortunately, the sample consisting of vesicles derived from iRBCs that were treated in the absence of DNase was lost. It prevents us from extrapolating any major conclusions from this preliminary experiment despite having a number of SYBR-positive vesicles remaining after DNase treatment (**Figures 16C** and **16D**). We also noticed that after digestion there a shift in the EV population, outside of the EV gate. We believe that the new population defined by high SYBR intensity and high side scatter population is due to the DNase enzyme remaining associated with the vesicles.

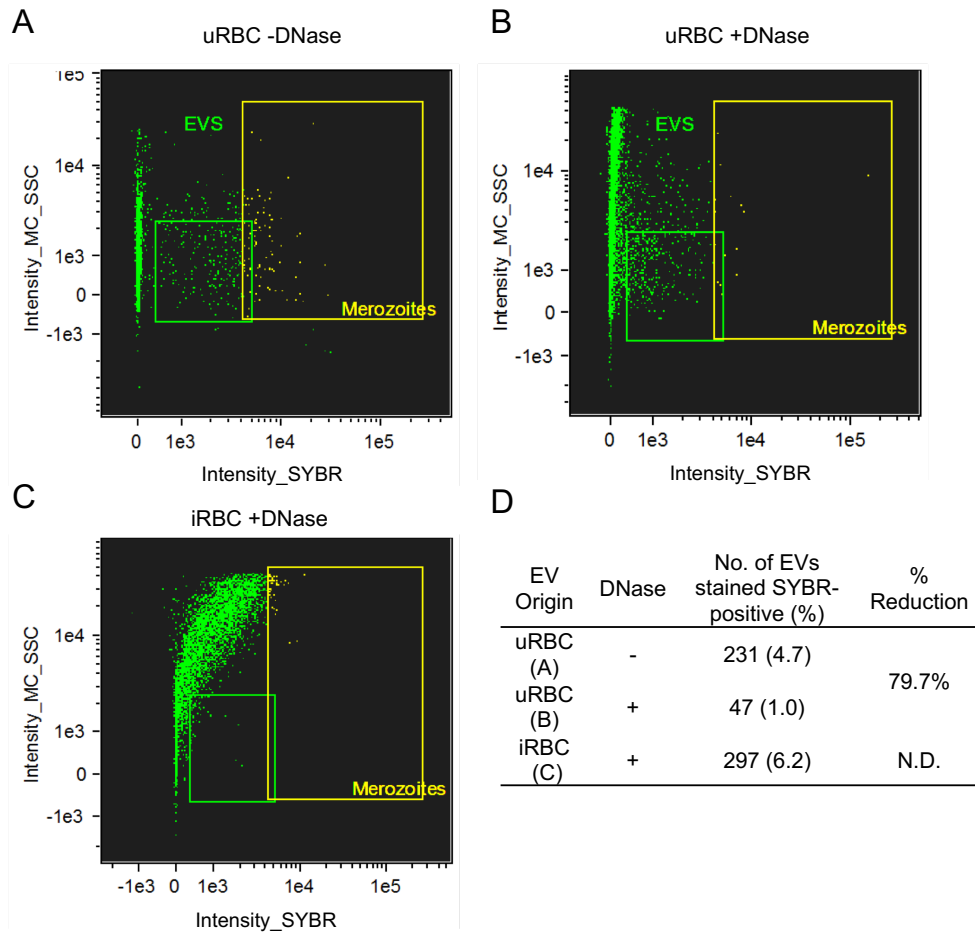


**Figure 16. Visualization of EVs treated in the absence and presence of DNase by ImageStream.** Samples were stained with SYBR before analysis on ImageStream. DNA derived from uRBCs in the (A) absence and (B) presence of DNase. C. DNA derived from iRBC vesicles treated in the presence of DNase. *Note: 2D plot displaying absence of DNase is not included due to loss of sample.* D. Quantification of the number of vesicles stained SYBR-positive and the reduction percentage of SYBR-stained vesicles after DNase treatment. DNA derived from uRBCs was reduced by 79.7%. N.D, not determined; n=1.

Future studies will explore the removal of the enzyme using standard purification methods and observing the presence or absence of the new population observed in **Figure 16B**.

### 3.4 Discussion

Our present study extends prior studies of EVs that contribute to malaria biology and pathogenesis (Combes et al., 2004; Mantel et al., 2013b; Nantakomol et al., 2011; Pankoui Mfonkeu et al., 2010; Regev-Rudzki et al., 2013; Sampaio et al., 2017; Sisquella et al., 2017). Here, we sought to characterize and distinguish vesicles from parasite or host origin. From our preliminary data, we hypothesize that parasite-derived vesicles are larger in size and closely reflect the genotype of its chromosomal origin. We provide *in vitro* evidence that drug resistant *Plasmodium* parasites are able to generate vesicles carrying endogenous, resistance-conferring genes. While the mechanisms delineating the secretory pathway in *Plasmodium* is unclear, our results suggest that vesicle exchange between a resistant donor and a sensitive recipient parasite may emerge as a new targetable mechanism to inhibit resistance propagation.

Using EM, we observed vesicles that were between 50-300nm in both iRBC and uRBC populations (mean of 200-300nm). This finding agrees with the previous observation that the Total Isolation Reagent recovers a broad range of EVs (Lobb, 2015; Tang, 2017). The larger vesicles are in the range of microparticles (100-1000nm), while the smaller vesicles fall within the classification of exosomes (50-100nm) (Szatanek et al., 2015). Compared to previous studies in malaria (Mantel et al., 2013b; Regev-Rudzki et al., 2013; Sisquella et al., 2017), our vesicles are larger compared to Regev-Rudzki et al. studies, but are similarly sized compared

to Sisquella et al. and Mantel et al studies. These differences are presumably due to varying isolation techniques and different commercial kits (i.e. Total Exosome Isolation Reagent v OptiPrep Density Gradient Medium) (reviewed in greater detail in **Chapter 1** (Szatanek et al., 2015)). These results emphasize that classifying vesicles by size alone is not sufficient due to a variety of isolation methods. One limitation of this study is the lack of RBC-specific and parasite-specific markers e.g. CD235a and PfPTP2, respectively (Babatunde et al., 2020; Regev-Rudzki et al., 2013).

The vesicles isolated in our studies contained a lipid bilayer, which is in agreement with other EM studies (Babatunde et al., 2020; Nantakomol et al., 2011; Sisquella et al., 2017) and suggests that they are not simply lipoproteins (Zaborowski, M et al., 2015). We did detect what we speculate to be lipoproteins (dark spots) within our vesicles (**Figure 12**). More experiments are required to identify lipoproteins with specific protein markers and, thus, these results should be interpreted with caution.

A key finding from our studies is that mutated DNA harboring CNVs is found within vesicles derived from *Plasmodium* parasites (**Figure 15**). While it is unclear how DNA is packaged into vesicles, this finding extends a previous study conducted by Regez-Rudzki et al. that provided support for episomal transmission (Regev-Rudzki et al., 2013) and a recent study by Sisquella et al. that provided support of genomic DNA transmission (Sisquella et al., 2017). In complement of these studies, we attempted to purify and amplify DNA before and after DNase treatment (**Figure 15**). High quality parasite DNA is found within the vesicles, as assessed by the presence of purified products after qPCR and ddPCR (**Figure 15**). One advantage of packaged DNA over cell free DNA is that packaged DNA can

evade degradation from cellular DNases while traveling between different organelles.

Although Sisquella et al. primarily focused on the stimulation of an immune response via RNA, our studies both demonstrate that DNA is indeed packaged inside of vesicles. In a similar fashion, we discovered genomic DNA *inside* of the vesicles confirmed using DNases and various DNA stains. An important result from their studies revealed that once internalized, cargo found within vesicles are biologically relevant and functional. Vesicle-derived DNA elicited a DNA sensing response that led to cytosolic signaling (Sisquella et al., 2017). Alternatively, we suggest that our endogenous EV-DNA has a role in resistance propagation i.e. the transmission of resistance-conferring genes. Our studies both agree that EV transmission is important for social interaction between parasites and, presumably, provides a fitness advantage.

Researchers also found that their iRBC-derived vesicles are between 50-300nm with a peak of 107nm and uRBC-derived vesicles are between 125-225nm (Sisquella et al., 2017). Our vesicles were also in that range, but majority of our iRBC-derived EVs were about 300nm in diameter. Some differences in size may reflect the employment of different vesicle isolation schemes as well as differences in the type of vesicles released during different parasitic stages. We isolated vesicles of mixed cultures (rings, trophs, and schizonts) and Sisquella et al. focused on the release of vesicles from rings. The group suggests only early stages during invasion including rings are responsible for DNA packaged vesicles and delivery (Sisquella et al., 2017). This finding warrants further investigations regarding whether or not different parasitic stages release different sized vesicles and cargo.

In the same study, researchers reported EV-DNA to be double-stranded, 15kb in length, and wrapped around histones (Sisquella et al., 2017). In this study, we observed a 4kb DNA fragment (**Figure 15C**). Vesicles devoid of full chromosome sized DNA implies some tightly ordered structure and compaction enforced by the vesicle itself. We also hypothesize that the difference in size may be due to differences in technical approaches; we employed PFGE for detection and Sisquella et al employed Agilent TapeStation.

The EV route is another major difference between the studies. We propose that our DNA cargo travels parasite to parasite to elicit natural transformation. We believe the vesicles investigated in our studies must reach the nucleus as its final destination to possibly alter gene expression as a result of harboring CNVs. Sisquella et al. investigated DNA cargo travelling from parasite to monocyte to elicit an immune response. In both cases, there may be some overlapping pathways to reach the cytosol to be further investigated. We are uncertain of full the details required to make the journey, but work from Mantel et al. has shown that vesicles concentrate at the recipient parasite nucleus by fluorescence microscopy.

The DNA investigated in our EV studies was *dhodh*-positive and harbored a similar copy number found in the genome at 6 copies, implying conservation of gene copy mutation. Interestingly, after DNase treatment, the copy number decreased to 3.6 copies. This result suggests that only a few copies are needed in the propagation of resistance. More research will focus on the characterization of DNA found within vesicles using other copy number analysis tools and next generation sequencing.

The oncosome field, which focuses on cancer-derived EVs, was the first to identify DNA in vesicles. A myriad of studies has provided support for EV-DNA that

contains mutations, both single nucleotide polymorphisms and CNVs (Kawamura, 2017). It is proposed that mutated genes found within oncosomes induces tumor favorable effects such as genetic instability in recipient cells (Kawamura, 2017). Drawing from this field, our next experiments will be designed to uncover the function of *Plasmodium* DNA contained in vesicles and assessment of its ability to transform sensitivity parasites to resistant parasites.

In conclusion, a thorough understanding of the biological mechanisms used by *P. falciparum* to communicate intercellularly to neighboring parasites will provide a useful mechanism to manipulate and disrupt highly adaptive messages for increased fitness.

### **3.3 Materials and methods**

#### *3.3.1 P. falciparum culture conditions.*

Cells were grown in complete media containing 2.5g of AlbuMAX II (AbII) Lipid-Rich BSA (ThermoFisher Scientific, Waltham, MA, USA) and 0.05g of hypoxanthine (Sigma-Aldrich, St. Louis, MO, USA) with final parasitemia 2-3% and 3% final hematocrit (Corning, Costar, Fisher Scientific). Subsequently, the parasite culture was diluted to about 1% and 2% hematocrit before transferring to transwell plates. A defined volume of the diluted culture was transferred to the upper chamber of each transwell. Cells were incubated 37°C (5% CO<sub>2</sub>, 5% O<sub>2</sub>) for 72hrs before collection. Parasite lines used were Dd2 (WT) and H1 (C710-1a , DSM1-resistant) (Guler et al., 2013).

#### *3.3.2 Isolation of EVs from P. falciparum.*

Instructions were followed according to manufacturer's instruction. After removing the media from lower chamber of the transwell or removing media directly from

culture flasks, 0.5x volume of Total Exosome Isolation Reagent (ThermoFisher Scientific, Waltham, MA, USA) was added to the media and stored overnight at 4°C. Samples were then filtered using a 0.1µm filter (Nalgene, ThermoFisher Scientific) to remove contamination prior to purification. Vesicles were recovered by centrifugation at 10,000xg for 1hr at 4°C in Oakridge tubes (Nalgene, ThermoFisher Scientific). An optional clearance step was used to remove any contaminating particles that may have co-purified. The supernatant was decanted and the pellet was resuspended in 250µl 1xfilter-sterilized PBS for downstream applications (i.e. flow cytometry or electron microscopy) or a DNA resuspension buffer (150mM NaCl and 50mM Tris, pH 7.5) for DNA analysis.

### 3.3.3 *Cryo-EM of EVs.*

Cryo-EM was performed with Tecnai F20 Twin transmission electron microscope (FEI, Hillsboro, OR, USA) electron microscope. Sample preparations for cryo-transmission electron microscopy (TEM) imaging of exosomes were based on a previously established protocol (Banizs et al., 2014). All EVs were embedded and sectioned by the Molecular Electron Microscopy Core at University of Virginia. Approximately number 25 images were taken per vesicle derived from iRBCs or uRBCs.

### 3.3.4 *ImageStreamX flow cytometry.*

Samples were stained with 2xSYBR Green Nucleic Acid Stain (ThermoFisher) DNA stain for 20min at room temperature prior to imaging on the Amnis ImageStreamX Mark II Flow Cytometry (Luminex, Austin, TX, USA). A PBS buffer only and buffer and SYBR control sample was also performed with each run (data not shown). Laser settings were adjusted to detect SYBR green channel (488nm). For every sample a collect >10,000 events were applied. Samples were stored on

ice (4°C) until they were ready to be analyzed using ImageStream. Gating strategies were used to distinguish EVs from merozoites. On average, a single merozoite is small, ~1µm in diameter and have a single genome of DNA. The merozoites also produced large scatter and were visible under brightfield microscopy, EVs were not (**Supplemental Figure 6**). The shift of large side scatter with positive SYBR stained was enough to gate the complete merozoite population. The EVs were gated due to its uniformity (SYBR staining), low scatter (**Supplemental Figure 6**). Particle concentration (particles/mL) was calculated by the ImageStream instrument.

#### *3.3.4 DNA extraction for electrophoresis.*

After resuspension of the pellet, DNase was added to remove any contaminating DNA associated with the outer membrane of the vesicles. To do so, 5U of Benzonase (Sigma-Aldrich, St. Louis, Missouri, USA) was incubated with samples for 140mins at 37°C while shaking (Ronquist et al., 2012). A final concentration of 10mM of EDTA was used to inactivate the DNase. Following, 1/100 of 10% Sarkosyl (L-loril sarcosil) (Teknova Inc, Hollister, CA, USA) and 200µg/mL proteinase K (Thermo Fisher Scientific) was added to the total volume and incubated overnight at 37°C. Nucleic acids were then extracted from vesicles with phenol/chloroform/isoamyl alcohol (25:24:1), pH 7.8-8.1 (Invitrogen, Waltham, MA, USA). DNA was extracted twice more as above, once with chloroform, and, then ethanol precipitated using standard methods.

#### *3.3.5 Pulse field gel electrophoresis (PFGE) of vesicle-derived DNA.*

DNA extracted in section 3.3.3 were loaded into the well of 1% pulse field-certified gel in 0.5X Tris/Boric acid/EDTA buffer (Bio-Rad Laboratories, Inc.) and run at 14°C on the PFGE-DR system with PFGE DNA standards (Bio-Rad Laboratories,

Inc.) at 6V, 1-10s switch rate, for 5hr. Completed gels were stained with SYBR Safe DNA Gel Stain (1:10,000, Life Technologies, Carlsbad, CA, USA). Gels were visualized using a Typhoon 9410 Variable Mode Imager (SYBR settings: fluorescence, Laser: blue (488nm), Emission filter: 520BP40).

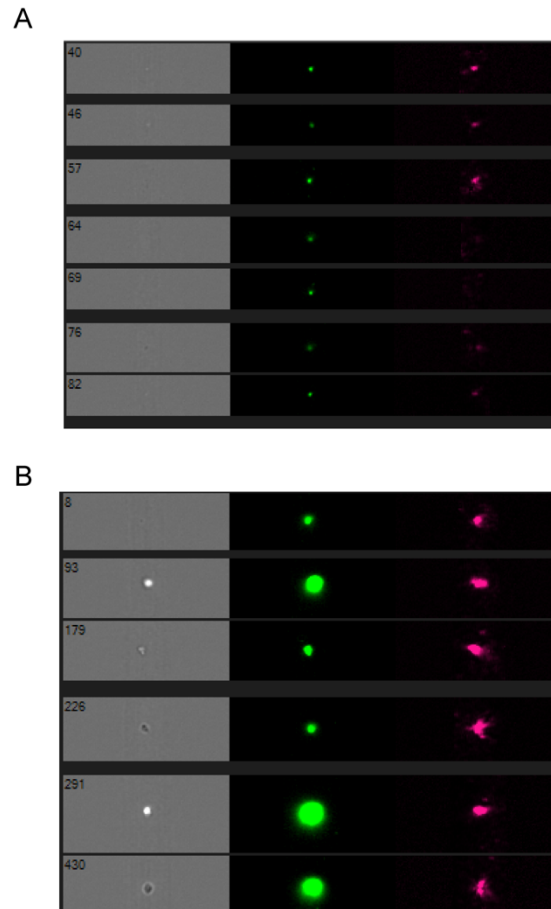
### 3.3.6 Quantitative RT-PCR.

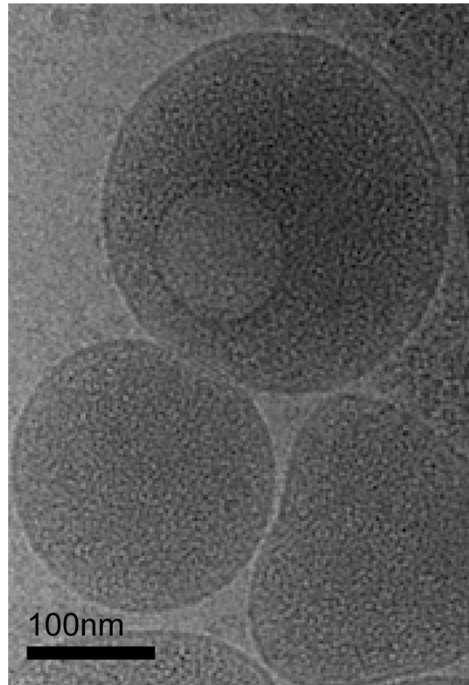
To measure the parasite DNA associated with vesicles, absolute quantitative real time (RT) PCR was used. The following reaction mixture went as follows: 5µl of template (50ng total), 0.1µl of forward and reverse primers (final concentration of 0.1µM), and 25µl of 2xSYBR green PCR Master Mix (ThermoFisher) for detection. The reaction mix was brought up to a final reaction volume of 50µl in nuclease free water. A negative control (no DNA template) was also added. Next, the reaction was moved to an Eppendorf Mastercycler pro PCR system thermocycler (FisherScientific). The reaction conditions involved initial denaturation for 15 minutes at 95°C, 50 cycles of denaturation for 15 seconds at 94°C, and annealing for 60 seconds at 60°C. Samples were ran in triplicate.

### 3.3.7 Copy number analysis with droplet digital(dd) PCR

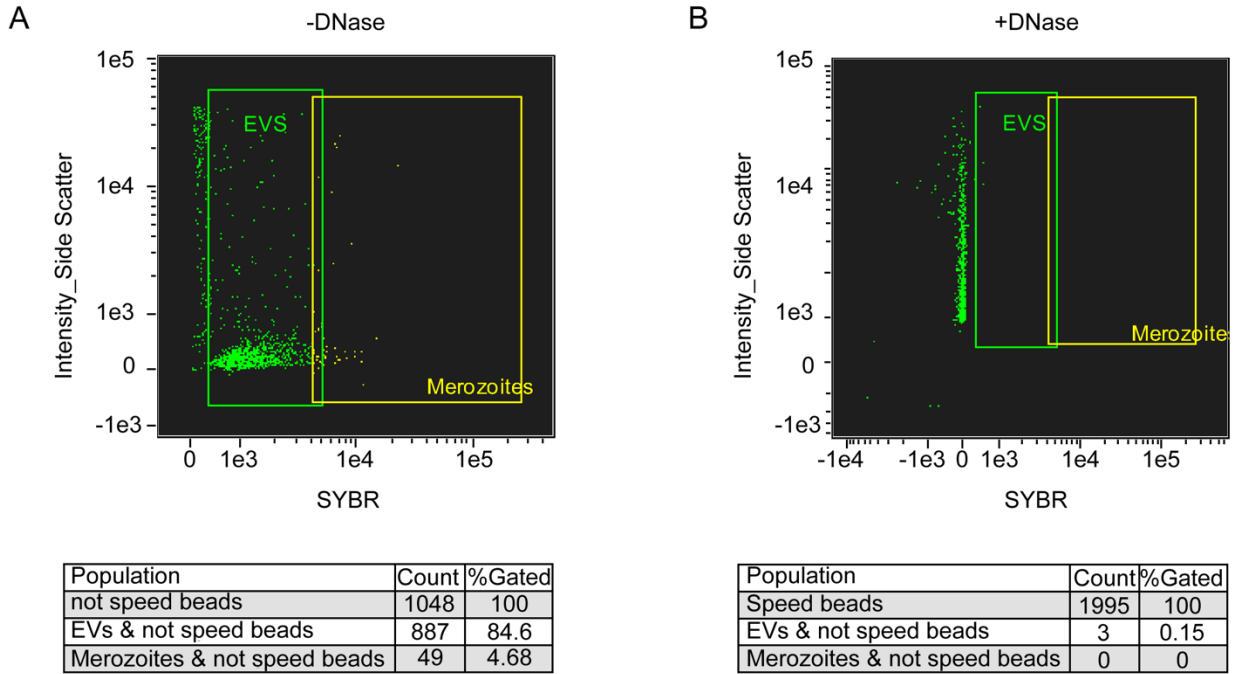
The PCR step was performed using ddPCR probe Supermix (Bio-Rad Laboratories, Inc.) with 5pg- 1ng of DNA. The TaqMan probe assay used 600nM final (using Seryl tRNA synthetase probe) and 900nM final (*dhodh* probe) multiplexed primers combined with a 50µM (final) probe (McDermott et al., 2013; Miotke et al., 2014). The reactions also contained the following detection probes: *Dihydroorotate dehydrogenase (dhodh)* probe 5'-56-FAM/CATTATTGCATCAGGAGGGA/3MGBEc-3' and *seryl tRNA synthetase* probe-5'-5HEX/ACATGAAGAAATGATACAAACA/3MGBEc-3'. The PCR protocol

for probe-based was 95°C for 10min, followed by 40 rounds of 95°C for 30sec and 60°C for 1min. Droplet generation (prior to PCR cycling) and fluorescence readings (post-PCR cycling) were performed per the manufacturer's instructions. The majority of samples measured fluorescence from a minimum of 8000 droplets. The ratio of positive droplets containing an amplified gene (*dhodh*, *D*) versus a single-copy gene (*seryl tRNA synthetase*, *S*) was calculated by QuantaSoft (BioRad Laboratories, Inc., D:S, ratio) and averaged between replicates. Poisson confidence intervals were provided by the software and the extreme values were reported (*i.e.* min and max across all experiments).





**Supplemental Figure 7. Parasite derived EVs appeared to contain vesicles bound vesicles.** A representative vesicle image derived from Dd2 parasite line. Scale bar, 100nm.



**Supplemental Figure 8. Assessment of DNase activity on DNA associated from uRBCs vesicles.** Visualization of DNA associated with vesicles without (**A**) and with (**B**) DNase treatment. **A.** Vesicles that displayed a higher SYBR intensity appeared in the merozoites gate although no merozoites were present. Analysis was performed using ImageStream.

## **Chapter 4: Persistent *pfprt* mutations in the genome of the malarial parasite, *Plasmodium falciparum*, from Southwestern Uganda**

This section is a version of a manuscript currently revised to be submitted to the Malaria Journal. The figures and tables have been renumbered to maintain sequence with other figures and tables in this dissertation.

Jennifer M. McDaniels<sup>1</sup>, Anna C. Long<sup>1</sup>, Kennedy Kassaza<sup>2,3</sup>, Mharlove Andre<sup>1</sup> Wasswa Fredrickson<sup>3</sup>, Dan Nyehangane<sup>2</sup>, Patrick Orikiriza<sup>2</sup>, Darwin J. Operario<sup>4</sup>, Joel Bazira<sup>3</sup>, Juliet A. Mwanga-Amumpaire<sup>2,5</sup>, Christopher C. Moore<sup>4</sup>, Jennifer L. Guler<sup>1,4</sup>, and Yap Boum II<sup>2,3</sup>

<sup>1</sup>Department of Biology, University of Virginia, Charlottesville, VA, USA, <sup>2</sup>Epicentre Mbarara Research Centre, Mbarara, Uganda, <sup>3</sup>Department of Microbiology, Mbarara University of Science and Technology, Mbarara, Uganda, <sup>4</sup>Division of Infectious Disease and International Health, University of Virginia, Charlottesville, VA, USA, <sup>5</sup>Department of Pediatrics and Child Health, Mbarara University of Science and Technology, Mbarara, Uganda

Author Contributions:

Conceived and designed the experiments: JMM JLG

Performed the experiments: JMM ACL KK MA WF

Analyzed the data: JMM ACL JLG

Contributed reagents, materials, and/or analysis tools: JB PO DO JB JM JLG

Wrote the paper: JMM ACL JLG

## 4.1 Introduction

In 2017, the World Health Organization (WHO) reported over 7 million annual cases of malaria and over 5 thousand attributable deaths in Uganda (WHO 2017; WHO 2018), which has the 6th highest number of malaria related fatalities per year in Africa (Ministry of Health 2016). The treatment of malaria is complicated on a global scale due to increased drug resistance to antimalarials including chloroquine (CQ), sulfadoxine-pyrimethamine (SP), mefloquine, and most recently, artemisinin (WHO 2015). CQ resistance is associated with mutations in the *P. falciparum* CQ resistance transporter (*pfcr*t) gene, which encodes a transmembrane protein localized to the parasite's digestive vacuole membrane (Djimde, et al. 2001). Mutations in residues 72-76 of *PfCRT* contribute to altered efflux of CQ from the vacuole, its site of action (Ecker, et al. 2012). The K76T mutation is a well-known marker of CQ resistance in Uganda (Dorsey, et al. 2001). While the normal haplotype across residues 72-76 is CVMNK, the mutant haplotype CVIET, confers the highest level of resistance (Fidock, et al. 2000a) and is the most common in Africa (Khalil, et al. 2005). The mutant SVMNT haplotype that is most common in South American isolates (Fidock, et al. 2000b; Keen, et al. 2007; Mehlotra, et al. 2001; Wellems and Plowe 2001) has a lower level of resistance compared to the CVIET haplotype (Sa and Twu 2010). This haplotype has recently been detected in Africa and surveillance of SVMNT is important due to possible cross-resistance to amodiaquine (Alifrangis, et al. 2006; Gama, et al. 2010).

Cessation of CQ use has led to the re-emergence of CQ-sensitive parasite populations in Malawi (Kublin, et al. 2003), Kenya and Tanzania (Mohammed, et al. 2013), Papua New Guinea (Sekihara, et al. 2018), and Eastern regions of Uganda (Mbogo, et al. 2014). Our goal in this study was to measure the prevalence of CQ resistance in Southwestern Uganda by assessing the *pfcr*t haplotypes using a PCR-based high-resolution melt (HRM) assay (Daniels, et al. 2012). HRM is a useful method in resource-limited settings due to its simplicity, cost, and sensitivity (Life Technologies Corporation 2009). HRM yields few false positives (Li, et al. 2011; Vossen, et al. 2009), exhibits high sensitivity and specificity (Kassaza, et al. 2018), and can be employed inexpensively to screen samples prior to sequencing (Vossen, et al. 2009).

Due to reports of artemisinin resistance in Southeast Asia, there is a need to find alternative effective antimalarial drugs (Ashley, et al. 2014; Dondorp, et al. 2010). One alternative therapy may be to revisit the once highly-effective antimalarial, CQ, and to pair it with new drug combinations (Untaroiu, et al. 2019; White 2016; Wirjanata, et al. 2017). We report 1) the persistence of CQ resistance in 2010 and 2015 and 2) significant regional variation across Southwestern Uganda. These results emphasize the need for local surveillance before CQ-based therapies are employed.

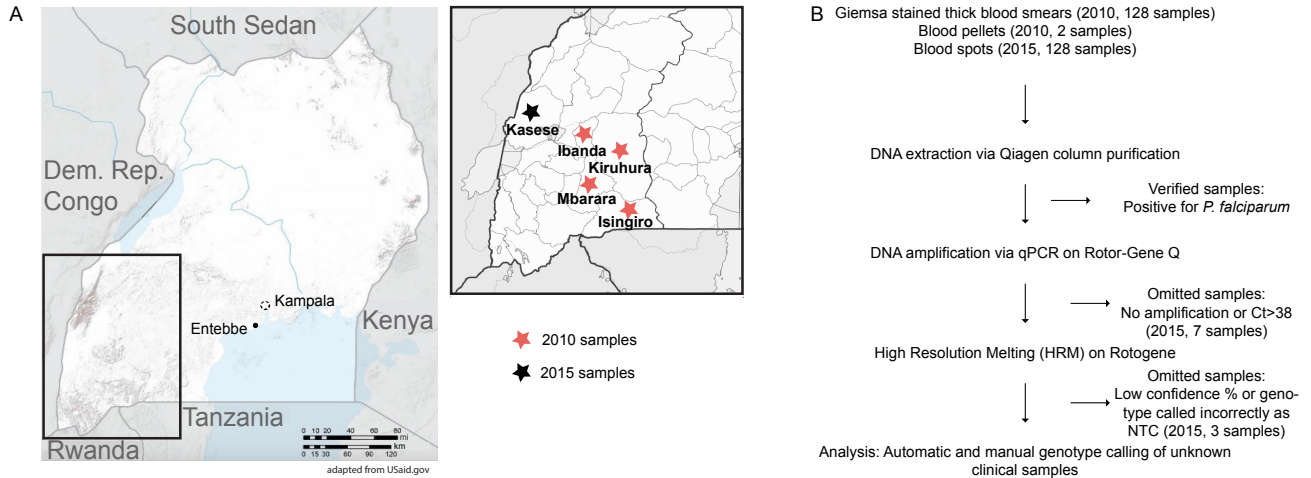


**Figure 17. Clinical sample collection sites in Uganda and schematic overview of methods for detection of pfCRT resistant and sensitive genotypes. A.** Samples were collected in Southwest Uganda in the districts of Ibanda, Isingiro, Kiruhura, and Mbarara in 2010 (orange stars) and the district of Kasese in 2015 (black star). **B.** Work flow of DNA isolation methods extracted from Giemsa stained thick blood smears, blood smears, and blood pellets used for 2010 samples or dried blood spots used for 2015 followed by HRM high resolution melting. Samples were omitted if DNA did not amplify, their Ct score was greater than 38, or confidence % was below a specific threshold, or genotype was incorrectly called as no template control (NTC). Of the 2015 samples, 10 were omitted and 118 samples were analyzed in this study.

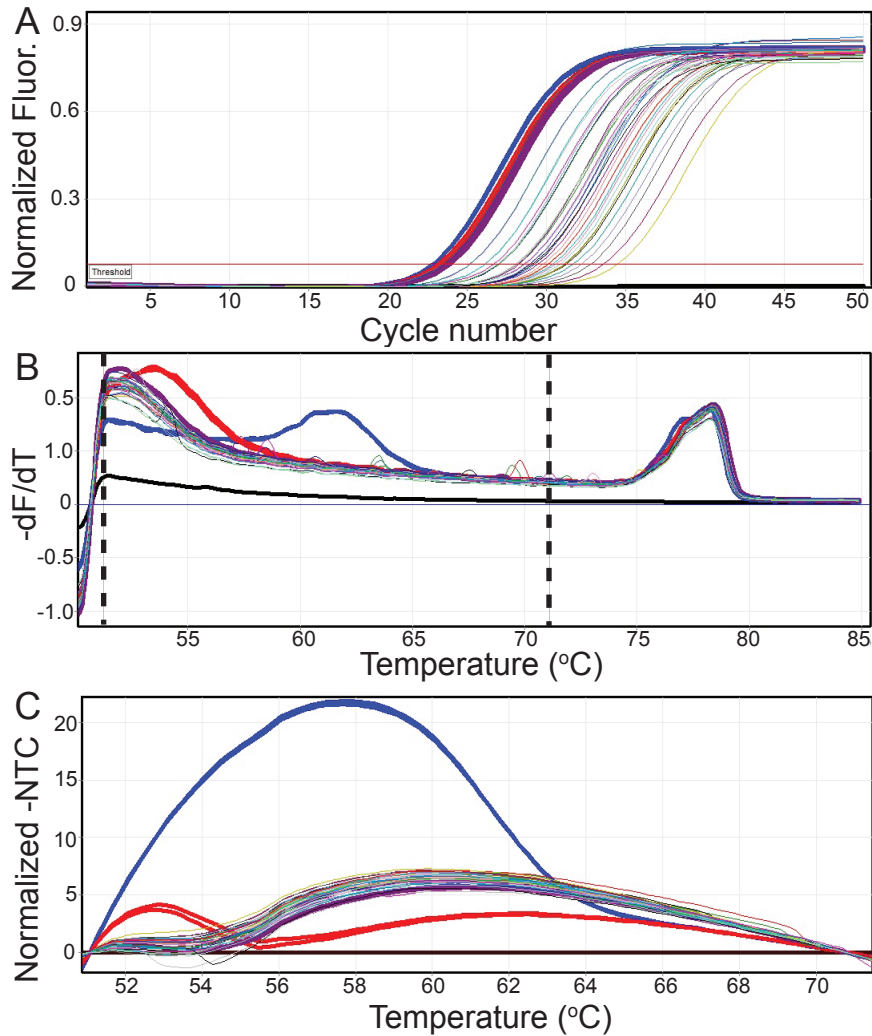


**Figure 18. PCR and HRM analysis.** Representative graphs of real time PCR and HRM of clinical samples (thin colored lines) and control samples (bold lines, blue: wild type control (CVMNK), red: mutant haplotype (SVMNT), and purple: mutant haplotype control (CVIET). **A.** Fluorescence-based real time detection of DNA amplification of clinical samples, genomic DNA, and no template controls. Horizontal red line denotes threshold, which was determined for each assay. **B.** A derivative plot displaying the melt analysis curve highlighting probe dissociation between normalization regions (denoted by dashed lines at 51 $^{\circ}\text{C}$  and 71 $^{\circ}\text{C}$ ). The change in fluorescence was recorded in 0.2 $^{\circ}\text{C}$  increments every 2sec. **C.**

Difference curve normalized to the no template control (NTC). All analysis was made using the Rotor-Gene Q software.

## 4.2. Results

### *4.2.1 Prevalence of CQ resistant genotypes in Southwestern Uganda*

A total of 248 total clinical samples were analyzed by HRM in this study (see results summarized in **Table 5**). A large majority of the 2010 samples were positive for the mutant, CVIET genotype (94.6%; 123/130 samples). Only ~5% (6/130 samples) showed the wild type, CVMNK haplotype. The CVIET genotypes were detected in 39% (46/118) of the 2015 samples. More than half of the 2015 samples (57.6%; 68/118) were positive for the CVMNK genotype. A single 2015 sample (1/118; 0.85%) was found to have a mutant SVMNT haplotype. However, due to a low confidence percentage (33.64%), we were unable to ensure accurate classification of this sample. Overall, only 4 clinical samples were detected as variations (1/130 and 3/118 from 2010 and 2015 samples, respectively); they had an unknown melting profile that was not identified to be CVMNK, SVMNK, or CVIET and produced a higher Ct score (**Table 5** and **Supplemental Figure 8**). A confidence value could not be assigned for these clinical samples for this reason. These variants could be novel CQ mutations, alternative haplotypes (non-CVMNK/SVMNT/CVIET), or mixed haplotypes (**Supplemental Table 5**).

To investigate this latter possibility, we first assessed the ability of the Rotor-Gene Q instrument to call mixed haplotypes using control samples at various ratios (90:10 (7G8:HB3), 50:50 (7G8:7C424), and 30:30:30 (HB3:7G8:7C424), see **Supplemental Figure 11**). Equally mixed samples (50:50) exhibited a prominent shoulder at a lower melting temperature.

**Table 5. Summary of *pfcr* genotypes.**

Year	Number of Samples Collected	Amino Acid Mutation	Phenotype	Number of Isolates (%)	Mean Confidence%	Mean Ct Value
2010	130	CVMNK	Wild type	6 (4.6) MaC: 2	84.60	30.21 MaC: 34.03
		<u>SVMNT</u>	Mutant	0 (0%) MaC:0	-	-
		<u>CVIET</u>	Mutant	123 (94.6) MaC:11	93.63	28.20 MaC: 34.14
		Unknown	Variation	1 (0.77) MaC:0	-	30.06
					Overall Mean: 93.63%	Overall Mean: 28.31
2015	118	CVMNK	Wild type	68 (57.6) MaC:0	88.24	31.06
		<u>SVMNT</u>	Mutant	1 (0.85%) MaC:0	*33.64	*26.79
		<u>CVIET</u>	Mutant	46 (39.0%) MaC:0	93.88	31.42
		Unknown	Variation	3 (2.5%) MaC:0	-	35.09
					Overall Mean: 91.06%	Overall Mean: 32.50

\*Denotes the exact value since an average could not be calculated; omitted from total average calculation.

Underline denotes amino acid changes that confers chloroquine (CQ) resistance and differs from CVMNK haplotype (CQ sensitive).

MaC, Manual Calls; CVMNK, Cys-Val-Met-Asn-Lys; SVMNT, Ser-Val-Met-Asn-Thr; CVIET, Cys-Val-Ile-Glu-Thr.

This shoulder was predicted to be from heteroduplex formation (a mixture of both genotypes present) and was less prominent in non-equal mixtures (30:30:30 and 90:10). The Rotor-Gene Q software did not have the capabilities to call the mixed haplotypes; as predicted, it called the predominant genotype with lower confidence. Given these findings, we manually reviewed any low confidence clinical samples and variation samples for the characteristic shoulder, but we failed to detect any samples with this instrument. Thus, mixed haplotypes were not likely the explanation for the variation calls and not common in our samples. Using the heteroduplex shoulder, we could manually identify mixtures of down to 10%, as seen with other HRM platforms (Andriantsoanirina, et al. 2009; Gan and Loh 2010); with Rotor-Gene Q, we were unable to reach a 1% detection limit as reported with mutant allele amplification bias (MAAB) on a LightScanner-32 instrument (Daniels, et al. 2012).

#### *4.2.2 HRM genotyping confidence and consistency*

Each sample was automatically called by the software and inspected manually for accuracy. Overall, the average confidence percentage produced by automatic calls was greater than 90% for CVMNK (wild type) or (CVIET) mutant parasites in both years (**Table 5**). Manual calls, which were made when a visual discrepancy was identified on the difference curve (**Supplemental Figure 10**), represented 8.5% of calls and were confined to 2010 samples (**Table 5**). We speculated that this could be due to the lower quality of DNA derived from Giemsa stained slides. In support of this, 2010 clinical samples that were manually called had higher mean Ct values than those called automatically (34.1 versus 29.2, **Table 5**). Additionally, a larger percentage of samples had to be repeated due to high Ct values, NTC or variant calls (~15% of the 2010 samples versus just ~3% of the 2015 samples

solely derived from blood spots) (**Supplemental Table 5**). Supporting the reliability of genotype calls, there was an inverse correlation between Ct value and confidence percentage for both sample sets with a p value of 2.243e-9 and R<sup>2</sup> value of 0.0968 (**Supplemental Figure 12**). Based on Ct values and confidence percentages, we did not observe a difference in performance between the reaction mixes used in these studies (**Supplemental Figure 8**). Samples analyzed from 2010 were collected from Giemsa stained slides and blood pellets using the LightScanner mix whereas samples analyzed from 2015 were collected from blood spots using the HotStarTaq mix. Assay performance was also similar by assigned Ct value and confidence percentages (**Supplemental Figure 6**). Thus, HotStarTaq and LightScanner mix are comparable mixes that can be used for similar high resolution melt assays for haplotype detection.

### 4.3. Discussion

With the discovery of artemisinin resistance (Dondorp, et al. 2010; Mbengue, et al. 2015; Straimer, et al. 2015), our catalog of effective antimalarials is dwindling. In response to growing resistance, there is a need to evaluate past effective treatments like CQ. Recent studies have assessed the response of parasite populations to CQ drug cessation in some African countries (Fidock, et al. 2000b; Kamugisha, et al. 2012; Keen, et al. 2007; Kiarie, et al. 2015; Mbogo, et al. 2014; Simon-Oke 2017), but there has been limited research on this topic conducted in Southwestern Uganda; patterns in Tororo, located in Eastern Uganda, have been the most documented.

In this study, we measured the prevalence of CQ resistance haplotypes in parasite populations from Southwestern Uganda. Clinical samples used in this

study were collected in 2010 and 2015. Using HRM-based assays, we observed persistence of the *pfcr*t resistance mutations in majority of *P. falciparum* parasites (~68.5% overall, 170 out of 248 total samples). One explanation for the delay in the return of sensitive parasites to Southwestern Uganda could be the continued use of therapeutic CQ. Indeed, up until recently, CQ paired with SP was still used as a combination therapy in home-based care (Frosch, et al. 2011; Kamugisha, et al. 2012; Ucakon, et al. 2011; Uganda 2016). CQ is also used as a pre-hospital medication for children with fevers (Tumwebaze, et al. 2017) and as a malaria prophylactic for children with sickle cell anemia (Nakibuuka, et al. 2009). Regional sources of CQ may have been prepared with lower doses or used in suboptimal treatment regimens, which may have exacerbated this effect (Asua, et al. 2019; Mulindwa, et al. 2002; Uganda 2016). Fortunately, the implementation of the CQ importation ban in 2009 will likely help to decrease CQ pressure on local parasites (Nabyonga-Orem, et al. 2014). Additionally, high quality, evidenced based studies on drug efficacy are helping to refine malaria treatment policies in Uganda (Nabyonga-Orem, et al. 2014).

The dominant presence of the mutant CVIET haplotype in our samples (**Table 5**) is consistent with what has been observed in other areas of Uganda and throughout sub-Saharan Africa during a similar time frame (Kamugisha, et al. 2012; Keen, et al. 2007; Mbogo, et al. 2014; Tumwebaze, et al. 2017). A similar persistence of CQ resistance has been reported in more recent years (Asua, et al. 2019; Ocan, et al. 2019; Rasmussen, et al. 2017). A study conducted in Tororo, Uganda in 2012 reported that 67% of samples exhibited the CVIET haplotype (Mbogo, et al. 2014). Similar to our study, the mutant SVMNT haplotype was not detected. Our data indicate that other haplotypes are not likely to be present in

these clinical samples; wild type CVMNK and mutant CVIET haplotypes together covered 99.2% of samples from 2010 and 96.6% of the samples from 2015. Despite this result, it is possible that other minor resistance haplotypes have moved into the area (i.e. CVIEK which has been detected in Sudan in 2000 (Fidock, et al. 2000b) and in Nigeria in 2015 (Zhou, et al. 2016)). However, further studies would be needed to explore this possibility in Uganda.

While we did detect a decline in highly resistant CQ parasites (from 94.6% in 2010 to 39% in 2015, Table 1), persistence at such levels 10-15 years following CQ monotherapy abandonment in 2000 highlights the slow progression back to sensitivity. A comparable trend was observed in other African countries; after 13 years of cessation in Kenya and 10 years of cessation in Nigeria, parasites harboring the CVIET haplotypes were observed at 41% and 95% prevalence, respectively (Kiarie, et al. 2015; Simon-Oke 2017). Similarly in Asia, greater than 50% prevalence of resistant parasites remained 20 years after cessation in China and resistance prevalence decreased by <10% after 8 years in Papua New Guinea (Liu, et al. 1995; Sekihara, et al. 2018; Wang, et al. 2005). The persistence of CQ resistance in these areas are counter to the almost complete return of CQ sensitivity observed in Malawi and Tanzania just 10 years after drug cessation (Laufer, et al. 2006; Mohammed, et al. 2013).

Since there has been apparent persistence of CQ resistance in the population (100% CVIET between 1998-2008) (Frosch, et al. 2011), our current report showing reduced prevalence of resistant parasites is mildly encouraging (39.0% CVIET in 2015 from Kasese). If CQ resistance is no longer consistently detected in the region, CQ may be part of a future effective combination therapy. Possible combinations include fosmidomycin or SP (Untaroiu, et al. 2019) or

pairing CQ with a reversal agent, for example, verapamil, chlorpheniramine, and cyproheptadine (Wirjanata, et al. 2017). Other possibilities include changing the CQ side chain by adding AQ-13, which is active against CQ resistant parasites, or using a CQ-related molecule called ferroquine paired with artesunate (Wirjanata, et al. 2017); (White 2016). CQ resistance reversal agents (CQRRAs) increase the organism's susceptibility to the drug without any deleterious effects; however, the mode of action of CQRRAs is not well understood (Wirjanata, et al. 2017). This approach may limit the return of resistant parasites to the area, but resistance dynamics are hard to predict.

We acknowledge some limitations of the current study. Firstly, the different resistant profiles that we observed between 2010 and 2015 samples could be due to factors related to location (instead of time). Our samples were collected from 2 districts of Southwestern Uganda that are separated by ~280km. There is evidence for significant regional variation in resistance rates during similar time periods, even in sites just 100km apart (compare Iganga (Kamugisha, et al. 2012) with Tororo (Mbogo, et al. 2014)). This could be due to variations in cultural practices and/or antimalarial use and availability. Certainly, parasites in Kasese (collected in 2015, ~40% resistance) may be under different selective forces than parasites in Mbarara (collected in 2010, ~95% resistance). This significant regional variation emphasizes the need to perform *local* assessment of resistant profiles to influence treatment policies. Of note, recent studies investigated the resistance profiles across Uganda that included 2 districts in Southwestern Uganda, which were Kanungu and Kabale (Asua, et al. 2019; Tumwebaze, et al. 2017). Similarly, these authors also reported differences in resistance profiles within a single country and a slow reversal to CQ sensitivity. High throughput surveillance may be possible

with the introduction of new tools such as the malaria-TaqMan Array Card (Pholwat, et al. 2017).

#### 4.4. Conclusions

In conclusion, we report the persistence of highly resistant CQ parasites in Southwestern Uganda. The results of this study suggest that there is still selection for CQ resistance in this area. The significant regional variation in Uganda, as well as other areas of the world, emphasizes the need to perform *local* assessment of resistant profiles to inform treatment policies. Further surveillance is required to determine if resistance will decline, as it has in other African countries, so that CQ may be considered as part of effective combination therapies against *P. falciparum* infection.

#### 4.5 Materials and methods

##### 4.5.1 Study area and clinical isolates

Southwestern Uganda is mesoendemic for malaria with a tropical climate with 2 peaks of high transmission (September-January and March-May) that occur following the rainy seasons (Ojuka, et al. 2015). The samples used in this study were originally collected during previous cross-sectional studies performed across Southwestern Uganda by Epicentre Mbarara Research Centre, a research arm of Médecins sans Frontières, and Mbarara University of Science and Technology (Boyce, et al. 2015; Oyet, et al. 2017), see **Figure 17A** and details below.

The 2010 samples were collected during household surveys of children <5 years old from the districts of Ibanda, Isingiro, Kiruhura, and Mbarara (Kassaza, et

al. 2018; Oyet, et al. 2017). Participants in this survey ranged from 6-60 months of age and sampling was performed during the low transmission season (Oyet, et al. 2017). The 2015 samples were collected from children between <5, 5-15, and >15 years of age during a study of rapid diagnostic tests for the identification of severe malaria from the district of Kasese in Southwestern Uganda (Boyce, et al. 2015). Likewise, samples were collected from children during low transmission season and extended during the high transmission season. In the 2010 and 2015 studies, children included in this study were diagnosed with malaria and confirmed by rapid diagnostic tests (RDT) and microscopy. The peak incidence of malaria in Uganda occurs in children <5 years (WHO 2017; WHO 2018).

#### *4.5.2 Clinical sample preparation*

Genomic DNA was extracted from blood pellets, blood spots, and Giemsa stained slides described in **Figure 17B**. Of the 130 total clinical samples included from the 2010 collections, 128 DNA samples were extracted by scraping Giemsa stained thick blood smears followed by column purification and 2 DNA samples were from frozen blood pellets (total volume of 100µl) as previously reported (Kassaza, et al. 2018). These samples were also previously verified positive for *P. falciparum* using a species-specific HRM assay (Kassaza, et al. 2018). A total of 118 samples were included from the 2015 collections and the DNA used in the following studies were all extracted from blood spots using the QIAamp DNA Mini Kit (Qiagen Inc., Germantown, Maryland, USA). A subset of these samples were verified positive for *P. falciparum* prior to proceeding (Kassaza, et al. 2018). All sample types (blood pellets, blood spots, and Giemsa stained slides) were successfully PCR amplified with acceptable mean cycle threshold (Ct) values (35.0, 32.5, and 28.3,

respectively, for a mean of 28.3 for 2010 samples and 32.5 for 2015 samples, **Supplemental Figure 6A and B**) at the Epicentre Mbarara Research Centre. The Epicentre laboratory is in compliance with the National Health Laboratory Services, South Africa.

#### 4.5.3 Reference DNA and gene loci

*P. falciparum* genomic DNA controls were included in each run to validate assay performance and assign genotypes to the clinical samples. Genomic DNA from three *P. falciparum* reference strains with known *pfcr* haplotypes (GenBank accession number NC\_004328.2:458600-461695, gene ID: 2655199) were obtained from BEI resources (NIAID, NIH, Manassas, VA, USA): *P. falciparum* HB3 (wild type CVMNK haplotype, MRA-155G, contributed by Thomas E. Wellems), 7G8 (mutant haplotype SVMNT, MRA-152G, contributed by David Walliker), 7C424 (mutant haplotype CVIET, MRA-175G, contributed by Thomas E. Wellems). To ensure accurate genotyping, each control line was sequenced and confirmed for correct *pfcr* mutations (**Supplemental Figure 7**). Control samples provided reproducible melt curves which were used to determine the correct genotype of clinical samples with heightened confidence.

#### 4.5.4 Real time PCR assays and cycling

The Rotor-Gene Q real-time PCR cycler (Qiagen Inc.) with a 72-well rotor was used for both PCR and HRM steps. Primers and probe with modified C3 spacer were purchased from Integrated DNA Technologies (IDT, Inc., Coralville, Iowa, USA). The primers and probe used were as follows (Daniels, et al. 2012): Forward Primer: 5'-GTAAAACGACGGCCAGTTTCTTGTCTTGGTAAATGTGCTCA-3', Reverse Primer: 3'-CAGGAAACAGCTATGACCGGATGTTACAAAACCTATAGTTACCAAT-5', HRM

Probe: 5'-GTGTATGTGTAATGAATAAAATTTTTG(3SpC3)-3'. Asymmetric PCRs were performed with reverse primer in 10-fold excess to promote the accumulation of single stranded DNA for probe binding (Sanchez, et al. 2004). The unlabeled HRM probe detected mutations across the 72-76 codon region. The C3 spacer on the end of the probe was necessary to prevent extension of the probe during PCR amplification. During the HRM steps, the probes disassociated from the mutant and wild type template DNA at distinct melting temperatures (Daniels, et al. 2012).

Two PCR master mixes were used over the course of this study due to varying accessibility of reagents LightScanner Master mix (BioFire™ Defense, Salt Lake City, Utah, USA) or HotstarTaq Master mix (Qiagen Inc.) paired with 10x LCGreen Melting Dye (BioFire™ Defense, Salt Lake City, Utah, USA). We did not detect differences in assay performance using the two mixes (**Supplemental Figure 8**). For LightScanner assays, the following components were added per 20µL reaction: 8µL of 2.5x LightScanner master mix, forward primer (1µM final), reverse primer (10µM final), probe (8µM final), and 3µL of sample DNA, reference DNA (1 ng), or nuclease-free water (no template control, NTC). For HotStarTaq assays, the following components were added per 20µL reaction: 10µL of 2x HotStarTaq master mix, 1µL of 10x LC Green, forward primer (1µM final), reverse primer (10µM final), probe (8µM final), and 3µL of sample DNA, reference DNA (1ng) or nuclease-free water (NTC). Sample material was not normalized prior to amplification because DNA purified from clinical samples contains both human and parasite genomes. However, through the use of parasite DNA controls of known concentration (HB3, 7G8, 7C424), we were able to estimate the clinical parasite DNA concentration range to be between ~1ng and 10<sup>-5</sup>ng. We also estimated the lowest DNA concentration used in this study and detected by HRM was between

$10^{-4}$  and  $10^{-5}$ ng per sample. This limit of detection for HRM has been published by other groups (Andriantsoanirina, et al. 2009; Daniels, et al. 2012; Gan and Loh 2010) and it allowed us to establish the Ct cutoff of 38 for our studies (i.e. samples with resulting Ct values of  $>38$  were excluded from our analysis).

PCR cycling conditions were performed with an initial 2min hold for LightScanner assays (15min hold for HotStarTaq assays) at  $95^{\circ}\text{C}$  followed by 50 cycles of  $90^{\circ}\text{C}$  for 30sec,  $60^{\circ}\text{C}$  for LightScanner assays ( $56^{\circ}\text{C}$  for HotStarTaq assays) for 30 sec, and  $72^{\circ}\text{C}$  for 30sec. Fluorescence data was acquired during the  $72^{\circ}\text{C}$  step. The last cycle was followed by a  $98^{\circ}\text{C}$  hold for 2min and a  $40^{\circ}\text{C}$  hold for 2min before continuing to the HRM analysis (see section 4.5.5). Fluorescence intensities of clinical samples, genomic DNA controls, and NTC were recorded in real time throughout amplification cycles, which was used to determine the cycle threshold values for each assay (**Figure 18A**).

#### *4.5.5 High Resolution Melt (HRM) parameters and analysis*

Following real time PCR conditions, the melting curve program consisted of the following: a 90 sec step of pre-melt conditioning at  $50^{\circ}\text{C}$  followed by an increase of temperature from  $50^{\circ}\text{C}$  to  $90^{\circ}\text{C}$  in  $0.2^{\circ}\text{C}$  increments every 2sec. The change in fluorescence was measured at each increment. Manual gain optimization settings were as follows: Set for  $60^{\circ}\text{C}$ , HRM gain optimization was turned on at tube position 1, and set to select the highest fluorescence less than 70. Gain was set to a minimum and maximum reading of 1FI and 3FI, and a minimum and maximum gain of -10 and 10. Rotor-Gene Q Series Software version 2.2.1, Build 49 (Qiagen Inc.) was used for analysis of PCR and HRM data. Melt analysis curves were normalized between  $51^{\circ}\text{C}$  and  $71^{\circ}\text{C}$  (manually set) to capture the melting of the unlabeled probe from the full template (**Figure 18B**). Narrower normalization

regions were assessed and did not change the outcome of our analysis (**Supplemental Figure 9**).

Unknown clinical samples were automatically called by the Rotor-Gene Q software against the known genomic DNA controls, which produced reproducible HRM profiles. The difference curve, normalized to the NTC, was used to compare the melting profile of the probe/template duplexes (**Figure 18C**). The confidence percentage threshold was set to 20% to allow for low confidence calls to be recognized by the software. Confidence percentages were used as an integrity check. Values that fall above the threshold were subject to auto-calls predicted by the software and values that fell below the threshold were called as a “variation” and were re-tested (described in **Figure 17B**) (Life Technologies Corporation 2009). If the amplitude or shape of the sample curve was different than the controls, the genotype was also determined by the program to be a “variation”. For increased accuracy, each automatic call was manually inspected through visual comparison of the normalized difference curve (**Figure 18C**). If a mistake in the genotype call was plainly discernible due to a visual discrepancy in the automatic genotype call and the difference curve, then a “manual call” was made. Examples of manual calls (MaC) are detailed in (**Supplemental Table 5** and **Supplemental Figure 10C**).

#### *4.5.6 Data quality control*

A Ct cutoff of 38 was used (see **Figure 18A**). The combination of the Ct value, confidence percentage, and manual inspection allowed for heightened confidence in correct genotype calling. Samples were repeated if their Ct was greater than 38, if they failed to amplify on the first run, or if an abnormal genotype needed to be

verified (see **Figure 17B**). Samples were omitted in three scenarios: 1) there was no amplification of the DNA and, therefore, no Ct value, 2) the Ct value of the samples were repeatedly above the 38 Ct cutoff, and 3) the samples displayed an acceptable Ct value, but the genotype call was “NTC” (no template control) (**Figure 17B**). NTC melt curves were flat and did not resemble any of the positive controls (*data not shown*). Of the 2015 samples, 10 were omitted and 118 samples were analyzed in this study (**Figure 17B**). Repeat samples that gave inconsistent calls were removed from the final analysis (identified in **Supplemental Table 5**). Of the 2010 and 2015 repeat samples, 17/19 (~78%) and 4/4 (100%) gave consistent calls, respectively.

#### *4.5.7 Statistical analysis*

Box plots were generated using Graphpad Prism 7.0 (GraphPad Prism, La Jolla, CA). Scatter plots were generated using the data visualization package ggplot2 in R package version 1.1.383 (R foundation for Statistical Computing, Vienna, Austria). A p value of <0.05 by an unpaired t test was considered significant.

**Supplemental Table 5. High Resolution Melt analysis of clinical samples.**

<u>2010 samples</u>				<u>2015 samples</u>			
Name	Ct	Genotype	Confidence%	Name	Ct	Genotype	Confidence%
b,g3_12_2	28.66	CVIET	86.81	a,sM010	33.23	CVIET	75.72
b,g10_1_1	29.81	CVIET	94.61	a,sM013	35.04	CVIET	65.11
b,g10_16_2	29.93	CVIET	92.70	a,sM033	31.42	CVIET	88.34
b,g10_2_2	34.41	CVIET	MaC	a,sM038	32.26	CVIET	68.24
b,g10_4_1	30.16	CVIET	93.50	a,sM041	32.59	CVIET	55.10
b,g10_9_2	29.34	CVIET	95.86	a,sM057	29.85	CVIET	96.90
b,g,r11_1_1	22.38	CVIET	99.60	a,*s,rM087	38.98	CVIET	97.80
b,g11_1_2	21.9	CVIET	98.74	a,sM089	35.46	CVIET	76.06
b,g,r11_12_1	30.41	CVIET	91.27	a,sM092	27.55	CVIET	95.78
b,g11_14_1	23.1	CVIET	93.69	a,sM094	29.44	CVIET	92.53
b,g11_2_2	22.46	CVIET	93.30	a,sM096	33.26	CVIET	77.92
b,g11_3_1	27.26	CVIET	95.45	a,sM098	26.57	CVIET	80.27
b,g11_3_2	24.99	CVIET	96.26	a,sM101	31.17	CVIET	99.07
b,g11_6_1	24.61	CVIET	95.99	a,sM111	31.02	CVIET	99.01
b,g11_8_1	26.27	CVIET	97.63	a,sM114	26.34	CVIET	96.56
b,g,r13_1_1	33.82	CVIET	74.77	a,sM119	29.71	CVIET	93.30
b,g13_3_1	30.05	CVIET	89.07	a,sM124	28.58	CVIET	97.15
b,g13_5_1	25.31	CVIET	88.28	a,sM127	28.47	CVIET	95.03
b,g13_8_1	25.07	CVIET	93.18	a,sM128	37.37	CVIET	92.88
b,g14_10_1	22.32	CVIET	94.26	a,sM129	25.27	CVIET	98.81
b,g14_8_1	30.54	CVIET	94.11	a,sM134	26.44	CVIET	62.60
b,g15_10_1	33.77	CVIET	83.25	a,sM140	30.55	CVIET	99.41
b,g15_11_1	23.18	CVIET	99.15	a,sM158	26.89	CVIET	99.53
b,g15_13_1	29.53	CVIET	86.56	a,sM149	30.00	CVIET	99.83
b,g17_13_1	29.08	CVIET	95.96	a,sM162	35.78	CVIET	92.89
b,g17_14_1	27.61	CVIET	98.00	a,sM166	27.15	CVIET	93.02
b,g17_15_1	32.04	CVIET	87.70	a,sM168	32.39	CVIET	97.42
b,g17_5_1	24.95	CVIET	98.38	a,sM169	30.04	CVIET	99.50
b,g17_8_1	28.54	CVIET	98.73	a,sM172	27.37	CVIET	98.55
b,g18_11_2	25.53	CVIET	97.51	a,sM173	24.7	CVIET	99.63
b,g18_11_3	32.90	CVIET	87.09	a,sM180	26.65	CVIET	94.82
				a,sM188	26.56	CVIET	99.82

b,g18_14_1	28.38	CVIET	97.71	a,sM189	27.52	CVIET	91.88
b,g18_5_1	28.94	CVIET	89.88	a,sM190	35.99	CVIET	98.54
b,g18_8_1	22.86	CVIET	96.80	a,sM191	29.46	CVIET	99.00
b,g19_12_2	30.99	CVIET	91.15	a,sM193	24.79	CVIET	89.52
b,g19_13_1	28.90	CVIET	96.61	a,sM194	37.12	CVIET	80.53
b,g19_2_1	28.31	CVIET	93.02	a,sM201	29.34	CVIET	99.05
b,g19_4_1	26.40	CVIET	98.48	a,sM202	31.95	CVIET	93.55
b,g19_8_1	33.73	CVIET	MaC	a,sM204	33.63	CVIET	96.58
b,g2_11_1	27.63	CVIET	91.03	a,sM205	24.64	CVIET	99.20
b,g2_11_2	28.82	CVIET	97.52	a,sM208	27.62	CVIET	99.42
b,g2_14_1	26.29	CVIET	98.56	a,sM209	30.09	CVIET	97.63
b,g2_2_1	27.94	CVIET	97.94	a,sM215	27.66	CVIET	63.64
b,g2_4_2	25.52	CVIET	95.16	a,sM182	31.78	CVIET	99.57
b,g,r2_7_1	34.75	CVIET	MaC	a,sM183	31.53	CVIET	99.14
b,g20_2_1	25.25	CVIET	93.67	a,sM007	29.14	CVIET	99.38
b,g20_7_2	24.16	CVIET	98.57	a,sM020	33.67	CVIET	97.52
b,g20_7_3	25.25	CVIET	91.51	a,sM027	29.64	CVIET	98.01
b,g,r21_1_1	31.30	CVIET	MaC	a,sM028	34.83	CVIET	95.14
b,g21_1_2	30.13	CVIET	84.82	a,sM029	30.02	CVIET	98.88
b,g21_4_7	25.26	CVIET	99	a,*sM054	39.71	SVMNT	23.02
b,g22_13_1	33.50	CVIET	88.20	a,*sM077	39.30	SVMNT	24.38
b,g,r22_7_1	30.32	CVIET	90.96	a,s,rM140	26.79	SVMNT	33.64
b,g23_13_1	27.92	CVIET	93.84	a,sM061	34.37	Variation	
b,g23_16_1	21.65	CVIET	97.02	a,sM065	36.94	Variation	
b,g,r23_5_1	33.19	CVIET	81.43	a,sM082	33.96	Variation	
b,g23_6_2	26.12	CVIET	98.55	a,*sM053		NTC	99.23
b,g23_9_1	31.64	CVIET	90.25	a,*sM056		NTC	98.68
b,g24_11_1	28.09	CVIET	99.35	a,*sM074		NTC	97.28
b,g24_2_3	27.44	CVIET	97.32	a,sM034	36.86	CVMNK	62.08
b,g24_2_4	26.39	CVIET	97.31	a,sM043	31.04	CVMNK	99.48
b,g,r24_4_1	21.73	CVIET	99.75	a,sM045	37.61	CVMNK	80.62
b,g24_7_1	33.27	CVIET	85.77	a,sM048	32.06	CVMNK	97.22
b,g25_5_1	25.58	CVIET	99.07	a,sM058	35.57	CVMNK	87.99
b,g,r25_8_2	22.26	CVIET	99.91	a,sM059	32.60	CVMNK	97.48

b,g27_1_1	35.30	CVIET	MaC	a,sM062	33.36	CVMNK	68.48
b,g27_8_1	34.42	CVIET	86.96	a,sM064	32.3	CVMNK	95.70
b,g28_7_2	25.74	CVIET	94.03	a,sM066	33.16	CVMNK	95.06
b,g29_1_1	20.53	CVIET	98.33	a,sM068	33.89	CVMNK	96.14
b,g29_11_1	31.76	CVIET	84.92	a,sM073	34.78	CVMNK	74.32
b,g29_4_1	22.24	CVIET	88.87	a,sM075	34.09	CVMNK	95.01
b,g29_4_2	23.12	CVIET	98.79	a,sM079	31.48	CVMNK	98.07
b,g3_5_1	23.93	CVIET	94.64	a,sM085	32.30	CVMNK	92.71
b,g3_6_1	24.61	CVIET	91.34	a,s,rM086	23.47	CVMNK	56.67
b,g3_9_1	27.46	CVIET	97.48	a,sM095	34.82	CVMNK	93.16
b,g32_13_18	23.16	CVIET	94.53	a,sM099	33.95	CVMNK	94.81
b,g33_13_1	29.24	CVIET	91.65	a,sM100	32.36	CVMNK	97.28
b,g34_15_1	30.44	CVIET	92.13	a,sM106	25.53	CVMNK	99.47
b,p,r35_8_1	34.85	CVIET	MaC	a,sM109	28.85	CVMNK	86.94
b,g37_4_1	26.47	CVIET	97.03	a,sM113	30.47	CVMNK	99.80
b,g4_10_1	23.65	CVIET	99.04	a,sM115	35.46	CVMNK	94.69
b,g4_11_1	30.59	CVIET	89.34	a,sM116	31.98	CVMNK	60.53
b,g4_6_1	31.38	CVIET	89.85	a,sM121	32.35	CVMNK	70.77
b,p,r4_7_2	35.20	CVIET	MaC	a,sM122	37.89	CVMNK	98.51
b,g4_7_3	27.71	CVIET	96.38	a,sM125	25.10	CVMNK	93.99
b,g46_10_3	28.00	CVIET	96.90	a,sM126	33.81	CVMNK	96.27
b,g46_4_1	25.74	CVIET	97.93	a,sM130	32.22	CVMNK	99.23
b,g53_8_1	28.29	CVIET	93.82	a,sM132	32.42	CVMNK	79.70
b,g,r55_1_2	27.57	CVIET	97.35	a,sM133	34.40	CVMNK	69.69
b,g56_12_1	33.59	CVIET	MaC	a,s,rM141	33.20	CVMNK	92.68
b,g56_12_2	31.01	CVIET	85.21	a,sM159	26.38	CVMNK	99.84
b,g60_10_3	27.41	CVIET	91.44	a,sM160	32.73	CVMNK	91.62
b,g62_02_1	26.92	CVIET	94.09	a,sM161	30.81	CVMNK	81.03
b,g62_4_1	28.68	CVIET	89.34	a,sM165	27.56	CVMNK	98.80
b,g63_9_1	28.66	CVIET	91.94	a,sM167	27.67	CVMNK	99.55
b,g64_14_1	27.52	CVIET	99.41	a,sM174	26.75	CVMNK	99.60
b,g64_16_1	25.56	CVIET	95.25	a,sM175	28.35	CVMNK	98.17
b,g64_9_1	23.13	CVIET	97.59	a,sM178	30.15	CVMNK	57.18
b,g65_16_1	35.79	CVIET	79.70	a,sM179	27.91	CVMNK	98.04

b,g,r7_9_1	36.31	CVIET	MaC	a,sM184	30.34	CVMNK	95.50
b,g8_11_1	25.89	CVIET	96.07	a,sM185	26.54	CVMNK	99.43
b,g8_14_1	27.27	CVIET	98.86	a,sM187	28.39	CVMNK	98.22
b,g8_4_1	28.96	CVIET	95.27	a,sM192	33.98	CVMNK	92.98
b,g9_11_1	28.46	CVIET	97.73	a,sM195	34.35	CVMNK	87.80
b,g9_12_1	29.77	CVIET	95.87	a,sM197	27.81	CVMNK	91.82
b,g9_2_1	24.67	CVIET	95.61	a,sM198	29.22	CVMNK	98.04
b,g9_3_1	26.81	CVIET	89.47	a,sM200	35.13	CVMNK	53.14
b,g9_4_1	28.87	CVIET	95.61	a,sM203	30.27	CVMNK	97.64
b,g9_6_1	30.50	CVIET	92.10	a,sM211	34.63	CVMNK	92.47
b,g9_6_2	28.50	CVIET	98.32	a,sM212	33.31	CVMNK	97.50
b,g9_7_2	28.31	CVIET	99.33	a,sM213	26.25	CVMNK	67.39
b,g9_9_1	30.08	CVIET	92.32	a,sM214	30.37	CVMNK	99.63
b,g,r13_9_1	30.06	Variation		a,sM016	37.40	CVMNK	77.98
b,g21_1_1	26.14	CVMNK	99.18	a,sM210	33.59	CVMNK	89.56
b,g27_1_2	26.03	CVMNK	63.62	a,sM002	31.54	CVMNK	85.22
b,g,r27_2_1	30.75	CVMNK	MaC	a,sM021	30.22	CVMNK	83.11
b,g44_5_4	37.30	CVMNK	MaC	a,sM030	31.22	CVMNK	50.38
b,g48_11_1	30.57	CVMNK	77.10	a,sM031	31.97	CVMNK	97.43
b,g55_1_2	30.44	CVMNK	98.51	a,sM035	31.81	CVMNK	90.95
				a,sM199	40.27	CVMNK	56.81
				a*,sM083	38.79	CVMNK	67.30
				a*,sM069	39.72	CVMNK	59.30
				a*,sM060	38.34	CVMNK	73.20
				a*,sM012	41.07	CVMNK	43.43

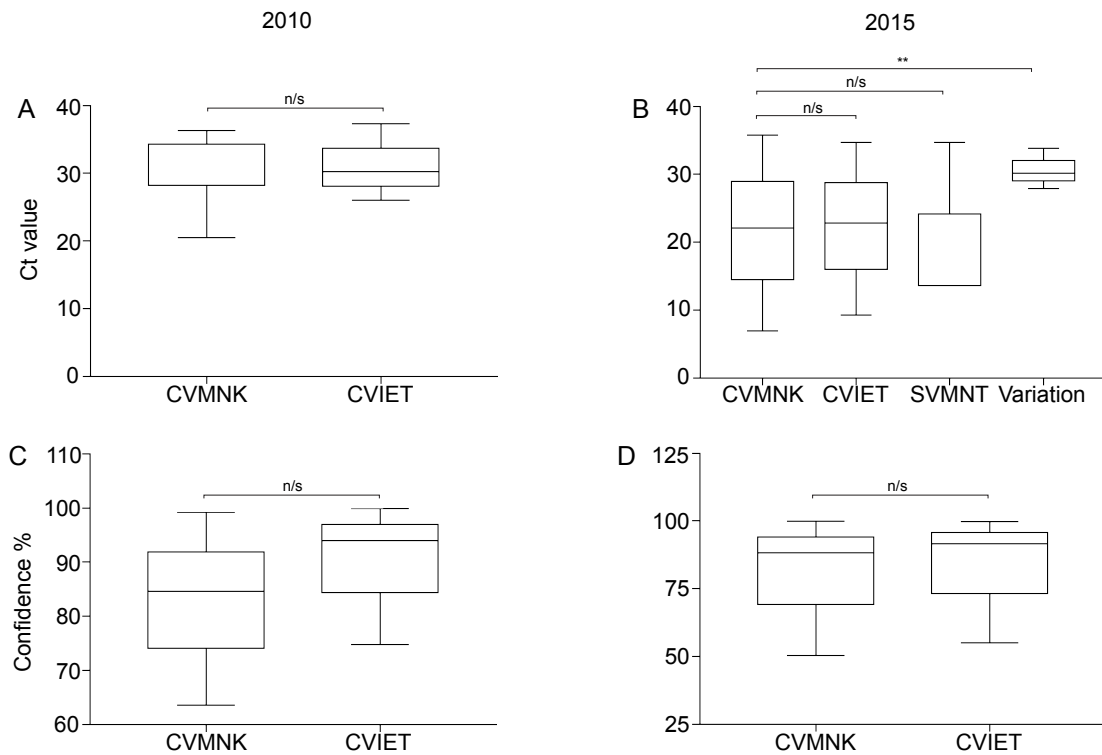
<sup>a</sup>denotes HotstarTaq reaction mix and <sup>b</sup> LightScanner reaction mix

\*denotes omitted samples if Ct value >38 or if genotype incorrectly calls as no template control (NTC)

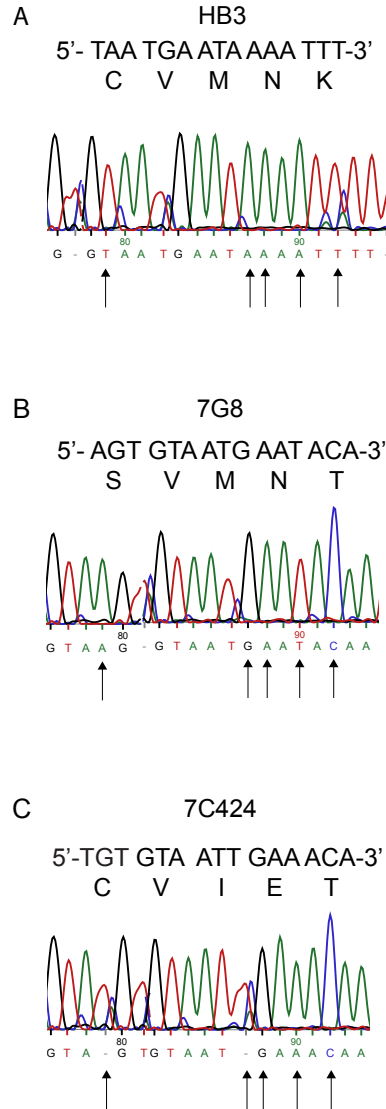
<sup>s</sup>denotes blood spots, <sup>p</sup>blood pellets, and <sup>g</sup>Giemsa-stained slides

<sup>r</sup>denotes samples that were repeated during the assay

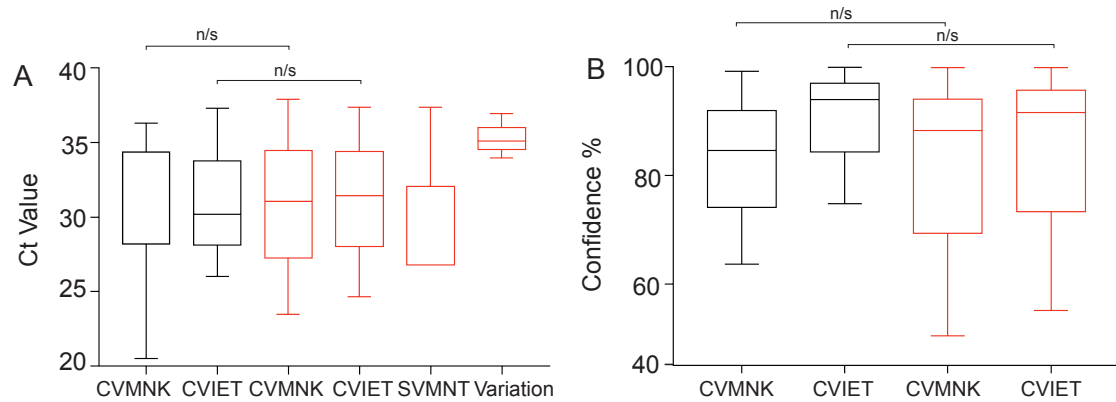
CVMNK, wild type control; SVMNT, mutant; CVIET, mutant; MaC, manual calls



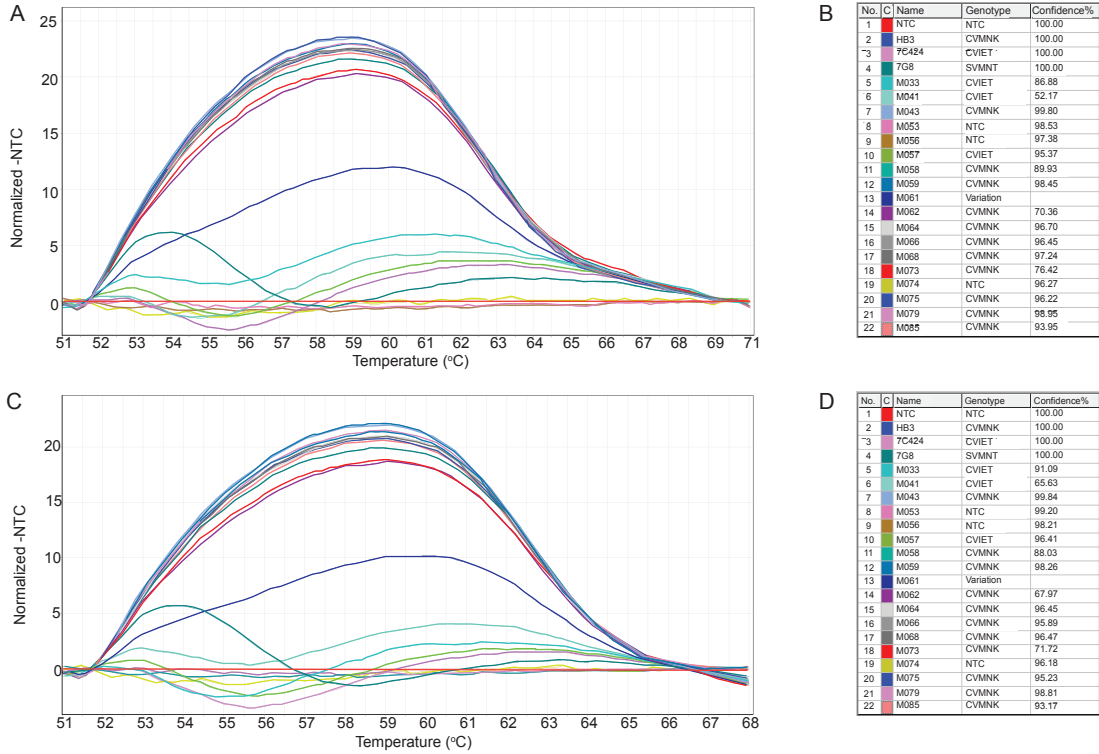
**Supplemental Figure 9. Evaluation of Ct values and confidence % by High Resolution Melt (HRM) assay.** Box plots showing average Ct values from 2010 (A) and 2015 (B) and confidence % from 2010 (C) and 2015 (D) from HRM analysis. Confidence values are automatically assigned by Rotor-Gene Q software to each sample according to their HRM melt profiles. Error bars reflect 95% confidence intervals. \*\*p=0.001, CVMNK vs variation; n/s (not significant), p>0.05. Variation are genotype calls below 95% confidence. CVMNK, wild type; SVMNT, mutant; CVIET, mutant.



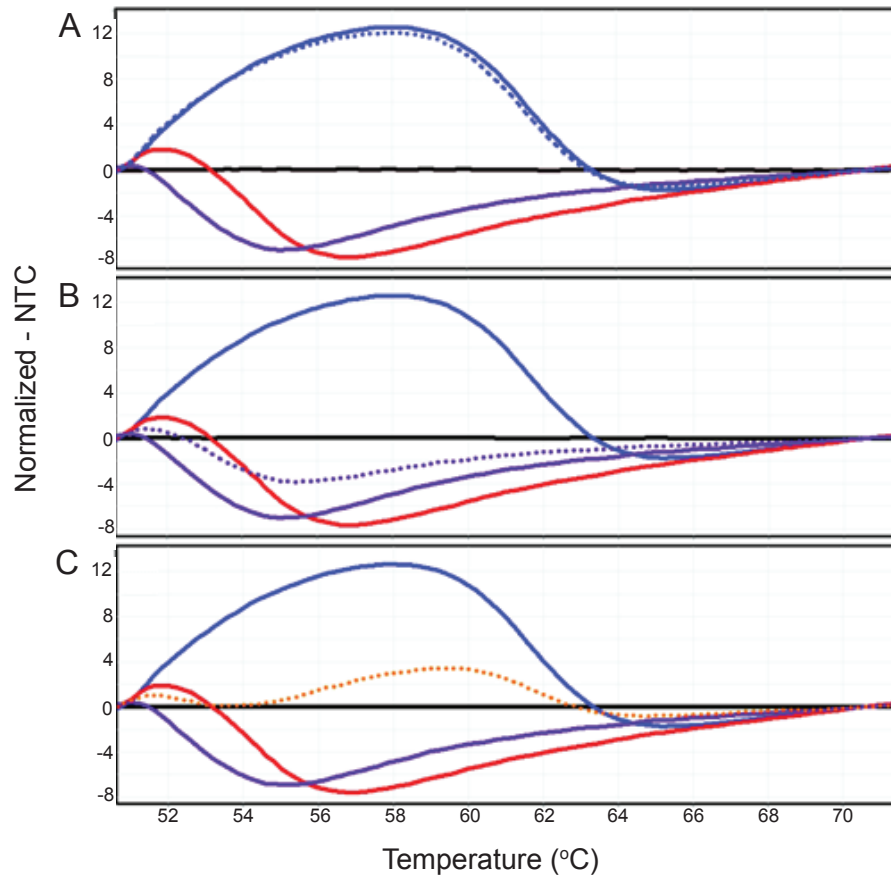
**Supplemental Figure 10. Evaluating sequencing profiles of the *pfcr* gene in control *Plasmodium* genomes.** A 300bp PCR product that includes amino acid residues 72-76 was sequenced to verify that the HRM genotyping call was accurate. **A.** Wild type, CVMNK, haplotype was confirmed by HB3 sequencing. **B.** Mutant, SVMNT, haplotype was confirmed by 7G8 sequencing. **C.** Mutant, CVIET, haplotype was confirmed by sequencing 7C424. Arrows denote nucleotide mutations that change amino acid sequences to C72S, M74I, N75E, K76T.



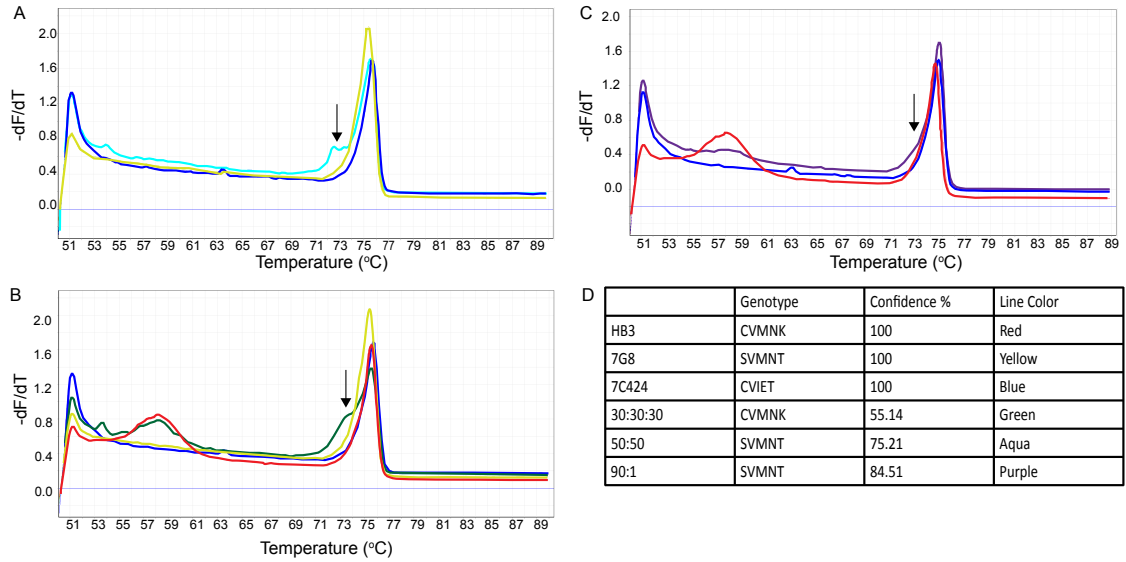
**Supplemental Figure 11. Evaluation of LightScanner and HotStarTaq mix performance.** Box plots showing average Ct values (A) and confidence % (B) between 2010 (black) and 2015 (orange) from HRM analysis. LightScanner mix was used to assess 2010 and HotStarTaq Mix was used to assess 2015 samples. n/s (not significant),  $p > 0.05$ ; CVMNK, wild type; SVMNT, mutant; CVIET, mutant.



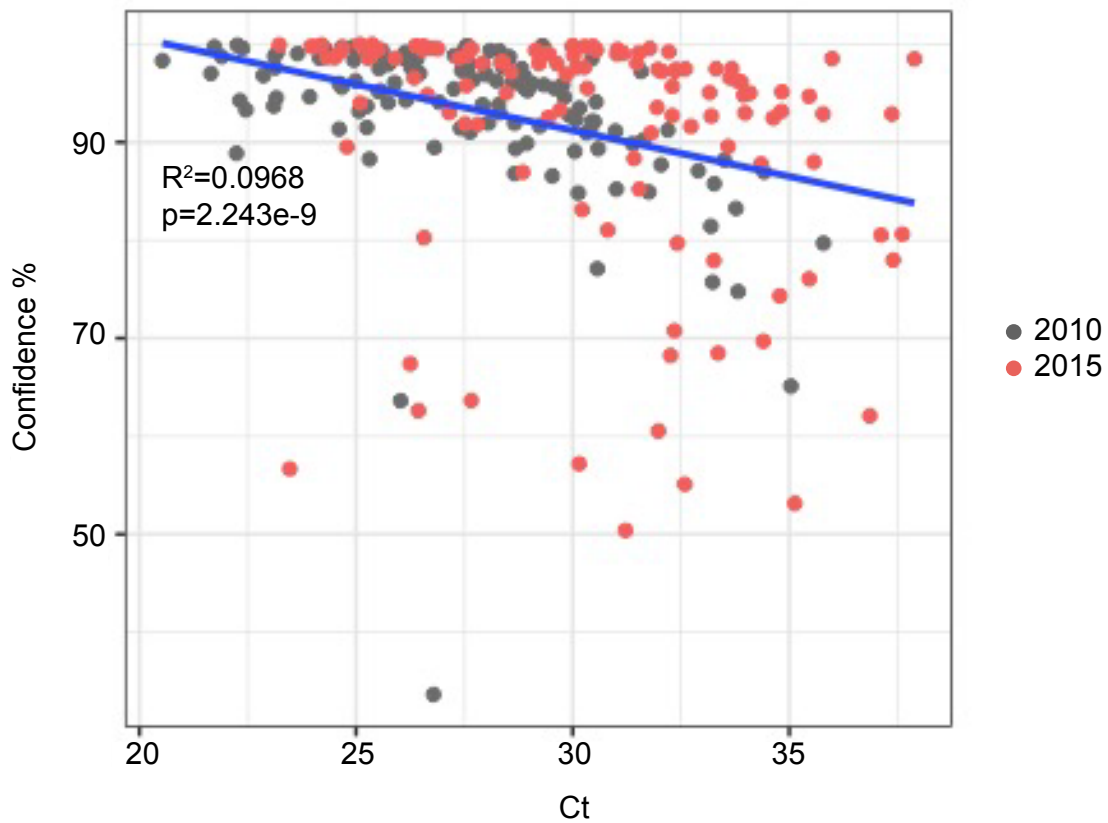
**Supplemental Figure 12. Assessment of the impact of narrower normalization regions on genotype calling.** Difference curves of a subset of clinical samples with normalization regions set to 51-52°C and 70-71°C (**A**) or 51-52°C and 65-68°C (**C**). Genotyping calls of these samples are listed in **B** and **D**. NTC, no template control.



**Supplemental Figure 13. Representatives of manual genotype calling.** Clinical samples were called against control genotypes by visual assessment. Displayed are the difference curves normalized to a no template control (NTC). Wild type control probe melt curve (solid blue line); Mutant genotype control probe melt curve (solid red line); Mutant genotype control probe melt curve (solid purple line); representative clinical samples (dashed colored lines). **A.** Example of a wild type genotype call. **B.** Example of a mutant genotype call. **C.** Example of a variation genotype call.



**Supplemental Figure 14. HRM analysis of mixed pfCRT haplotypes using Rotor-Gene Q.** Derivative plots of 50:50 mixture (**A**, 7G8:7C424 controls), 30:30:30 mixture (**B**, HB3:7G8:7C424), and 90:10 mixture (**C**, 7G8:HB3). The heteroduplex ‘shoulder’ (arrow) is likely due to the formation and melting of a heteroduplex of both DNA sequences. **D**. Summary table of genotype, confidence % called by Rotor-Gene Q, and corresponding line color.



**Supplemental Figure 15. Ct values vs confidence % generated by High Resolution Melt (HRM) assay.** A total of 248 clinical samples were plotted from 2010 (grey) and 2015 (orange) and genotyped. Confidence percentages are inversely proportional to Ct values with a linear correlation coefficient of 0.09684. High confidence was reported for both years which correlates to accurate, auto-called genotypes using Rotor-Gene Q Software. Blue line indicates trend line. Plot and statistical analysis were made using ggplot2 in RStudio.

## Chapter 5: Discussion and open questions

I have presented here in this thesis, work that spans across 3 major topics: ecDNA, vesicles, and surveillance of genotypes, as it relates to antimalarial resistance. Each topic is presented in a manner of a resistance strategy used by the malaria parasite, *P. falciparum*, which allows the parasite to consistently evolve and adapt to stress such as drug challenge. I believe I have successfully unveiled a novel strategy that has never been detected until now and I have built upon previous research and a number of long held assumptions. I will first reiterate the key observations from **Chapters 2** through **4**, since these studies are to be published. Then, I will discuss a series of open questions that will guide future investigations.

### EcDNA

Nearly fifty percent of the world's population is at risk for developing malaria. One of the greatest hurdles in eradicating this disease is antimalarial resistance; *P. falciparum* has developed resistance to every antimalarial used clinically, including our current frontline artemisinin. Little is known about **how** genomic changes that confer resistance (i.e. mutations that prevent drug binding or amplifications that increase target protein) arise when this haploid parasite is under selection. Understanding how resistance is acquired will be a powerful tool used in preventative strategies. Also, ecDNA research is a developing field and there are gaps in how these elements are maintained and generated.

Building upon previous mechanistic studies in our lab (Guler et al., 2013) and critical DNA structures that result in CNV generation (Huckaby et al., 2019),

we now report ecDNA in highly resistant parasites harboring significant CNVs. We successfully used a combination of innovative methods to isolate, measure, and sequence the putative ecDNA. Our methods involved isolating ecDNA after PFGE electrophoresis, which allowed the purification of 2 elements termed gel-competent and gel-incompetent ecDNA of different size and topology. We further characterized the elements using ddPCR and Illumina sequencing, relying on the enrichment of specific genes over genomic copies and its unique association with resistant parasites. These sensitive detection strategies provided the opportunity to detect an otherwise, invisible molecule. We concluded that ecDNA is 1) tunable, meaning copy number can increase or decrease in the presence of selection, 2) heterogeneous, indicating its complexity and 3) a highly adaptive feature of the *P. falciparum* haploid genome.

In addition to the details outlined above, we believe the work in this thesis is important because:

- it provides novel insights into the generation of drug resistance that extends beyond the malaria parasite (i.e. molecules that are present at undetectable levels could be contributing to/propagating resistance in other organisms).
- it raises the possibility that these elements could be transferred between parasites through recently described vesicles for intercellular communication.
- it uses an original approach to detect the enrichment of ecDNA following purification. It can serve as a guide to determine if endogenous ecDNA are formed in response to other selective drugs (not limited to *Plasmodium*).

- the mechanisms of ecDNA generation are likely targetable and their inhibition could prevent the development of resistance in this organism.
- the study strategy and findings are of intellectual interest to many scientific communities, including those studying microbiology, evolutionary biology, genomics, and cell biology.

### **Extra-cellular vesicles (EVs)**

As previously described, *P. falciparum* is highly adaptive when faced with a hostile environment so much so that strategies to block acquired resistance are highly studied. Common mechanisms of drug resistance are mediated through genetic mutations, efflux pumps, and metabolism alterations to list a few. Interestingly, proteins, lipids, nucleic acids, and other small molecules can be carried inside of EVs to perform those same common mechanisms. EVs have been shown to play a role in many biological processes and the pathogenesis of disease. Multiple studies have shown that in cases of severe malaria, EV levels are elevated in patients. Many questions remain: What are the messages that parasites are communicating? Can malaria parasites spread resistance using EVs?

Recently, it has been shown that *Plasmodium* parasites have the ability to transmit resistance through an episomal plasmid via vesicles. It was also found that the next generation of parasites also harbored those same resistance-conferring genes. The work presented in this thesis describes, for the first time, the packaging of endogenous resistance-conferring genes found in parasite-derived vesicles. The novelty of this study lies in the finding of conserved mutations,

specifically copy number variations, in both chromosomal and vesicle-derived DNA. Additionally, this study revealed a promising characteristic to distinguish vesicles secreted from uninfected and infected parasites. We also characterized the biophysical properties of vesicles to extend our current knowledge base.

In addition to the details outlined above, our studies contribute to the field because:

- we discuss the current challenges and advantages of extra-cellular vesicle characterization.
- the targeting of EV pathways would be a promising avenue to overcome antimalarial resistance.
- transmission of endogenous resistance-conferring genes implies a new strategy for sensitive parasites to acquire resistance. It will encourage future DNA-centric investigations of genetic material found in vesicles after antimalarial selection.
- it emphasizes the need to understand factors that trigger the secretion of vesicles and the pathway of vesicle trafficking in *Plasmodium*.

Lastly, these efforts can serve as a beginning point for other researchers studying the role of vesicles in malaria to ensure continued development of resistance blocking strategies.

### ***Pf*CRT resistance surveillance in SW Uganda**

Following with the theme of rampant drug resistance by the malaria parasite, **Chapter 4** highlights the evaluation of parasite genotypes in SW Uganda *after* CQ withdrawal in 2004. If artemisinin resistance spreads to Africa, greater mortality ensues. Instead of focusing on a novel targetable mechanism of resistance (as presented in **Chapters 2** and **3**), we consider another ‘new’ alternative in combating resistance.

A central question in the field is: can we return to using a once effective antimalarial, CQ after its withdrawal and after the documented appearance of drug susceptible parasites? Being safe, inexpensive, and ubiquitous are just some benefits of using former antimalarial drugs. We aimed to study SW Uganda because there are very few reports for Uganda despite ranking the 6<sup>th</sup> highest country with the highest malaria related deaths.

Recently, there has been a trend to assess drug resistance genotypes in malaria-stricken countries including Kenya, Tanzania, eastern Uganda and Malawi. After >12 years of documented CQ withdrawal in Malawi, clinical efficacy increased to 99%. In our current study, **we identified persistent chloroquine resistant parasites for the years 2010 and 2015 in Southwestern Uganda using a sensitive technology called high-resolution melt analysis (HRM)**. HRM is a technique that employs the use of unlabeled probes to bind with high specificity to a target sequence paired with a fluorescent dsDNA dye used as a readout to determine the temperature range at which the probe disassociates. Wild type and mutant probes create a distinct melt profile in which we use to assign our clinical samples. We concluded that there is still a selective pressure in this area

for CQ. The impact of this study lies in the ability to influence policy change regarding stricter regulations of CQ use, distribution, and production In Uganda.

We would like to highlight:

- our reported data is congruent with research in other locations and during a similar time frame, suggesting CQ pressure is still present in Southwestern Uganda.
- that we identified a decline in CQ resistant parasites from samples collected in Southwestern Uganda from 2010 and 2015 using a very sensitive PCR-based methodology called HRM. CQ may gain effectiveness again with new small molecules and new drug pairings, which has been recently published.
- surveillance of CQ resistant parasites is an essential step before drug implementation. In determining the resistance profile of Southwestern Uganda, an underrepresented region of Uganda, we also found differences in the number of CQ resistant parasites within a single country.
- the impact of this study lies in the ability to influence policy change regarding stricter regulations of chloroquine use, distribution, and production In Uganda.

## Open questions

### Is ecDNA a common mechanism of antimalarial resistance?

The strategy to answer this question is delineated in this thesis. My novel method includes: 1) running PFGE with parasites embedded in agarose blocks, 2) isolating putative ecDNA directly from agarose gels using a modified freeze and squeeze technique (Thuring et al., 1975) and 3) using a highly sensitive instrument for copy number variation analysis. Successful isolation of ecDNA should be validated by methods including but not limited to enzymatic digest and deep sequencing.

First, validation of ecDNA in other DSM1 resistant lines, H2 and H3, should occur (see summary of clone names in **Figure 2**). H2 and H3 are similar to H1 in which there is a disproportionality between copy number and resistance measured by  $EC_{50}$  (**Figure 2**) (Guler et al., 2013). H2 and H3 also shares a heterogenous smear migration of 50-200kb and retains DNA in its loading well as with H1. With the sequencing of H1 gel incompetent ecDNA, we observed a super-peak located near *sac3*, which also spans across a highly rich A/T track (**Figure 8**). This unique feature defined as a super-peak (for maximum coverage of over 36,000-fold) can be used as confirmation of ecDNA in future studies. If the super-peak is indeed present in the other parasite lines, it also builds strong evidence for its biological function. We predict a centromere-like or origin of replication-like function. In summary, by first isolating ecDNA in our DSM1 resistance model, the search for ecDNA in other resistance lines may move forward in high confidence.

When it comes to other resistance drug lines, one must ask, have we overlooked ecDNA in many of our low or high throughput methods (examined in

**Chapter 1**). Our proposed model (**Figure 10**) suggests that ecDNA is excised from locations of the genome harboring CNVs. A multitude of CNVs have been discovered in malaria in response to drug pressure (Bilsland et al., 2018; Cheeseman et al., 2009; Cowman et al., 1994; Foote et al., 1990; Heinberg et al., 2013; Kidgell et al., 2006; Nair et al., 2008a, 2007; Sidhu et al., 2006; Triglia et al., 1991; Wilson et al., 1989). Further exploration would prompt the building of an ecDNA database consisting of essential genes and motifs required for ecDNA maintenance (replication and segregation) derived from future ecDNA studies. Another good follow up study I would suggest is to add *sac3* super-peak sequence to episomes to determine if stability and segregation efficiency increases; transfection is a tedious process as it can take up to 6-12 months (Balu et al., 2005). This prediction is based off the assumption that if ecDNA is endogenous to *P. falciparum*, it should have higher transformation efficiencies.

Although we believe that ecDNA that has been described is in fact a by-product of the *dhodh* amplicon, one could argue what if it is not? In other words, ecDNA is not a valid resistance strategy used by the parasite. Three prominent results will refute this idea. First, gel-competent and -incompetent DNA is only observed in the resistant clones (**Supplemental Figure 1 and 2**). We argue that both CNVs and the repetitive nature of the *Plasmodium* genome (over 82% A/T-richness (Hamilton et al., 2017; Weber, 1987)) can facilitate recombination and thus generate ecDNA (see **Figure 10**). We believe that this process occurs *within the parasite* because PFGE allows the electrophoresis of DNA directly from the cell, with minimal manipulation. The ecDNA sequence shares high sequence identity to its home chromosome 6 location (**Supplemental Table 1**). Second,

ecDNA is only detected with primers (and probes) that are specific to the *dhodh* amplicon (**Figure 4**). Southern blotting and ddPCR results indicate that high CN are **not** observed when using probes outside of the amplicon (**Figure 4**, **Supplemental Figure 1**, and see **Table 1** for reference of *dhodh* and external probes). Lastly, we observed a super-peak that was enriched over 36,000-fold (**Figure 8** and **Supplemental Table 2**). Split read analysis revealed that the super-peak is in a tandem (head to tail) orientation. Although we used a common mechanism to amplify the gel-incompetent DNA, a head to tail amplification is not stochastic, meaning a regulated step-wise process is at play. For reference, the *dhodh* amplicon is also arranged tandemly (**Supplemental Figure 6, compare D to C**). See review in **Chapter 2**.

To my knowledge, there has only been one paper that suggested the idea of one type of ecDNA in *Plasmodium* as this research explored the idea of cell-cycle-associated genomic-DNA fragments, termed CAGFs (Li, 2018), but these studies cast a small doubt. CAGFs are described as fragmented ssDNA released from the genome that is necessary for the progression of cell cycle progression (Li, 2018). A large difference between Li's work and the work presented in this thesis is that our ecDNA carries multiple copies of *dhodh* or CNVs. Li makes a clear distinction that his version precludes CNVs (Li, 2018). Our ddPCR results draw on CN found in resistant parasites measured relative to wild type parasites using primer and probe specificity versus Li's results using an arbitrary primer that Li used. One drawback of this study is that a single arbitrary primer can result in non-specific binding, artificial amplification from a template, and low reproducibility (Black, 1993). Li also reports that after increasing concentrations of CQ, both the

resistant parasites (K1) and wild type parasites (HB3) releases CAGFs. This work is limited to an observation solely based on a PCR result without consideration of whether or not CAGFs actually contributes to cell cycle progression or if the ecDNA described here is heritable, thus showing necessity. Previous studies has suggested that CQ releases ROS (Farombi et al., 2003; Gupta et al., 2016; Monti et al., 2002; Percário et al., 2012), which can then result in DNA breaks presumably observed by Li. Our results highlight distinct differences found in wild type and highly resistant parasite lines that suggests a survival advantage (Guler et al., 2013 and McDaniels et al. In prep). Only our resistant parasites carry ecDNA with heightened resistance factors shown by  $EC_{50}$  ((Guler et al., 2013) and **Figure 2**). This provided us with the first opportunity to critically evaluate ecDNA in *P. falciparum*.

### **How is ecDNA replicated or regulated?**

One way to resolve this question is to arrest replication using inhibitors. For example, aphidicolin, a DNA polymerase inhibitor, and flavopiridol, a PfPK5 (a putative member of cyclin dependent protein kinase) have already been shown to impact *Plasmodium* growth (Graeser et al., 1996; Matthews et al., 2018). Assessment of replication inhibition, presumably after synchronization of parasite life cycle, can occur by fluorescent staining, i.e. SYBR DNA staining, and using 2D gels to detect the presence of stalled replication forks and other DNA structures. Essentially, ecDNA would be assessed in the same manner provided in this thesis in the presence and absence of the inhibitor. This experiment can generate 2 results: ecDNA is formed in the presence of a replication inhibitor, meaning that it

is using a replication-independent mechanism or ecDNA is not formed in the presence of a replication inhibitor, indicating a replication-dependent mechanism. This would also assess (and potentially modify) our proposed model of ecDNA generation (**Figure 10**). Independent replication generation would confirm that ecDNA is generated by excision at the chromosomal location followed by subsequent loss and the genomic location, which there is mild support for (see **Chapter 2**).

We draw on published reports of replication of ecDNA that occurs in *P. falciparum*—the apicoplast and mitochondria. There are still some unaddressed questions related to replication due to the lack of annotation and characterization of the *Plasmodium* proteins as well as the abundance of hypothetical proteins in the genome (Milton and Nelson, 2016; Wilson and Williamson, 1997). Due to gaps in research, it is unclear which method is favored under which circumstance. Thus, we can only state that rolling circle and recombination-dependent replication used by the mitochondria (Preiser et al., 1996; Wilson and Williamson, 1997) and rolling circle and D-loop replication (recombination-independent) used by the apicoplast (Milton and Nelson, 2016) are probable. Additional studies are needed to discern regulation between the two pathways. Determining how the ecDNA is replicated can emerge as a new strategy to prevent the propagation of resistance and would lead to the future development of antimalarials.

**What is the functional role of packaged DNA found in parasite-derived vesicles?**

We hypothesize that linear extra-chromosomal DNA homologous to the *dhodh* amplicon can initiate and maintain CNVs via amplicon border homology. To address this hypothesis, it will be pertinent to investigate if CNVs can be induced in *P. falciparum* using a method called small fragment-driven DNA amplification (SFDA). SFDA is a method recently described by Mukherjee *et al.* where 80bp oligonucleotides with homology to either end of the desired amplicon were used to trigger CNVs in yeast (Mukherjee and Storici, 2012).

We expect SFDA to work as a mechanism that triggers amplification in *P. falciparum*; furthermore, this mechanism offers a way to follow parasite DNA as it becomes packaged into red blood cell-derived exosomes. We anticipate that SFDA will be used to increase the rate and amount of amplifications driving extra-chromosomal DNA generation. Another advantage of using the SFDA technology is to induce amplification elsewhere in the genome simply by making an 80-mer oligonucleotide. If this was to work, investigating how CNVs maintains strict boundaries and what regions in the genome are more susceptible for amplification to occur would also be insightful. This is still an unanswered question in the field. To test and confirm that this method works, I suggest designing oligonucleotides to other regions in the genome responsible for drug resistance to artificially induce amplification.

I also suggest synthesizing 80bp oligonucleotides that have homology to the *dhodh* amplicon breakpoints from low and high level resistant parasites. Oligonucleotides designed against randomly chosen sequences from across the

genome would serve as a control. In this case, even if amplification does occur, they will not confer DSM1 resistance and the parasite will die. These custom oligonucleotides can be easily transfected into RBCs. As in a typical transfection scheme used in the malaria field, these “loaded” red blood cells function to pass the desired DNA on to *P. falciparum* upon invasion (transfection method described in (O’Donnell et al., 2001b)). Finally, in order to determine whether SFDA is contributing to amplicon generation, it would be worth applying DSM1 drug pressure and comparing the time required to develop low level and high level resistance ( $EC_{50}$ , **Figure 2**) of SFDA-transfected parasites to that of typical DSM1-sensitive parasites (~30-45 days). qPCR and ddPCR can be used to validate that *dhodh* amplicons have been generated in resistant parasites, regardless of their origin.

If initial attempts prove unsuccessful, longer stretches of homology should be assessed if favored by *P. falciparum* replication machinery. If our hypothesis is correct, we expect that the transfection of SFDA oligonucleotides specific for previously successful *dhodh* amplicon boundaries will *decrease* the time required to develop DSM1 resistance. Furthermore, boundaries of the newly generated amplicons will match those that were used in the design of the oligonucleotides. If novel amplicon boundaries are generated in resistant parasites (as was the case for each low level clone in the initial selection), it is likely that the SFDA did not work as we expected. If successful, detection of an *increase* in 1) the amount of ecDNA via PFGE and 2) the representation of amplicons carried in EVs derived from resistant parasites is expected. These results would link ecDNA and vesicles together to make for a great continuation of this thesis project.

One additional advantage of using the SFDA technology may induce CNVs elsewhere in the genome. This possibility will extend beyond our current DSM1 resistance model to investigate what regions in the genome are more or less prone to CNV generation. This investigation could potentially address a number of unanswered questions in the malaria field.

**Appendix 1. Freeze and squeeze extraction of DNA from agarose gels  
protocol**

1. Cut out the band of interest with a sterile spatula and place it in a 1.5mL tube.  
Crush the gel slice with the spatula or razor.
2. Add 250µl of nuclease free H<sub>2</sub>O.
3. Place in heat block for 10min at 65°C.
4. Freeze at -80°C.
5. Thaw the sample at room temperature. Gently flick the tube to make sure that no ice remains. Centrifuge at full speed (20,000xg) for 6min. Remove and save the supernatant. Put in a new tube.
6. If using multiple tubes, pool saved supernatants from steps 4 and 6 and centrifuge at full speed (20,000xg) for 6min.
7. Remove and save the supernatant with a pipet tip to a fresh tube.
8. If there is more than 0.4mL of liquid, divide it into multiple tubes so there is a maximum of 0.4mL per tube.
9. Add an equal volume of PCI. Spin at 5min at 2000xg. Add an equal volume of chloroform. Spin for 5min at 2000xg.
10. Add 1/10<sup>th</sup> volume of 3M sodium acetate and 1µl of glycogen (20mg/mL) to each tube. Add 2 volumes of 95% ethanol, mix, and place at -20°C overnight.
11. Centrifuge at full speed (20,000xg) for 15min.
12. Decant the supernatant and invert the tube on a paper towel.
13. Add 0.5mL of 70% ethanol and vortex. Centrifuge at full speed (20,000xg) for 5min.
14. Decant the supernatant and invert the tube on a paper towel.

15. Dry the pellet.

16. Resuspend the pellet in 20 $\mu$ L of 1xTE or EB buffer.

## References

- Adepoju, P., 2019. RTS,S malaria vaccine pilots in three African countries. *Lancet* 393, 1685. [https://doi.org/10.1016/S0140-6736\(19\)30937-7](https://doi.org/10.1016/S0140-6736(19)30937-7).
- Agarwal, M., Bhowmick, K., Shah, K., Krishnamachari, A., Dhar, S.K., 2017. Identification and characterization of ARS-like sequences as putative origin(s) of replication in human malaria parasite *Plasmodium falciparum*. *The Federation of European Biochemical Societies Journal* 284, 2674–2695. <https://doi.org/10.1111/febs.14150>.
- Albertson, D.G., 2006. Gene amplification in cancer. *Trends in Genetics* 22, 447–455. <https://doi.org/10.1016/j.tig.2006.06.007>.
- Anderson, Tim J. C., Patel, J., Ferdig, M.T., 2009. Gene copy number and malaria biology. *Trends in Parasitology* 25, 336–343. <https://doi.org/10.1016/j.pt.2009.04.005>.
- Anderson, Tim J.C., Patel, J., Ferdig, M.T., 2009. Gene copy number and malaria biology. *Trends in Parasitology* 25, 336–343. <https://doi.org/10.1016/j.pt.2009.04.005>.
- Arlt, M.F., Mulle, J.G., Schaibley, V.M., Ragland, R.L., Durkin, S.G., Warren, S.T., Glover, T.W., 2009. Replication Stress Induces Genome-wide Copy Number Changes in Human Cells that Resemble Polymorphic and Pathogenic Variants. *American Journal of Human Genetics* 84, 339–350. <https://doi.org/10.1016/j.ajhg.2009.01.024>.
- Ashley, E.A., Dhorda, M., Fairhurst, R.M., Amaratunga, C., Lim, P., Suon, S., Sreng, S., Anderson, J.M., Mao, S., Sam, B., Sopha, C., Chuor, C.M., Nguon, C., Sovannaroeth, S., Pukrittayakamee, S., Jittamala, P.,

Chotivanich, K., Chutasmit, K., Suchatsoonthorn, C., Runcharoen, R., Hien, T.T., Thuy-Nhien, N.T., Thanh, N.V., Phu, N.H., Htut, Y., Han, K.-T., Aye, K.H., Mokuolu, O.A., Olaosebikan, R.R., Folaranmi, O.O., Mayxay, M., Khanthavong, M., Hongvanthong, B., Newton, P.N., Onyamboko, M.A., Fanello, C.I., Tshefu, A.K., Mishra, N., Valecha, N., Phyo, A.P., Nosten, F., Yi, P., Tripura, R., Borrmann, S., Bashraheil, M., Peshu, J., Faiz, M.A., Ghose, A., Hossain, M.A., Samad, R., Rahman, M.R., Hasan, M.M., Islam, A., Miotto, O., Amato, R., MacInnis, B., Stalker, J., Kwiatkowski, D.P., Bozdech, Z., Jeeyapant, A., Cheah, P.Y., Sakulthaew, T., Chalk, J., Intharabut, B., Silamut, K., Lee, S.J., Vihokhern, B., Kunasol, C., Imwong, M., Tarning, J., Taylor, W.J., Yeung, S., Woodrow, C.J., Flegg, J.A., Das, D., Smith, J., Venkatesan, M., Plowe, C.V., Stepniewska, K., Guerin, P.J., Dondorp, A.M., Day, N.P., White, N.J., Tracking Resistance to Artemisinin Collaboration (TRAC), 2014. Spread of artemisinin resistance in *Plasmodium falciparum* malaria. *New England Journal of Medicine* 371, 411–423.  
<https://doi.org/10.1056/NEJMoa1314981>.

Aurrecoechea, C., Brestelli, J., Brunk, B.P., Dommer, J., Fischer, S., Gajria, B., Gao, X., Gingle, A., Grant, G., Harb, O.S., Heiges, M., Innamorato, F., Iodice, J., Kissinger, J.C., Kraemer, E., Li, W., Miller, J.A., Nayak, V., Pennington, C., Pinney, D.F., Roos, D.S., Ross, C., Stoeckert, C.J., Treatman, C., Wang, H., 2009. PlasmoDB: a functional genomic database for malaria parasites. *Nucleic Acids Research* 37, D539–D543.  
<https://doi.org/10.1093/nar/gkn814>.

- Babatunde, K.A., Mbagwu, S., Hernández-Castañeda, M.A., Adapa, S.R., Walch, M., Filgueira, L., Falquet, L., Jiang, R.H.Y., Ghiran, I., Mantel, P.-Y., 2018. Malaria infected red blood cells release small regulatory RNAs through extracellular vesicles. *Scientific Reports* 8, 1–15. <https://doi.org/10.1038/s41598-018-19149-9>.
- Babatunde, K.A., Yesodha Subramanian, B., Ahouidi, A.D., Martinez Murillo, P., Walch, M., Mantel, P.-Y., 2020. Role of Extracellular Vesicles in Cellular Cross Talk in Malaria. *Frontiers in Immunology* 11, 22. <https://doi.org/10.3389/fimmu.2020.00022>.
- Balu, B., Shoue, D.A., Fraser, M.J., Adams, J.H., 2005. High-efficiency transformation of *Plasmodium falciparum* by the lepidopteran transposable element piggyBac. *Proceedings of the National Academy of Sciences of the United States of America* 102, 16391–16396. <https://doi.org/10.1073/pnas.0504679102>.
- Banizs, A.B., Huang, T., Dryden, K., Berr, S.S., Stone, J.R., Nakamoto, R.K., Shi, W., He, J., 2014. *In vitro* evaluation of endothelial exosomes as carriers for small interfering ribonucleic acid delivery. *International Journal of Nanomedicine* 9, 4223–4230. <https://doi.org/10.2147/IJN.S64267>.
- Baruch, D.I., Pasloske, B.L., Singh, H.B., Bi, X., Ma, X.C., Feldman, M., Taraschi, T.F., Howard, R.J., 1995. Cloning the *P. falciparum* gene encoding PfEMP1, a malarial variant antigen and adherence receptor on the surface of parasitized human erythrocytes. *Cell* 82, 77–87. [https://doi.org/10.1016/0092-8674\(95\)90054-3](https://doi.org/10.1016/0092-8674(95)90054-3).
- Basiji, D.A., Ortyn, W.E., Liang, L., Venkatachalam, V., Morrissey, P., 2007. Cellular Image Analysis and Imaging by Flow Cytometry. *Clinics in*

Laboratory Medicine 27, 653–670, viii.

<https://doi.org/10.1016/j.cll.2007.05.008>.

Beghain, J., Langlois, A.-C., Legrand, E., Grange, L., Khim, N., Witkowski, B.,

Duru, V., Ma, L., Bouchier, C., Ménard, D., Paul, R.E., Arieu, F., 2016.

*Plasmodium* copy number variation scan: gene copy numbers evaluation in haploid genomes. Malaria Journal 15, 206.

<https://doi.org/10.1186/s12936-016-1258-x>.

Beverley, S.M., 1988. Characterization of the “unusual” mobility of large circular DNAs in pulsed field-gradient electrophoresis. Nucleic Acids Research 16, 925–939.

Beverley, S.M., Coderre, J.A., Santi, D.V., Schimke, R.T., 1984. Unstable DNA amplifications in methotrexate resistant Leishmania consist of extrachromosomal circles which relocalize during stabilization. Cell 38, 431–439. [https://doi.org/10.1016/0092-8674\(84\)90498-7](https://doi.org/10.1016/0092-8674(84)90498-7).

Bhattacharjee, S., Coppens, I., Mbengue, A., Suresh, N., Ghorbal, M., Slouka, Z., Safeukui, I., Tang, H.-Y., Speicher, D.W., Stahelin, R.V., Mohandas, N., Haldar, K., 2018. Remodeling of the malaria parasite and host human red cell by vesicle amplification that induces artemisinin resistance. Blood 131, 1234–1247. <https://doi.org/10.1182/blood-2017-11-814665>.

Bilsland, E., van Vliet, L., Williams, K., Feltham, J., Carrasco, M.P., Fotoran, W.L., Cubillos, E.F.G., Wunderlich, G., Grøtli, M., Hollfelder, F., Jackson, V., King, R.D., Oliver, S.G., 2018. *Plasmodium* dihydrofolate reductase is a second enzyme target for the antimalarial action of triclosan. Scientific Reports 8, 1–8. <https://doi.org/10.1038/s41598-018-19549-x>.

- Bindra, R.S., Schaffer, P.J., Meng, A., Woo, J., Måseide, K., Roth, M.E., Lizardi, P., Hedley, D.W., Bristow, R.G., Glazer, P.M., 2004. Down-regulation of Rad51 and decreased homologous recombination in hypoxic cancer cells. *Molecular and Cellular Biology* 24, 8504–8518.  
<https://doi.org/10.1128/MCB.24.19.8504-8518.2004>.
- Birnbaum, J., Scharf, S., Schmidt, S., Jonscher, E., Hoeijmakers, W.A.M., Flemming, S., Toenhake, C.G., Schmitt, M., Sabitzki, R., Bergmann, B., Fröhlke, U., Mesén-Ramírez, P., Soares, A.B., Herrmann, H., Bártfai, R., Spielmann, T., 2020. A Kelch13-defined endocytosis pathway mediates artemisinin resistance in malaria parasites. *Science* 367, 51–59.  
<https://doi.org/10.1126/science.aax4735>.
- Black, W.C., 1993. PCR with arbitrary primers: approach with care. *Insect Molecular Biology* 2, 1–6. <https://doi.org/10.1111/j.1365-2583.1993.tb00118.x>.
- Boddey, J.A., Moritz, R.L., Simpson, R.J., Cowman, A.F., 2009. Role of the *Plasmodium* Export Element in Trafficking Parasite Proteins to the Infected Erythrocyte. *Traffic* 10, 285–299. <https://doi.org/10.1111/j.1600-0854.2008.00864.x>.
- Bray, P.G., Martin, R.E., Tilley, L., Ward, S.A., Kirk, K., Fidock, D.A., 2005. Defining the role of PfCRT in *Plasmodium falciparum* chloroquine resistance. *Molecular Microbiology* 56, 323–333.  
<https://doi.org/10.1111/j.1365-2958.2005.04556.x>.
- Burrows, J., 2015. Malaria runs rings round artemisinin. *Nature* 520, 628–630.  
<https://doi.org/10.1038/nature14387>.

- Bzymek, M., Lovett, S.T., 2001. Instability of repetitive DNA sequences: The role of replication in multiple mechanisms. *Proceedings of the National Academy of Sciences of the United States of America* 98, 8319–8325. <https://doi.org/10.1073/pnas.111008398>.
- Cantsilieris, S., Baird, P.N., White, S.J., 2013. Molecular methods for genotyping complex copy number polymorphisms. *Genomics* 101, 86–93. <https://doi.org/10.1016/j.ygeno.2012.10.004>.
- Carret, C.K., Horrocks, P., Konfortov, B., Winzeler, E., Qureshi, M., Newbold, C., Ivens, A., 2005. Microarray-based comparative genomic analyses of the human malaria parasite *Plasmodium falciparum* using Affymetrix arrays. *Molecular and Biochemical Parasitology* 144, 177–186. <https://doi.org/10.1016/j.molbiopara.2005.08.010>.
- Center for Disease Control and Prevention, 2019. CDC - Malaria - Malaria Worldwide - How Can Malaria Cases and Deaths Be Reduced? - Vaccines [WWW Document]. URL [https://www.cdc.gov/malaria/malaria\\_worldwide/reduction/vaccine.html](https://www.cdc.gov/malaria/malaria_worldwide/reduction/vaccine.html) (accessed 3.10.20).
- Cheeseman, I.H., Gomez-Escobar, N., Carret, C.K., Ivens, A., Stewart, L.B., Tetteh, K.K.A., Conway, D.J., 2009. Gene copy number variation throughout the *Plasmodium falciparum* genome. *BioMed Central Genomics* 10, 353. <https://doi.org/10.1186/1471-2164-10-353>.
- Cheeseman, I.H., Miller, B., Tan, J.C., Tan, A., Nair, S., Nkhoma, S.C., De Donato, M., Rodulfo, H., Dondorp, A., Branch, O.H., Mesia, L.R., Newton, P., Mayxay, M., Amambua-Ngwa, A., Conway, D.J., Nosten, F., Ferdig, M.T., Anderson, T.J.C., 2016. Population Structure Shapes Copy Number

- Variation in Malaria Parasites. *Molecular Biology and Evolution* 33, 603–620. <https://doi.org/10.1093/molbev/msv282>.
- Cohen, S., 2001. A novel cell-free system reveals a mechanism of circular DNA formation from tandem repeats. *Nucleic Acids Research* 29, 2542–2548. <https://doi.org/10.1093/nar/29.12.2542>.
- Cohen, S., Segal, D., 2009. Extrachromosomal Circular DNA in Eukaryotes: Possible Involvement in the Plasticity of Tandem Repeats. *Cytogenetic and Genome Research* 124, 327–338. <https://doi.org/10.1159/000218136>.
- Cohen, Z., Lavi, S., 2009. Replication Independent Formation of Extrachromosomal Circular DNA in Mammalian Cell-Free System. *PLOS ONE* 4, e6126. <https://doi.org/10.1371/journal.pone.0006126>.
- Cole, K.D., Tellez, C.M., 2002. Separation of Large Circular DNA by Electrophoresis in Agarose Gels. *Biotechnology Progress* 18, 82–87. <https://doi.org/10.1021/bp010135o>.
- Combes, V., Taylor, T.E., Juhan-Vague, I., Mège, J.-L., Mwenechanya, J., Tembo, M., Grau, G.E., Molyneux, M.E., 2004. Circulating endothelial microparticles in Malawian children with severe *falciparum* malaria complicated with coma. *Journal of American Medical Association* 291, 2542–2544. <https://doi.org/10.1001/jama.291.21.2542-b>.
- Coquelle, A., Toledo, F., Stern, S., Bieth, A., Debatisse, M., 1998. A new role for hypoxia in tumor progression: induction of fragile site triggering genomic rearrangements and formation of complex DMs and HSRs. *Molecular Cell* 2, 259–265. [https://doi.org/10.1016/s1097-2765\(00\)80137-9](https://doi.org/10.1016/s1097-2765(00)80137-9).
- Cowman, A.F., Galatis, D., Thompson, J.K., 1994. Selection for mefloquine resistance in *Plasmodium falciparum* is linked to amplification of the

*pfmdr1* gene and cross-resistance to halofantrine and quinine.

Proceedings of the National Academy of Science of the United States of America 91, 1143–1147.

Cowman, A.F., Healer, J., Marapana, D., Marsh, K., 2016. Malaria: Biology and Disease. Cell 167, 610–624. <https://doi.org/10.1016/j.cell.2016.07.055>.

Cox, F.E., 2010. History of the discovery of the malaria parasites and their vectors. Parasites & Vectors 3, 5. <https://doi.org/10.1186/1756-3305-3-5>.

Crabb, B.S., de Koning-Ward, T.F., Gilson, P.R., 2010. Protein export in *Plasmodium* parasites: from the endoplasmic reticulum to the vacuolar export machine. International Journal of Parasitology 40, 509–513. <https://doi.org/10.1016/j.ijpara.2010.02.002>.

Davies, H.M., Nofal, S.D., McLaughlin, E.J., Osborne, A.R., 2017. Repetitive sequences in malaria parasite proteins. Federation of the European Microbiological Societies Microbiology Reviews 41, 923–940. <https://doi.org/10.1093/femsre/fux046>.

Delabranche, X., Berger, A., Boisramé-Helms, J., Meziani, F., 2012. Microparticles and infectious diseases. Médecine et Maladies Infectieuses 42, 335–343. <https://doi.org/10.1016/j.medmal.2012.05.011>.

Dennin, R.H., 2018. Overlooked: Extrachromosomal DNA and Their Possible Impact on Whole Genome Sequencing. The Malaysian Journal of Medical Sciences 25, 20–26. <https://doi.org/10.21315/mjms2018.25.2.3>.

Deshpande, V., Luebeck, J., Nguyen, N.-P.D., Bakhtiari, M., Turner, K.M., Schwab, R., Carter, H., Mischel, P.S., Bafna, V., 2019. Exploring the landscape of focal amplifications in cancer using Amplicon Architect.

Nature Communications 10, 1–14. <https://doi.org/10.1038/s41467-018-08200-y>.

Dharia, N.V., Sidhu, A.B.S., Cassera, M.B., Westenberger, S.J., Bopp, S.E., Eastman, R.T., Plouffe, D., Batalov, S., Park, D.J., Volkman, S.K., Wirth, D.F., Zhou, Y., Fidock, D.A., Winzeler, E.A., 2009. Use of high-density tiling microarrays to identify mutations globally and elucidate mechanisms of drug resistance in *Plasmodium falciparum*. *Genome Biology* 10, 2 R21. <https://doi.org/10.1186/gb-2009-10-2-r21>.

Dillon, L.W., Kumar, P., Shibata, Y., Wang, Y.-H., Willcox, S., Griffith, J.D., Pommier, Y., Takeda, S., Dutta, A., 2015. Production of Extrachromosomal MicroDNAs Is Linked to Mismatch Repair Pathways and Transcriptional Activity. *Cell Reports* 11, 1749–1759. <https://doi.org/10.1016/j.celrep.2015.05.020>.

Dominical, V., Samsel, L., McCoy, J.P., 2017. Masks in Imaging Flow Cytometry. *Methods* 112, 9–17. <https://doi.org/10.1016/j.ymeth.2016.07.013>.

Duraisingh, M.T., Cowman, A.F., 2005. Contribution of the *pfmdr1* gene to antimalarial drug-resistance. *Acta Tropica* 94, 181. <https://doi.org/10.1016/j.actatropica.2005.04.008>.

Erdbrügger, U., Rudy, C.K., Etter, M.E., Dryden, K.A., Yeager, M., Klibanov, A.L., Lannigan, J., 2014. Imaging flow cytometry elucidates limitations of microparticle analysis by conventional flow cytometry. *Cytometry Part A* 85, 756–770. <https://doi.org/10.1002/cyto.a.22494>.

Farombi, E.O., Shyntum, Y.Y., Emerole, G.O., 2003. Influence of chloroquine treatment and *Plasmodium falciparum* malaria infection on some enzymatic and non-enzymatic antioxidant defense indices in humans.

Drug and Chemical Toxicology 26, 59–71. <https://doi.org/10.1081/dct-120017558>.

Faust, C., Dobson, A.P., 2015. Primate malarias: Diversity, distribution and insights for zoonotic *Plasmodium*. *One Health* 1, 66–75. <https://doi.org/10.1016/j.onehlt.2015.10.001>.

Foote, S.J., Galatis, D., Cowman, A.F., 1990. Amino acids in the *dihydrofolate reductase-thymidylate synthase* gene of *Plasmodium falciparum* involved in cycloguanil resistance differ from those involved in pyrimethamine resistance. *Proceedings of the National Academy of Science of the United States of America* 87, 3014–3017.

Gardner, M.J., Hall, N., Fung, E., White, O., Berriman, M., Hyman, R.W., Carlton, J.M., Pain, A., Nelson, K.E., Bowman, S., Paulsen, I.T., James, K., Eisen, J.A., Rutherford, K., Salzberg, S.L., Craig, A., Kyes, S., Chan, M.-S., Nene, V., Shallom, S.J., Suh, B., Peterson, J., Angiuoli, S., Pertea, M., Allen, J., Selengut, J., Haft, D., Mather, M.W., Vaidya, A.B., Martin, D.M.A., Fairlamb, A.H., Fraunholz, M.J., Roos, D.S., Ralph, S.A., McFadden, G.I., Cummings, L.M., Subramanian, G.M., Mungall, C., Venter, J.C., Carucci, D.J., Hoffman, S.L., Newbold, C., Davis, R.W., Fraser, C.M., Barrell, B., 2002. Genome sequence of the human malaria parasite *Plasmodium falciparum*. *Nature* 6906, 498-511. <https://doi.org/10.1038/nature01097>.

Genois, M.-M., Paquet, E.R., Laffitte, M.-C.N., Maity, R., Rodrigue, A., Ouellette, M., Masson, J.-Y., 2014. DNA Repair Pathways in Trypanosomatids: from DNA Repair to Drug Resistance. *Microbiology and Molecular Biology Reviews* 78, 40–73. <https://doi.org/10.1128/MMBR.00045-13>.

- Graeser, R., Wernli, B., Franklin, R.M., Kappes, B., 1996. *Plasmodium falciparum* protein kinase 5 and the malarial nuclear division cycles. *Molecular and Biochemical Parasitology* 82, 37–49. [https://doi.org/10.1016/0166-6851\(96\)02716-8](https://doi.org/10.1016/0166-6851(96)02716-8).
- Gresham, D., Usaite, R., Germann, S.M., Lisby, M., Botstein, D., Regenberg, B., 2010. Adaptation to diverse nitrogen-limited environments by deletion or extrachromosomal element formation of the GAP1 locus. *Proceedings of the National Academy of Sciences of the United States of America* 107, 18551–18556. <https://doi.org/10.1073/pnas.1014023107>.
- Guler, J.L., Freeman, D.L., Ahyong, V., Patrapuvich, R., White, J., Gujjar, R., Phillips, M.A., DeRisi, J., Rathod, P.K., 2013. Asexual Populations of the Human Malaria Parasite, *Plasmodium falciparum*, Use a Two-Step Genomic Strategy to Acquire Accurate, Beneficial DNA Amplifications. *PLOS Pathogens* 9, e1003375. <https://doi.org/10.1371/journal.ppat.1003375>.
- Gupta, D.K., Patra, A.T., Zhu, L., Gupta, A.P., Bozdech, Z., 2016. DNA damage regulation and its role in drug-related phenotypes in the malaria parasites. *Scientific Reports* 6, 23603. <https://doi.org/10.1038/srep23603>.
- Gurrieri, S., Smith, S.B., Bustamante, C., 1999. Trapping of megabase-sized DNA molecules during agarose gel electrophoresis. *Proceedings of the National Academy of Sciences of the United States of America* 96, 453–458. <https://doi.org/10.1073/pnas.96.2.453>.
- Gutteridge, W.E., Dave, D., Richards, W.H., 1979. Conversion of dihydroorotate to orotate in parasitic protozoa. *Biochimica et Biophysica Acta- General Subjects* 582, 390–401. [https://doi.org/10.1016/0304-4165\(79\)90131-4](https://doi.org/10.1016/0304-4165(79)90131-4).

- Haase, S., de Koning-Ward, T.F., 2010. New insights into protein export in malaria parasites. *Cellular Microbiology* 12, 580–587.  
<https://doi.org/10.1111/j.1462-5822.2010.01455.x>.
- Hamilton, W.L., Claessens, A., Otto, T.D., Kekre, M., Fairhurst, R.M., Rayner, J.C., Kwiatkowski, D., 2017. Extreme mutation bias and high AT content in *Plasmodium falciparum*. *Nucleic Acids Research* 45, 1889–1901.  
<https://doi.org/10.1093/nar/gkw1259>.
- Hastings, P., Lupski, J.R., Rosenberg, S.M., Ira, G., 2009. Mechanisms of change in gene copy number. *Nature Review Genetics* 10, 551–564.  
<https://doi.org/10.1038/nrg2593>.
- Haynes, J.D., Diggs, C.L., Hines, F.A., Desjardins, R.E., 1976. Culture of human malaria parasites *Plasmodium falciparum*. *Nature* 263, 767–769.  
<https://doi.org/10.1038/263767a0>.
- Heinberg, A., Siu, E., Stern, C., Lawrence, E.A., Ferdig, M.T., Deitsch, K.W., Kirkman, L.A., 2013. Direct evidence for the adaptive role of copy number variation on antifolate susceptibility in *Plasmodium falciparum*. *Molecular Microbiology* 88, 702–712. <https://doi.org/10.1111/mmi.12162>.
- Hernandez-Rivas, R., Scherf, A., 1997. Separation and mapping of chromosomes of parasitic protozoa. *Memorias do Instituto Oswaldo Cruz* 92, 815–819. <https://doi.org/10.1590/s0074-02761997000600017>.
- Hindson, B.J., Ness, K.D., Masquelier, D.A., Belgrader, P., Heredia, N.J., Makarewicz, A.J., Bright, I.J., Lucero, M.Y., Hiddessen, A.L., Legler, T.C., Kitano, T.K., Hodel, M.R., Petersen, J.F., Wyatt, P.W., Steenblock, E.R., Shah, P.H., Bousse, L.J., Troup, C.B., Mellen, J.C., Wittmann, D.K., Erndt, N.G., Cauley, T.H., Koehler, R.T., So, A.P., Dube, S., Rose, K.A.,

Montesclaros, L., Wang, S., Stumbo, D.P., Hodges, S.P., Romine, S., Milanovich, F.P., White, H.E., Regan, J.F., Karlin-Neumann, G.A., Hindson, C.M., Saxonov, S., Colston, B.W., 2011. High-Throughput Droplet Digital PCR System for Absolute Quantitation of DNA Copy Number. *Analytical Chemistry* 83, 8604–8610.  
<https://doi.org/10.1021/ac202028g>.

Hoeijmakers, W.A.M., Flueck, C., François, K.-J., Smits, A.H., Wetzel, J., Volz, J.C., Cowman, A.F., Voss, T., Stunnenberg, H.G., Bártfai, R., 2012. *Plasmodium falciparum* centromeres display a unique epigenetic makeup and cluster prior to and during schizogony. *Cellular Microbiology* 14, 1391–1401. <https://doi.org/10.1111/j.1462-5822.2012.01803.x>.

Hosono, S., Faruqi, A.F., Dean, F.B., Du, Y., Sun, Z., Wu, X., Du, J., Kingsmore, S.F., Egholm, M., Lasken, R.S., 2003. Unbiased Whole-Genome Amplification Directly From Clinical Samples. *Genome Research* 13, 954–964. <https://doi.org/10.1101/gr.816903>.

Huckaby, A.C., Granum, C.S., Carey, M.A., Szlachta, K., Al-Barghouthi, B., Wang, Y.-H., Guler, J.L., 2019. Complex DNA structures trigger copy number variation across the *Plasmodium falciparum* genome. *Nucleic Acids Research* 47, 1615–1627. <https://doi.org/10.1093/nar/gky1268>.

Hull, R., King, M., Pizza, G., Krueger, F., Vergara, X., Houseley, J., 2019. Transcription-induced formation of extrachromosomal DNA during yeast ageing. *PLoS Biology* 12, e3000471. <https://doi.org/10.1101/744896>.

Iwanaga, S., Kato, T., Kaneko, I., Yuda, M., 2012. Centromere Plasmid: A New Genetic Tool for the Study of *Plasmodium falciparum*. *PloS One* 3, e3326. <https://doi.org/10.1371/journal.pone.0033326>.

- Iwanaga, S., Khan, S.M., Kaneko, I., Christodoulou, Z., Newbold, C., Yuda, M., Janse, C.J., Waters, A.P., 2010. Functional Identification of the *Plasmodium* Centromere and Generation of a *Plasmodium* Artificial Chromosome. *Cell Host Microbe* 7, 245–255.  
<https://doi.org/10.1016/j.chom.2010.02.010>.
- Jørgensen, T.S., Kiil, A.S., Hansen, M.A., Sørensen, S.J., Hansen, L.H., 2015. Current strategies for mobilome research. *Frontiers in Microbiology* 5, 750.  
<https://doi.org/10.3389/fmicb.2014.00750>.
- Kanda, T., Kamiya, M., Maruo, S., Iwakiri, D., Takada, K., 2007. Symmetrical localization of extrachromosomally replicating viral genomes on sister chromatids. *Journal of Cell Science* 120, 1529–1539.  
<https://doi.org/10.1242/jcs.03434>.
- Kanda, T., Wahl, G.M., 2000. The dynamics of acentric chromosomes in cancer cells revealed by GFP-based chromosome labeling strategies. *Journal of Cellular Biochemistry* 35, 107–114. [https://doi.org/10.1002/1097-4644\(2000\)79:35+<107::aid-jcb1133>3.0.co;2-y](https://doi.org/10.1002/1097-4644(2000)79:35+<107::aid-jcb1133>3.0.co;2-y).
- Kariuki, S.N., Williams, T.N., 2020. Human genetics and malaria resistance. *Human Genetics* In press. <https://doi.org/10.1007/s00439-020-02142-6>.
- Kawamura, Y., 2017. Extracellular vesicles as trans-genomic agents: Emerging roles in disease and evolution. *Cancer Science* 108, 824–830.
- Khan, S.R., Kuzminov, A., 2017. Pulsed-field gel electrophoresis does not break *E. coli* chromosome undergoing excision repair after UV irradiation. *Analytical Biochemistry* 526, 66–68.  
<https://doi.org/10.1016/j.ab.2017.03.019>.

- Khan, S.R., Kuzminov, A., 2013. Trapping and breaking of in vivo nicked DNA during pulsed-field gel electrophoresis. *Analytical Biochemistry* 443, 269–281. <https://doi.org/10.1016/j.ab.2013.06.001>.
- Kidgell, C., Volkman, S.K., Daily, J., Borevitz, J.O., Plouffe, D., Zhou, Y., Johnson, J.R., Le Roch, K.G., Sarr, O., Ndir, O., Mboup, S., Batalov, S., Wirth, D.F., Winzeler, E.A., 2006. A Systematic Map of Genetic Variation in *Plasmodium falciparum*. *PLoS Pathogens* 2, e57. <https://doi.org/10.1371/journal.ppat.0020057>.
- Koenderink, J.B., Kavishe, R.A., Rijpma, S.R., Russel, F.G.M., 2010. The ABCs of multidrug resistance in malaria. *Trends in Parasitology* 26, 440–446. <https://doi.org/10.1016/j.pt.2010.05.002>.
- Kondrashov, F.A., 2012. Gene duplication as a mechanism of genomic adaptation to a changing environment. *Proceedings of the Royal Society B: Biological Sciences* 279, 5048–5057. <https://doi.org/10.1098/rspb.2012.1108>.
- Konoshenko, M.Yu., Lekchnov, E.A., Vlassov, A.V., Laktionov, P.P., 2018. Isolation of Extracellular Vesicles: General Methodologies and Latest Trends. *Biomedical Research International* 2018, 8545347. <https://doi.org/10.1155/2018/8545347>.
- Kraemer, S.M., Smith, J.D., 2006. A family affair: var genes, PfEMP1 binding, and malaria disease. *Current Opinion in Microbiology* 9, 374–380. <https://doi.org/10.1016/j.mib.2006.06.006>.
- Krogstad, D.J., Gluzman, I.Y., Herwaldt, B.L., Schlesinger, P.H., Wellems, T.E., 1992. Energy dependence of chloroquine accumulation and chloroquine

- efflux in *Plasmodium falciparum*. *Biochemical Pharmacology* 43, 57–62.  
[https://doi.org/10.1016/0006-2952\(92\)90661-2](https://doi.org/10.1016/0006-2952(92)90661-2).
- Kuo, W.P., Tigges, J.C., Toxavidis, V., Ghiran, I., 2017. Red Blood Cells: A Source of Extracellular Vesicles. *Methods in Molecular Biology* 1660, 15–22. [https://doi.org/10.1007/978-1-4939-7253-1\\_2](https://doi.org/10.1007/978-1-4939-7253-1_2).
- Lane, K.D., Mu, J., Lu, J., Windle, S.T., Liu, A., Sun, P.D., Wellems, T.E., 2018. Selection of *Plasmodium falciparum* cytochrome B mutants by putative PfNDH2 inhibitors. *Proceedings of the National Academy of Sciences of the United States of America* 115, 6285–6290.  
<https://doi.org/10.1073/pnas.1804492115>.
- Langreth, S.G., Nguyen-Dinh, P., Trager, W., 1978. *Plasmodium falciparum*: Merozoite invasion *in vitro* in the presence of chloroquine. *Experimental Parasitology* 46, 235–238. [https://doi.org/10.1016/0014-4894\(78\)90136-4](https://doi.org/10.1016/0014-4894(78)90136-4).
- Lannigan, J., Erdbruegger, U., 2017. Imaging flow cytometry for the characterization of extracellular vesicles. *Methods, Flow Cytometry* 112, 55–67. <https://doi.org/10.1016/j.ymeth.2016.09.018>.
- Lasken, R.S., Stockwell, T.B., 2007. Mechanism of chimera formation during the Multiple Displacement Amplification reaction. *BioMed Central Biotechnology* 7, 19. <https://doi.org/10.1186/1472-6750-7-19>.
- Lauer, S.A., Rathod, P.K., Ghori, N., Haldar, K., 1997. A membrane network for nutrient import in red cells infected with the malaria parasite. *Science* 276, 1122–1125. <https://doi.org/10.1126/science.276.5315.1122>.
- Lázaro-Ibáñez, E., 2019. DNA analysis of low- and high-density fractions defines heterogeneous subpopulations of small extracellular vesicles based on

- their DNA cargo and topology. *Journal of Extracellular Vesicles* 8, 1656993. <https://doi.org/10.1080/20013078.2019.1656993>.
- Leprohon, P., Fernandez-Prada, C., Gazanion, É., Monte-Neto, R., Ouellette, M., 2014. Drug resistance analysis by next generation sequencing in *Leishmania*. *International Journal of Parasitology- Drugs and Drug Resistance* 5, 26–35. <https://doi.org/10.1016/j.ijpddr.2014.09.005>.
- Li, G.-D., 2018. Cell-Cycle-Associated Amplified Genomic-DNA Fragments (CAGFs) Might Be Involved in Chloroquine Action and Resistance in *Plasmodium falciparum*. Cornell University arXiv:1702.02076 [q-bio].
- Li, W., Olivier, M., 2012. Current analysis platforms and methods for detecting copy number variation. *Physiological Genomics* 45, 1–16. <https://doi.org/10.1152/physiolgenomics.00082.2012>.
- Lobb, R., 2015. Optimized exosome isolation protocol for cell culture supernatant and human plasma. *Journal of Extracellular Vesicles*, 4, 27031. <https://doi.org/10.3402/jev.v4.27031>.
- Maacha, S., Bhat, A.A., Jimenez, L., Raza, A., Haris, M., Uddin, S., Grivel, J.-C., 2019. Extracellular vesicles-mediated intercellular communication: roles in the tumor microenvironment and anti-cancer drug resistance. *Molecular Cancer* 18, 55. <https://doi.org/10.1186/s12943-019-0965-7>.
- Maier, A.G., Rug, M., O'Neill, M.T., Brown, M., Chakravorty, S., Szeszak, T., Chesson, J., Wu, Y., Hughes, K., Coppel, R.L., Newbold, C., Beeson, J.G., Craig, A., Crabb, B.S., Cowman, A.F., 2008. Exported proteins required for virulence and rigidity of *Plasmodium falciparum*-infected human erythrocytes. *Cell* 134, 48–61. <https://doi.org/10.1016/j.cell.2008.04.051>.

Manson-Bahr, P., 1938. The Jubilee of Sir Patrick Manson (1878-1938): A

Tribute to his Work on the Malaria Problem. *Postgraduate Medical Journal* 14, 345–357. <https://doi.org/10.1136/pgmj.14.157.345>.

Mantel, P.-Y., Hoang, A.N., Goldowitz, I., Potashnikova, D., Hamza, B., Vorobjev,

I., Ghiran, I., Toner, M., Irimia, D., Ivanov, A.R., Barteneva, N., Marti, M., 2013a. Malaria-infected erythrocyte-derived microvesicles mediate cellular communication within the parasite population and with the host immune system. *Cell Host Microbe* 13, 521–534.

<https://doi.org/10.1016/j.chom.2013.04.009>.

Mantel, P.-Y., Hoang, A.N., Goldowitz, I., Potashnikova, D., Hamza, B., Vorobjev,

I., Ghiran, I., Toner, M., Irimia, D., Ivanov, A.R., Barteneva, N., Marti, M., 2013b. Malaria-infected erythrocyte-derived microvesicles mediate cellular communication within the parasite population and with the host immune system. *Cell Host Microbe* 13, 521–534.

<https://doi.org/10.1016/j.chom.2013.04.009>.

Mantel, P.-Y., Marti, M., 2014. The role of extracellular vesicles in *Plasmodium* and other protozoan parasites. *Cell Microbiology* 16, 344–354.

<https://doi.org/10.1111/cmi.12259>.

Martin, R.E., Ginsburg, H., Kirk, K., 2009. Membrane transport proteins of the malaria parasite. *Molecular Microbiology* 74, 519–528.

<https://doi.org/10.1111/j.1365-2958.2009.06863.x>.

Martinsen, E.S., Perkins, S.L., Schall, J.J., 2008. A three-genome phylogeny of malaria parasites (*Plasmodium* and closely related genera): Evolution of life-history traits and host switches. *Molecular Phylogenetics and Evolution* 47, 261–273. <https://doi.org/10.1016/j.ympev.2007.11.012>.

- Matthews, H., Duffy, C.W., Merrick, C.J., 2018. Checks and balances? DNA replication and the cell cycle in *Plasmodium*. *Parasites & Vectors* 11, 216.  
<https://doi.org/10.1186/s13071-018-2800-1>.
- Mbengue, A., Bhattacharjee, S., Pandharkar, T., Liu, H., Estiu, G., Stahelin, R.V., Rizk, S.S., Njimoh, D.L., Ryan, Y., Chotivanich, K., Nguon, C., Ghorbal, M., Lopez-Rubio, J.-J., Pfrender, M., Emrich, S., Mohandas, N., Dondorp, A.M., Wiest, O., Haldar, K., 2015. A molecular mechanism of artemisinin resistance in *Plasmodium falciparum* malaria. *Nature* 520, 683–687.  
<https://doi.org/10.1038/nature14412>.
- McDermott, G.P., Do, D., Litterst, C.M., Maar, D., Hindson, C.M., Steenblock, E.R., Legler, T.C., Jouvenot, Y., Marrs, S.H., Bemis, A., Shah, P., Wong, J., Wang, S., Sally, D., Javier, L., Dinio, T., Han, C., Brackbill, T.P., Hodges, S.P., Ling, Y., Klitgord, N., Carman, G.J., Berman, J.R., Koehler, R.T., Hiddessen, A.L., Walse, P., Bousse, L., Tzonev, S., Hefner, E., Hindson, B.J., Cauly, T.H., Hamby, K., Patel, V.P., Regan, J.F., Wyatt, P.W., Karlin-Neumann, G.A., Stumbo, D.P., Lowe, A.J., 2013. Multiplexed target detection using DNA-binding dye chemistry in droplet digital PCR. *Analytical Chemistry* 85, 11619–11627.  
<https://doi.org/10.1021/ac403061n>.
- McGill, J.R., Beitzel, B.F., Nielsen, J.L., Walsh, J.T., Drabek, S.M., Meador, R.J., Von Hoff, D.D., 1993. Double minutes are frequently found in ovarian carcinomas. *Cancer Genetics and Cytogenetics* 71, 125–131.  
[https://doi.org/10.1016/0165-4608\(93\)90017-G](https://doi.org/10.1016/0165-4608(93)90017-G).
- Mehrotra, M., 2016. PCR-Based Detection of DNA Copy Number Variation, in: Luthra, R., Singh, R.R., Patel, K.P. (Eds.), *Clinical Applications of PCR*,

Methods in Molecular Biology. Springer, New York, NY, pp. 27–32.

[https://doi.org/10.1007/978-1-4939-3360-0\\_3](https://doi.org/10.1007/978-1-4939-3360-0_3).

Meshnick, S.R., 2002. Artemisinin: mechanisms of action, resistance and toxicity.

International Journal for Parasitology, Malaria Progress, Problems and

Plans in the Genomic Era 32, 1655–1660. [https://doi.org/10.1016/S0020-](https://doi.org/10.1016/S0020-7519(02)00194-7)

[7519\(02\)00194-7](https://doi.org/10.1016/S0020-7519(02)00194-7).

Milton, M.E., Nelson, S.W., 2016. Replication and maintenance of the

*Plasmodium falciparum* apicoplast genome. Molecular and Biochemical

Parasitology 208, 56–64.

<https://doi.org/10.1016/j.molbiopara.2016.06.006>.

Miotke, L., Lau, B.T., Rumma, R.T., Ji, H.P., 2014. High sensitivity detection and

quantitation of DNA copy number and single nucleotide variants with

single color droplet digital PCR. Analytical Chemistry 86, 2618–2624.

<https://doi.org/10.1021/ac403843j>.

Mita, T., Tanabe, K., Kita, K., 2009. Spread and evolution of *Plasmodium*

*falciparum* drug resistance. International Journal of Parasitology 58, 201–

209. <https://doi.org/10.1016/j.parint.2009.04.004>.

Mitamura, T., Palacpac, N.M.Q., 2003. Lipid metabolism in *Plasmodium*

*falciparum*-infected erythrocytes: possible new targets for malaria

chemotherapy. Microbes Infection 5, 545–552.

[https://doi.org/10.1016/s1286-4579\(03\)00070-4](https://doi.org/10.1016/s1286-4579(03)00070-4).

Mohandas, N., Chasis, J.A., 1993. Red blood cell deformability, membrane

material properties and shape: regulation by transmembrane, skeletal and

cytosolic proteins and lipids. Seminars in Hematology 30, 171–192.

Møller, H.D., Parsons, L., Jørgensen, T.S., Botstein, D., Regenberg, B., 2015.

Extrachromosomal circular DNA is common in yeast. *Proceedings of the National Academy of Sciences of the United States of America* 112, e3114-3122. <https://doi.org/10.1073/pnas.1508825112>.

Montaner, S., Galiano, A., Trelis, M., Martin-Jaular, L., Del Portillo, H.A., Bernal, D., Marcilla, A., 2014. The Role of Extracellular Vesicles in Modulating the Host Immune Response during Parasitic Infections. *Frontiers in Immunology* 5, 433. <https://doi.org/10.3389/fimmu.2014.00433>.

Monti, D., Basilico, N., Parapini, S., Pasini, E., Olliaro, P., Taramelli, D., 2002.

Does chloroquine really act through oxidative stress? *Federation of European Biochemical Societies Letters* 522, 3–5. [https://doi.org/10.1016/S0014-5793\(02\)02881-8](https://doi.org/10.1016/S0014-5793(02)02881-8).

Mukherjee, K., Storici, F., 2012. A mechanism of gene amplification driven by small DNA fragments. *PLoS Genetics* 8, e1003119.

<https://doi.org/10.1371/journal.pgen.1003119>.

Müller, O., Lu, G.Y., von Seidlein, L., 2019. Geographic expansion of artemisinin resistance. *Journal of Travel Medicine* 26, taz030.

<https://doi.org/10.1093/jtm/taz030>.

Mundwiler-Pachlatko, E., Beck, H.-P., 2013. Maurer's clefts, the enigma of *Plasmodium falciparum*. *Proceedings of the National Academy of Sciences of the United States of America* 110, 19987–19994.

<https://doi.org/10.1073/pnas.1309247110>.

Nair, S., Miller, B., Barends, M., Jaidee, A., Patel, J., Mayxay, M., Newton, P.,

Nosten, F., Ferdig, M.T., Anderson, T.J.C., 2008a. Adaptive copy number

evolution in malaria parasites. *PLoS Genetics* 4, e1000243.

<https://doi.org/10.1371/journal.pgen.1000243>.

Nair, S., Miller, B., Barends, M., Jaidee, A., Patel, J., Mayxay, M., Newton, P., Nosten, F., Ferdig, M.T., Anderson, T.J.C., 2008b. Adaptive Copy Number Evolution in Malaria Parasites. *PLoS Genetics* 4, e1000243.

<https://doi.org/10.1371/journal.pgen.1000243>.

Nair, S., Nash, D., Sudimack, D., Jaidee, A., Barends, M., Uhlemann, A.-C., Krishna, S., Nosten, F., Anderson, T.J.C., 2007. Recurrent gene amplification and soft selective sweeps during evolution of multidrug resistance in malaria parasites. *Molecular Biology and Evolution* 24, 562–573. <https://doi.org/10.1093/molbev/msl185>.

Nantakomol, D., Dondorp, A.M., Krudsood, S., Udomsangpetch, R., Pattanapanyasat, K., Combes, V., Grau, G.E., White, N.J., Viriyavejakul, P., Day, N.P.J., Chotivanich, K., 2011. Circulating red cell-derived microparticles in human malaria. *Journal of Infectious Disease* 203, 700–706. <https://doi.org/10.1093/infdis/jiq104>.

O'Donnell, R.A., Preiser, P.R., Williamson, D.H., Moore, P.W., Cowman, A.F., Crabb, B.S., 2001a. An alteration in concatameric structure is associated with efficient segregation of plasmids in transfected *Plasmodium falciparum* parasites. *Nucleic Acids Research* 29, 716–724.

<https://doi.org/10.1093/nar/29.3.716>.

Ofir-Birin, Y., Abou karam, P., Rudik, A., Giladi, T., Porat, Z., Regev-Rudzki, N., 2018. Monitoring Extracellular Vesicle Cargo Active Uptake by Imaging Flow Cytometry. *Frontiers in Immunology* 9, 1011.

<https://doi.org/10.3389/fimmu.2018.01011>.

- O'Neill, P.M., Barton, V.E., Ward, S.A., 2010. The molecular mechanism of action of artemisinin--the debate continues. *Molecules* 15, 1705–1721. <https://doi.org/10.3390/molecules15031705>.
- Pankoui Mfonkeu, J.B., Gouado, I., Fotso Kuate, H., Zambou, O., Amvam Zollo, P.H., Grau, G.E.R., Combes, V., 2010. Elevated cell-specific microparticles are a biological marker for cerebral dysfunctions in human severe malaria. *PLoS ONE* 5, e13415. <https://doi.org/10.1371/journal.pone.0013415>.
- Parish, L.A., Rayner, J.C., 2009. Plasmodium falciparum secretory pathway: Characterization of PfStx1, a plasma membrane Qa-SNARE. *Molecular and Biochemical Parasitology* 164, 153–156. <https://doi.org/10.1016/j.molbiopara.2008.11.011>.
- Paulsen, T., Kumar, P., Koseoglu, M.M., Dutta, A., 2018a. Discoveries of Extrachromosomal Circles of DNA in Normal and Tumor Cells. *Trends in Genetics* 34, 270–278. <https://doi.org/10.1016/j.tig.2017.12.010>.
- Paulsen, T., Kumar, P., Koseoglu, M.M., Dutta, A., 2018b. New discoveries of extrachromosomal circles of DNA in normal and tumor cells. *Trends in Genetics* 34, 270–278. <https://doi.org/10.1016/j.tig.2017.12.010>.
- Paulsen, T., Shibata, Y., Kumar, P., Dillon, L., Dutta, A., 2019. Small extrachromosomal circular DNAs, microDNA, produce short regulatory RNAs that suppress gene expression independent of canonical promoters. *Nucleic Acids Research* 47, 4586–4596. <https://doi.org/10.1093/nar/gkz155>.
- Percário, S., Moreira, D.R., Gomes, B.A.Q., Ferreira, M.E.S., Gonçalves, A.C.M., Laurindo, P.S.O.C., Vilhena, T.C., Dolabela, M.F., Green, M.D., 2012.

Oxidative Stress in Malaria. *International Journal of Molecular Science* 13, 16346–16372. <https://doi.org/10.3390/ijms131216346>.

Phillips, M.A., Gujjar, R., Malmquist, N.A., White, J., El Mazouni, F., Baldwin, J., Rathod, P.K., 2008. Triazolopyrimidine-based dihydroorotate dehydrogenase inhibitors with potent and selective activity against the malaria parasite *Plasmodium falciparum*. *Journal of Medicinal Chemistry* 51, 3649–3653. <https://doi.org/10.1021/jm8001026>.

Phillips, M.A., Lotharius, J., Marsh, K., White, J., Dayan, A., White, K.L., Njoroge, J.W., Mazouni, F.E., Lao, Y., Kokkonda, S., Tomchick, D.R., Deng, X., Laird, T., Bhatia, S.N., March, S., Ng, C.L., Fidock, D.A., Wittlin, S., Lafuente-Monasterio, M., Benito, F.J.G., Alonso, L.M.S., Martinez, M.S., Jimenez-Diaz, M.B., Bazaga, S.F., Angulo-Barturen, I., Haselden, J.N., Louttit, J., Cui, Y., Sridhar, A., Zeeman, A.-M., Kocken, C., Sauerwein, R., Dechering, K., Avery, V.M., Duffy, S., Delves, M., Sinden, R., Ruecker, A., Wickham, K.S., Rochford, R., Gahagen, J., Iyer, L., Riccio, E., Mirsalis, J., Bathurst, I., Rueckle, T., Ding, X., Campo, B., Leroy, D., Rogers, M.J., Rathod, P.K., Burrows, J.N., Charman, S.A., 2015. A long-duration dihydroorotate dehydrogenase inhibitor (DSM265) for prevention and treatment of malaria. *Science Translational Medicine* 7, 296ra111-296ra111. <https://doi.org/10.1126/scitranslmed.aaa6645>.

Pinheiro, L.B., Coleman, V.A., Hindson, C.M., Herrmann, J., Hindson, B.J., Bhat, S., Emslie, K.R., 2012. Evaluation of a droplet digital polymerase chain reaction format for DNA copy number quantification. *Analytical Chemistry* 84, 1003–1011. <https://doi.org/10.1021/ac202578x>.

- Poliakov, A., Spilman, M., Dokland, T., Amling, C.L., Mobley, J.A., 2009. Structural heterogeneity and protein composition of exosome-like vesicles (prostasomes) in human semen. *Prostate* 69, 159–167. <https://doi.org/10.1002/pros.20860>.
- Prada-Luengo, I., Krogh, A., Maretty, L., Regenbreg, B., 2019. Sensitive detection of circular DNAs at single-nucleotide resolution using guided realignment of partially aligned reads. *BioMed Central Bioinformatics* 20, 663. <https://doi.org/10.1186/s12859-019-3160-3>.
- Preiser, P.R., Wilson, R.J., Moore, P.W., McCready, S., Hajibagheri, M.A., Blight, K.J., Strath, M., Williamson, D.H., 1996. Recombination associated with replication of malarial mitochondrial DNA. *European Molecular Biology Organization Journal* 15, 684–693.
- Prevention, C.-C. for D.C. and, 2019. CDC - Malaria - About Malaria - Biology [WWW Document]. URL <https://www.cdc.gov/malaria/about/biology/index.html> (accessed 2.5.20).
- Prugnolle, F., Durand, P., Ollomo, B., Duval, L., Ariey, F., Arnathau, C., Gonzalez, J.-P., Leroy, E., Renaud, F., 2011. A Fresh Look at the Origin of *Plasmodium falciparum*, the Most Malignant Malaria Agent. *PLOS Pathogens* 7, e1001283. <https://doi.org/10.1371/journal.ppat.1001283>.
- Qidwai, T., 2020. Exploration of copy number variation in genes related to anti-malarial drug resistance in *Plasmodium falciparum*. *Gene* 736, 144414. <https://doi.org/10.1016/j.gene.2020.144414>.
- Rathod, P.K., Leffers, N.P., Young, R.D., 1992. Molecular targets of 5-fluoroorotate in the human malaria parasite, *Plasmodium falciparum*.

Antimicrobial Agents and Chemotherapy 36, 704–711.

<https://doi.org/10.1128/aac.36.4.704>.

Regev-Rudzki, N., Wilson, D.W., Carvalho, T.G., Sisqueira, X., Coleman, B.M., Rug, M., Bursac, D., Angrisano, F., Gee, M., Hill, A.F., Baum, J., Cowman, A.F., 2013. Cell-cell communication between malaria-infected red blood cells via exosome-like vesicles. *Cell* 153, 1120–1133.

<https://doi.org/10.1016/j.cell.2013.04.029>.

Ribacke, U., Mok, B.W., Wirta, V., Normark, J., Lundeberg, J., Kironde, F., Egwang, T.G., Nilsson, P., Wahlgren, M., 2007. Genome wide gene amplifications and deletions in *Plasmodium falciparum*. *Molecular Biochemistry Parasitology* 155, 33–44.

<https://doi.org/10.1016/j.molbiopara.2007.05.005>.

Ronquist, G.K., Larsson, A., Stavreus-Evers, A., Ronquist, G., 2012.

Prostasomes are heterogeneous regarding size and appearance but affiliated to one DNA-containing exosome family. *Prostate* 72, 1736–1745.

<https://doi.org/10.1002/pros.22526>.

Roper, C., Alifrangis, M., Ariey, F., Talisuna, A., Menard, D., Mercereau-Puijalon, O., Ringwald, P., 2014. Molecular surveillance for artemisinin resistance in Africa. *The Lancet Infectious Diseases* 14, 668–670.

[https://doi.org/10.1016/S1473-3099\(14\)70826-6](https://doi.org/10.1016/S1473-3099(14)70826-6).

Rosenthal, P.J., 2018. Artemisinin Resistance Outside of Southeast Asia. *The American Journal of Tropical Medicine and Hygiene* 99, 1357–1359.

<https://doi.org/10.4269/ajtmh.18-0845>.

Ross, L.S., Gamo, F.J., Lafuente-Monasterio, M.J., Singh, O.M.P., Rowland, P., Wiegand, R.C., Wirth, D.F., 2014. *In vitro* resistance selections for

*Plasmodium falciparum* dihydroorotate dehydrogenase inhibitors give mutants with multiple point mutations in the drug-binding site and altered growth. *Journal of Biological Chemistry* 289, 17980–17995.

<https://doi.org/10.1074/jbc.M114.558353>.

Rottmann, M., McNamara, C., Yeung, B.K.S., Lee, M.C.S., Zou, B., Russell, B., Seitz, P., Plouffe, D.M., Dharia, N.V., Tan, J., Cohen, S.B., Spencer, K.R., González-Páez, G.E., Lakshminarayana, S.B., Goh, A., Suwanarusk, R., Jegla, T., Schmitt, E.K., Beck, H.-P., Brun, R., Nosten, F., Renia, L., Dartois, V., Keller, T.H., Fidock, D.A., Winzeler, E.A., Diagana, T.T., 2010. Spiroindolones, a potent compound class for the treatment of malaria. *Science* 329, 1175–1180. <https://doi.org/10.1126/science.1193225>.

RTS,S Clinical Trials Partnership, 2014. Efficacy and safety of the RTS,S/AS01 malaria vaccine during 18 months after vaccination: a phase 3 randomized, controlled trial in children and young infants at 11 African sites. *PLoS Medicine* 11, e1001685.

<https://doi.org/10.1371/journal.pmed.1001685>.

Sampaio, N.G., Cheng, L., Eriksson, E.M., 2017. The role of extracellular vesicles in malaria biology and pathogenesis. *Malaria Journal* 16, 245.

<https://doi.org/10.1186/s12936-017-1891-z>.

Sau, S., Ghosh, S.K., Liu, Y.-T., Ma, C.-H., Jayaram, M., 2019. Hitchhiking on chromosomes: A persistence strategy shared by diverse selfish DNA elements. *Plasmid* 102, 19–28.

<https://doi.org/10.1016/j.plasmid.2019.01.004>.

- Scherf, A., Lopez-Rubio, J.J., Riviere, L., 2008. Antigenic Variation in *Plasmodium falciparum*. *Annual Review of Microbiology* 62, 445–470. <https://doi.org/10.1146/annurev.micro.61.080706.093134>.
- Schimke, R.T., Sherwood, S.W., Hill, A.B., Johnston, R.N., 1986. Overreplication and recombination of DNA in higher eukaryotes: potential consequences and biological implications. *Proceedings of the National Academy of Sciences of the United States of America* 83, 2157–2161. <https://doi.org/10.1073/pnas.83.7.2157>.
- Schorey, J.S., Cheng, Y., Singh, P.P., Smith, V.L., 2015. Exosomes and other extracellular vesicles in host-pathogen interactions. *European Molecular Biology Organization Reports* 16, 24–43. <https://doi.org/10.15252/embr.201439363>.
- Shibata, Y., Kumar, P., Layer, R., Willcox, S., Gagan, J.R., Griffith, J.D., Dutta, A., 2012. Extrachromosomal microDNAs and chromosomal microdeletions in normal tissues. *Science* 336, 82–86. <https://doi.org/10.1126/science.1213307>.
- Sidhu, A.B.S., Uhlemann, A.-C., Valderramos, S.G., Valderramos, J.-C., Krishna, S., Fidock, D.A., 2006. Decreasing *pfmdr1* Copy Number in *Plasmodium falciparum* Malaria Heightens Susceptibility to Mefloquine, Lumefantrine, Halofantrine, Quinine, and Artemisinin. *Journal of Infectious Disease* 194, 528–535. <https://doi.org/10.1086/507115>.
- Sidhu, A.B.S., Verdier-Pinard, D., Fidock, D.A., 2002. Chloroquine Resistance in *Plasmodium falciparum* Malaria Parasites Conferred by *pfcr1* Mutations. *Science* 298, 210–213. <https://doi.org/10.1126/science.1074045>.

- Singh, A., Rosenthal, P.J., 2004. Selection of cysteine protease inhibitor-resistant malaria parasites is accompanied by amplification of falcipain genes and alteration in inhibitor transport. *Journal of Biological Chemistry* 279, 35236–35241. <https://doi.org/10.1074/jbc.M404235200>.
- Singh, D., Chaubey, S., Habib, S., 2003. Replication of the *Plasmodium falciparum* apicoplast DNA initiates within the inverted repeat region. *Molecular and Biochemistry Parasitology* 126, 9–14. [https://doi.org/10.1016/s0166-6851\(02\)00251-7](https://doi.org/10.1016/s0166-6851(02)00251-7).
- Sisquella, X., Ofir-Birin, Y., Pimentel, M.A., Cheng, L., Abou Karam, P., Sampaio, N.G., Penington, J.S., Connolly, D., Giladi, T., Scicluna, B.J., Sharples, R.A., Waltmann, A., Avni, D., Schwartz, E., Schofield, L., Porat, Z., Hansen, D.S., Papenfuss, A.T., Eriksson, E.M., Gerlic, M., Hill, A.F., Bowie, A.G., Regev-Rudzki, N., 2017. Malaria parasite DNA-harboring vesicles activate cytosolic immune sensors. *Nature Communications* 8, 1–15. <https://doi.org/10.1038/s41467-017-02083-1>.
- Slater, A.F.G., 1993. Chloroquine: Mechanism of drug action and resistance in *Plasmodium falciparum*. *Pharmacology & Therapeutics* 57, 203–235. [https://doi.org/10.1016/0163-7258\(93\)90056-J](https://doi.org/10.1016/0163-7258(93)90056-J).
- Smith, J.D., Chitnis, C.E., Craig, A.G., Roberts, D.J., Hudson-Taylor, D.E., Peterson, D.S., Pinches, R., Newbold, C.I., Miller, L.H., 1995. Switches in expression of *Plasmodium falciparum* var genes correlate with changes in antigenic and cytoadherent phenotypes of infected erythrocytes. *Cell* 82, 101–110. [https://doi.org/10.1016/0092-8674\(95\)90056-x](https://doi.org/10.1016/0092-8674(95)90056-x).
- Soekmadji, C., Nelson, C.C., 2015. The Emerging Role of Extracellular Vesicle-Mediated Drug Resistance in Cancers: Implications in Advanced Prostate

- Cancer. Biomedical Research International 2015, 454837.  
<https://doi.org/10.1155/2015/454837>.
- Soni, R., Sharma, D., Bhatt, T.K., 2016. *Plasmodium falciparum* Secretome in Erythrocyte and Beyond. *Frontiers in Microbiology* 7, 194.  
<https://doi.org/10.3389/fmicb.2016.00194>.
- Sun, T., Wang, K., Liu, C., Wang, Y., Wang, J., Li, P., 2019. Identification of Extrachromosomal Linear microDNAs Interacted with microRNAs in the Cell Nuclei. *Cells* 8, 111. <https://doi.org/10.3390/cells8020111>.
- Szataneck, R., Baran, J., Siedlar, M., Baj-Krzyworzeka, M., 2015. Isolation of extracellular vesicles: Determining the correct approach (Review). *International Journal of Molecular Medicine* 36, 11–17.  
<https://doi.org/10.3892/ijmm.2015.2194>.
- Tang, Y.T., Tang, Y. T., Huang, Y. Y., Zheng, L., Qin, S. H., Xu, X. P., An, T. X., Xu, Y., Wu, Y. S., Hu, X. M., Ping, B. H., & Wang, Q. 2017. Comparison of isolation methods of exosomes and exosomal RNA from cell culture medium and serum. *International Journal of Molecular Medicine* 40, 834–844. <https://doi.org/10.3892/ijmm.2017.3080>.
- Theisen, A., 2008. Microarray-based Comparative Genomic Hybridization (aCGH) [WWW Document]. Nature Education. URL <https://www.nature.com/scitable/topicpage/microarray-based-comparative-genomic-hybridization-acgh-45432/> (accessed 3.10.20).
- Thuring, R.W., Sanders, J.P., Borst, P., 1975. A freeze-squeeze method for recovering long DNA from agarose gels. *Analytical Biochemistry* 66, 213–220. [https://doi.org/10.1016/0003-2697\(75\)90739-3](https://doi.org/10.1016/0003-2697(75)90739-3).

- Tilley, L., Straimer, J., Gnädig, N.F., Ralph, S.A., Fidock, D.A., 2016. Artemisinin Action and Resistance in *Plasmodium falciparum*. *Trends in Parasitology* 32, 682–696. <https://doi.org/10.1016/j.pt.2016.05.010>.
- Toledo, F., Buttin, G., Debatisse, M., 1993. The origin of chromosome rearrangements at early stages of AMPD2 gene amplification in Chinese hamster cells. *Current Biology* 3, 255–264. [https://doi.org/10.1016/0960-9822\(93\)90175-n](https://doi.org/10.1016/0960-9822(93)90175-n).
- Trager, W., Jensen, J.B., 1976. Human malaria parasites in continuous culture. *Science* 193, 673–675. <https://doi.org/10.1126/science.781840>.
- Triglia, T., Foote, S.J., Kemp, D.J., Cowman, A.F., 1991. Amplification of the multidrug resistance gene *pfmdr1* in *Plasmodium falciparum* has arisen as multiple independent events. *Molecular and Cellular Biology* 11, 5244–5250. <https://doi.org/10.1128/mcb.11.10.5244>.
- Tun, K.M., Imwong, M., Lwin, K.M., Win, A.A., Hlaing, T.M., Hlaing, T., Lin, K., Kyaw, M.P., Plewes, K., Faiz, M.A., Dhorda, M., Cheah, P.Y., Pukrittayakamee, S., Ashley, E.A., Anderson, T.J.C., Nair, S., McDew-White, M., Flegg, J.A., Grist, E.P.M., Guerin, P., Maude, R.J., Smithuis, F., Dondorp, A.M., Day, N.P.J., Nosten, F., White, N.J., Woodrow, C.J., 2015. Spread of artemisinin-resistant *Plasmodium falciparum* in Myanmar: a cross-sectional survey of the K13 molecular marker. *The Lancet Infectious Diseases* 15, 415–421. [https://doi.org/10.1016/S1473-3099\(15\)70032-0](https://doi.org/10.1016/S1473-3099(15)70032-0).
- Turmel, C., Brassard, E., Slater, G.W., Noolandi, J., 1990. Molecular detrapping and band narrowing with high frequency modulation of pulsed field electrophoresis. *Nucleic Acids Research*. 18, 569–575. <https://doi.org/10.1093/nar/18.3.569>.

Vaidya, A.B., and Arasu, P., 1987. Tandemly arranged gene clusters of malarial parasites that are highly conserved and transcribed. *Molecular and Biochemistry Parasitology* 22, 249–257. [https://doi.org/10.1016/0166-6851\(87\)90056-9](https://doi.org/10.1016/0166-6851(87)90056-9).

van den Berg, M., Ogutu, B., Sewankambo, N.K., Biller-Andorno, N., Tanner, M., 2019. RTS,S malaria vaccine pilot studies: addressing the human realities in large-scale clinical trials. *Trials* 20, 316. <https://doi.org/10.1186/s13063-019-3391-7>.

Varshavsky, A., 1981. On the possibility of metabolic control of replicon “misfiring”: relationship to emergence of malignant phenotypes in mammalian cell lineages. *Proceedings of the National Academy of Sciences of the United States of America* 78, 3673–3677. <https://doi.org/10.1073/pnas.78.6.3673>.

Verhaak, R.G.W., Bafna, V., Mischel, P.S., 2019. Extrachromosomal oncogene amplification in tumour pathogenesis and evolution. *Nature Reviews Cancer* 19, 283–288. <https://doi.org/10.1038/s41568-019-0128-6>.

Verma, G., Surolia, N., 2018. Centromere and its associated proteins—what we know about them in *Plasmodium falciparum*. *International Union of Biochemistry and Molecular Biology Life* 70, 732–742. <https://doi.org/10.1002/iub.1878>.

Viret, J.F., Bravo, A., Alonso, J.C., 1991. Recombination-dependent concatemeric plasmid replication. *Microbiology Reviews* 55, 675–683.

Vogt, N., Lefèvre, S.-H., Apiou, F., Dutrillaux, A.-M., Cör, A., Leuraud, P., Poupon, M.-F., Dutrillaux, B., Debatisse, M., Malfoy, B., 2004. Molecular structure of double-minute chromosomes bearing amplified copies of the

- epidermal growth factor receptor gene in gliomas. *Proceedings of the National Academy of Sciences of the United States of America* 101, 11368–11373. <https://doi.org/10.1073/pnas.0402979101>.
- Wagner, W., So, M., 1992. Identification of a novel large extrachromosomal DNA (LED) in the *Trypanosomatidae*. *Molecular Microbiology* 6, 2299–2308. <https://doi.org/10.1111/j.1365-2958.1992.tb01405>.
- Wang, Y., Nair, S., Nosten, F., Anderson, T.J.C., 2009. Multiple Displacement Amplification for Malaria Parasite DNA. *Journal of Parasitology* 95, 253–255. <https://doi.org/10.1645/GE-1706.1>.
- Weaver, S., Dube, S., Mir, A., Qin, J., Sun, G., Ramakrishnan, R., Jones, R.C., Livak, K.J., 2010. Taking qPCR to a higher level: Analysis of CNV reveals the power of high throughput qPCR to enhance quantitative resolution. *Methods* 50, 271–276. <https://doi.org/10.1016/j.ymeth.2010.01.003>.
- Weber, J.L., 1987. Analysis of sequences from the extremely A + T-rich genome of *Plasmodium falciparum*. *Gene* 52, 103–109. [https://doi.org/10.1016/0378-1119\(87\)90399-4](https://doi.org/10.1016/0378-1119(87)90399-4).
- Wengelnik, K., Daher, W., Lebrun, M., 2018. Phosphoinositides and their functions in apicomplexan parasites. *International Journal for Parasitology* 48, 493–504. <https://doi.org/10.1016/j.ijpara.2018.01.009>.
- Whale, A.S., Huggett, J.F., Cowen, S., Speirs, V., Shaw, J., Ellison, S., Foy, C.A., Scott, D.J., 2012. Comparison of microfluidic digital PCR and conventional quantitative PCR for measuring copy number variation. *Nucleic Acids Research* 40, e82–e82. <https://doi.org/10.1093/nar/gks203>.
- Williamson, Donald H., Janse, C.J., Moore, P.W., Waters, A.P., Preiser, P.R., 2002. Topology and replication of a nuclear episomal plasmid in the

- rodent malaria *Plasmodium berghei*. *Nucleic Acids Research* 30, 726–731. <https://doi.org/10.1093/nar/30.3.726>.
- Williamson, D. H., Preiser, P.R., Moore, P.W., McCready, S., Strath, M., Wilson, R.J.M. (Iain), 2002. The plastid DNA of the malaria parasite *Plasmodium falciparum* is replicated by two mechanisms. *Molecular Microbiology* 45, 533–542. <https://doi.org/10.1046/j.1365-2958.2002.03033>.
- Wilson, C.M., Serrano, A.E., Wasley, A., Bogenschutz, M.P., Shankar, A.H., Wirth, D.F., 1989. Amplification of a gene related to mammalian *mdr* genes in drug-resistant *Plasmodium falciparum*. *Science* 244, 1184–1186. <https://doi.org/10.1126/science.2658061>.
- Wilson, R.J., Williamson, D.H., 1997. Extrachromosomal DNA in the Apicomplexa. *Microbiology and Molecular Biology Reviews* 61, 1–16.
- Wiser, M.F., 2011. *Protozoa and Human Disease*. Garland Science.
- Wolfson, R., Higgins, K.G., Sears, B.B., 1991. Evidence for replication slippage in the evolution of *Oenothera* chloroplast DNA. *Molecular Biology Evolution* 8, 709–720. <https://doi.org/10.1093/oxfordjournals.molbev.a040680>.
- World Health Organization, 2018. *World malaria report 2018*. World Health Organization.
- Wu, S., Turner, K.M., Nguyen, N., Raviram, R., Erb, M., Santini, J., Luebeck, J., Rajkumar, U., Diao, Y., Li, B., Zhang, W., Jameson, N., Corces, M.R., Granja, J.M., Chen, X., Coruh, C., Abnoui, A., Houston, J., Ye, Z., Hu, R., Yu, M., Kim, H., Law, J.A., Verhaak, R.G.W., Hu, M., Furnari, F.B., Chang, H.Y., Ren, B., Bafna, V., Mischel, P.S., 2019. Circular ecDNA promotes

accessible chromatin and high oncogene expression. *Nature* 575, 699–703. <https://doi.org/10.1038/s41586-019-1763-5>.

Wu, Y., Sifri, C.D., Lei, H.H., Su, X.Z., Wellems, T.E., 1995. Transfection of *Plasmodium falciparum* within human red blood cells. *Proceedings of the National Academy of Sciences of the United States of America* 92, 973–977. <https://doi.org/10.1073/pnas.92.4.973>.

Yuana, Y., Koning, R.I., Kuil, M.E., Rensen, P.C.N., Koster, A.J., Bertina, R.M., Osanto, S., 2013. Cryo-electron microscopy of extracellular vesicles in fresh plasma. *Journal of Extracellular Vesicles* 2, 10.3402/jev.v2i0.21494. <https://doi.org/10.3402/jev.v2i0.21494>.